Synthesis of Conjugated Polymers and their use in Photovoltaic Cells

Thesis presented for the degree of
Doctor of Philosophy

By

Walid Daoud

The University of Sheffield

Departments of Materials Engineering, Chemistry and Physics

July 2001

To My Parents

Acknowledgments

I would like to thank my supervisor Doctor Mike Turner for his great assistance, advice and patience during my studies.

I would also like to thank my wife, Ayeh, for her love, care and patience during the tough times.

Thanks also go to Professor Donal Bradley, Dr Brian McQuillin and Professor Angela Seddon for their assistance and stimulating discussions.

Thanks are also due to Steven Whitelegg and Dr Carsten Giebler in the Department of Physics, University of Sheffield, for help with device fabrication and characterisation.

Finally I would like to thank all the members of what was laboratory F3B and now D22, Department of Chemistry, for help and friendship. Thanks to the University of Sheffield and Sheffield Hallam University for funding.

Abstract

The work described in this thesis involved the synthesis of novel conjugated organic polymers for use as photosensitisers in all solid-state photovoltaics. The polymers of interest are poly(1,4-phenylene-vinylenes) and poly(1,4-phenylene-ethynylenes).

Palladium catalysed cross coupling of tributyl-vinyl-stannane with dialkyl and dialkoxy substituted 1,4-dihalobenzenes gives 1,4-dialkyl and 1,4-dialkoxy substituted 2,5-divinylbenzenes. 1,4-Dialkoxy substituted 2,5-diethynylbenzenes are prepared in a similar fashion on coupling with trimethylsilylacetylene.

Novel polymers with enhanced conjugation and controlled energy gaps can be synthesised by coupling these compounds with various dihaloaryls. 1,4-Dialkoxy-2,5-bis(chloromethyl)benzenes are prepared by a novel chloromethylation of 1,4-dialkoxy substituted benzenes for use as starting materials for a dehydrohalogenation polymerisation reaction.

Sol-gel processing is utilised for the preparation of highly dense thin films of TiO_2 for use as electron acceptor in all solid-state photovoltaic devices.

Solid-state solar cells are fabricated using the synthesised phenylene vinylene polymers. Thin films of these polymers were spin-coated on to the surface of highly dense sol-gel processed TiO_2 substrates. The exciton dissociation at the interface is thermodynamically favoured through the given energy levels of MEH-PPV and TiO_2.

Using electrodes with similar work function, the current-voltage characteristics show very low leakage currents and an open circuit voltage on illumination of 0.8 V. The energy conversion values of the best devices are 0.38% when monochromatic light is used and 0.15% when illuminated by simulated solar light AM1.5 (844 Watt m^{-2}).

Table of Contents

List of Abbreviations

CCD	Charge Coupled Plasma Detector
DCM	Dichloromethane
DMA	Dimethylacetamide
DMF	Dimethylformamide
DSC	Differential Scanning Calorimetry
GPC	Gel Permeation Chromatography
HOMO	Highest Occupied Molecular Orbital
HPLC	High Performance Liquid Chromatography
ITO	Indium Tin Oxide
LED	Light Emitting Diode
LCD	Liquid Crystal Display
LUMO	Lowest Unoccupied Molecular Orbital
NMR	Nuclear Magnetic Resonance
PPV	Poly(phenylene-vinylene)
PPE	Poly(phenylene-ethynylene)
TEM	Transmission Electron Microscope
THF	Tetrahydrofuran
TLC	Thin Layer Chromatography
XRD	X-Ray Diffraction

Chapter 1: Introduction

During the second half of this Century, the science and technology of synthetic polymers and materials has advanced rapidly. Synthetic polymers play an important role in almost each facet of our daily lives, from the mundane to the extraordinary. Polymers have traditionally been considered as insulating materials by chemists and physicists alike. Indeed a conventional application of polymers is the safe isolation of metallic conductors. The amazing discovery of highly conducting polyacetylene marked the birth of a new field and resulted in the award of the Nobel Prize for chemistry in 2000[1]. The study of this new class of compounds is often termed "molecular electronics". Chemists, physicists and theorists alike are continually exploring new materials and devising novel technologies. Early studies[2,3,4,5] focussed on improving the conductivity of organic polymers upon doping, but it has been generally accepted that most real devices are likely to exploit the intrinsic semiconducting properties of these materials[6].

Most polymers in use are based on a saturated carbon backbone e.g. polystyrene, polyethylene and polypropylene. Conjugated polymers differ from the more common saturated polymers by having a delocalised π-electron bonding along the polymer chain. The π (bonding) and π^* (antibonding) orbitals form delocalised valence and conduction wavefunctions, which can accommodate mobile charge carrying species (*e.g.* holes or electrons). This delocalisation results in conjugated polymers having semiconducting properties[7].

There are various types of conjugated polymers such as poly(1,4-phenylene-vinylenes), poly(1,4-phenylenes), poly(1,4-phenylene-vinylene-thienylenes), poly(thiophenes), poly(1,4-phenylene-ethynylene-thienylenes),

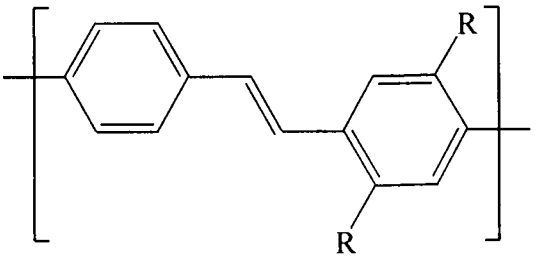

Poly(1,4-phenylene-vinylene)

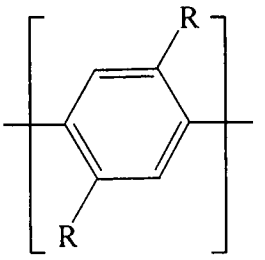

Poly(1,4-phenylene)

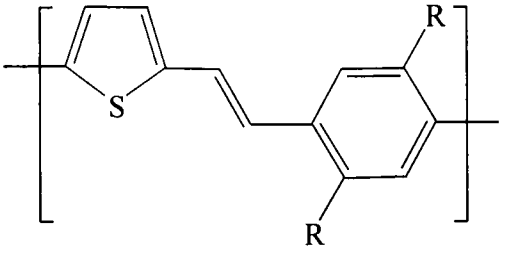

Poly(1,4-phenylene-vinylene-thienylene)

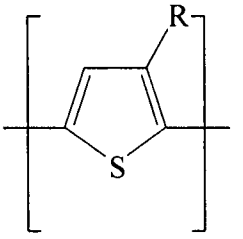

Poly(thiophene)

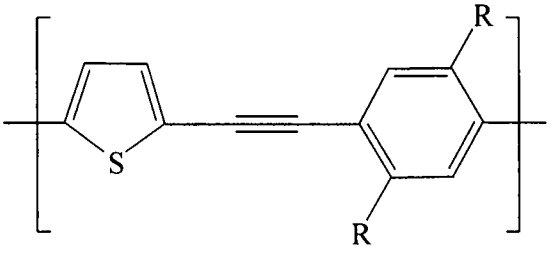

Poly(1,4-phenylene-ethynylene-thienylene)

The $\pi - \pi^*$ energy gap in these materials is given by the energy required to excite an electron from the highest occupied level (HOMO) to the lowest unoccupied level (LUMO).

The conducting properties of an extended solid depend on the electronic structure of that material. The occupancy of the energy bands is very important. If the energy gap (E_g) between the highest occupied level and the lowest unoccupied level is small enough (generally less than 3.0 eV), then the material is a semiconductor. Materials with particularly small energy gaps are termed intrinsic semiconductors as thermal excitation of electrons from the valence band into the conduction band becomes possible. Materials with energy gaps that are too large for thermal excitation at room temperature are often termed insulators, however through appropriate doping they can often be made conducting and are then termed extrinsic semiconductors. The doping can lead to the preponderance of either positive carriers (holes) in 'p-type' or negative carriers (electrons) as in 'n-type' semiconductors[5].

Conjugated polymers have recently stimulated intense research activity due to their interesting optoelectronic properties. These were first discovered at the University of Cambridge in 1990, where it was found that poly(1,4-phenylene-vinylene) (PPV) emits light when sandwiched between hole and electron injecting contacts[8]. These initial studies led to the investigation of huge number of PPV derivatives and other types of conjugated polymers in order to improve the efficiency of organic polymer based light emitting devices (PLEDs)[9,10].

For use in PLEDs, semiconducting polymers must provide both charge transport and efficient electroluminescence. However, they should also be easily processed using well-established techniques for the preparation of thin films, such as spin coating or dip coating. As most highly conjugated materials show poor solubility in common

solvents, approaches to useful conjugated polymers have involved strategies such as the use of a processible precursor, the attachment of solubilising side groups, the use of solubilising spacers between conjugated segments, or a combination of these strategies[10].

In this Chapter, a general introduction to optoelectronic devices will be followed by a more detailed discussion of the use of conjugated polymers in these devices.

1.1 Introduction to optoelectronic devices

Optoelectronics are those devices that combine light with electronics. Such devices refer to the generation of new solid-state components rather than those that are currently in use such as neon lamps and television picture tubes, which are vacuum-state devices.

1.1.1 Liquid crystal displays

Although LEDs are relatively efficient when compared with filament lamps, they nevertheless use a lot of power compared to some types of integrated circuit. Hence, there was a need for a low power display system that could operate for a long time from a battery small enough to go inside items such as wristwatches. The solution proved to be the liquid crystal display (LCD). The flat-panel display industry is currently dominated by liquid crystal technology. Starting in the 1970s with their introduction in watches, liquid crystal displays first took over most of the instrument panel business, then flourished as the laptop computer market grew, originally with

monochrome screens and now increasingly with colour. The LCD does not emit light as in LEDs, but is read like the page of this book, by reflected light. The operation of these devices[11] is beyond the scope of this thesis and they will not be discussed in any further detail.

1.1.2 Light emitting diodes

The light emitting diode (LED) is an extremely useful device, and replaces miniature incandescent lamps in a whole range of applications. Current LEDs, based on inorganic semiconductors, are cheap (nearly 10p each) and use little power. They have found application wherever an indicator lamp is required. The most usual colour is red, but yellow and green are also available.

Electroluminescence has been seen by a wide range of semiconductors[9], for organic semiconductors it was first reported for anthracene single crystals in the 1960s[12,13].

These early studies established that the process responsible for the electroluminescence requires injection of electrons from one electrode and holes from the other, the capture of oppositely charged carriers (electron-hole recombination), and the radiative decay of the excited electron-hole state (exciton) produced by this recombination process[9].

1.1.3 Photodiodes

Illumination of a photodiode with light of energy greater than the band gap energy, results in the production of electrons and holes. In many inorganic semiconductors,

photon absorption produces free electrons and holes directly[14]. However, in molecular organic semiconductors absorption creates electron-hole pairs (excitons), which are bound at room temperature[15], so that charge collection requires their dissociation. Exciton dissociation is known to be efficient at interfaces between materials with different electron affinities and ionisation potentials, where the electron is accepted by the material with larger electron affinity and the hole by the material with lower ionisation potential[16]. Thus, a two-layer diode can be used, in which excitons generated in either layer diffuse towards the interface between the layers. However, the exciton diffusion range is typically at least a factor of 10 smaller than the optical absorption depth, thus limiting the efficiency of charge collection[16].

1.1.4 Photovoltaics

Commonly known as solar cells, photovoltaic cells convert light energy directly into electrical energy. The term Photo stems from the Greek word Phos, which means light, while the term volt is named for Alessandro Volta, a pioneer in the study of electricity, so photovoltaic literally means light-electricity.

The photovoltaic effect was first described by the French physicist Edmond Bequerel in 1839. In 1870, Heinrich Hertz first studied this effect in solids such as selenium. Commercial solar cells were first developed by Chapin, Fuller, and Pearson in 1954 using a silicon p-n junction[17]. Subsequently, the cadmium sulfide solar cell was developed by Reynolds *et al*[18]. There has been a massive research effort in this field in the last three decades[19,20,21,22,23].

Early photovoltaic cells were very inefficient in terms of energy conversion, and produced very small currents and voltages. Since the 1960s intensive development has taken place, partly because it has been proved that in some conventional applications solar power, generated by means of photovoltaic cells, is a useful source of energy. For example, in the inner solar system, the sun represents a useful source of free energy for a space vehicle, an energy that involves no payload of fuel, and will not run out in the anticipated lifetime of the space vehicle. Telecommunications satellites are invariably powered by photovoltaic cells, and the present designs are surprisingly efficient, converting about 20% of the light falling on them into electrical power[24,25]. Silicon photovoltaic cells are simply a pn junction, made with a very thin layer of n-type silicon that is placed over a relatively thicker layer of p-type silicon, and connected through an external circuit. The top n-type layer should be thin enough to allow incident light to penetrate to the junction region easily[17].

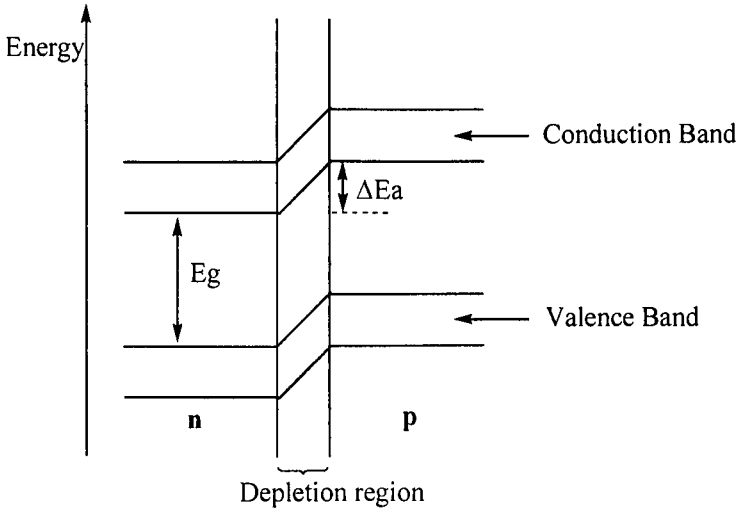

Fig. 1.1.4: Energy level diagram for a pn junction

1.1.4.1 Mechanism of charge separation

When p- and n-semiconductors are placed in intimate contact, electrons flow from the n-type to fill the holes in the p-type, until an equilibrium is established at the interface building a potential difference, the junction potential. When light is able to reach the junction, energy will be absorbed to promote an electron from the valence band of the semiconductor to the conduction band, resulting in the formation of electron-hole pair. Because of the electric field in the depletion region at the interface, these electron-hole pairs are separated and current will flow in an external circuit[26].

The first photovoltaic cell used selenium as a semiconductor. A single crystal silicon photovoltaic cell in the average efficiency range, about 10 cm diameter, will produce a current of ca. 2 A in bright sunlight, with a potential of around 0.5 V. Since roughly 1 kW falls on every square metre of the earth's surface, this means that just under 8 W falls on the cell. With an output of 1.6 W, this means that the efficiency is about 20%. Single crystal silicon photovoltaic cells are expensive, and the most efficient types (up to 24%) are used only for defence and aerospace applications[25].

1.1.4.2 Types of photovoltaics

The most widely studied photovoltaics are fabricated from silicon and gallium arsenide. These are currently the most efficient solar-light energy converters and are widely used.

Among the silicon-based photovoltaics, there are single crystal, amorphous and polycrystalline silicon devices. Single crystal silicon based devices are the most

efficient of silicon photovoltaics with an overall efficiency of nearly 20%, but unfortunately these are very expensive. Polycrystalline silicon is cheaper to produce, but devices made from this material have defects in the whole structure as a result of the grain boundaries, where the charges get trapped. Thus, these devices are less efficient (16%) than single crystal devices. Amorphous silicon cells are the cheapest to produce and the least efficient (11%) as amorphous silicon has very poor charge mobility. Amorphous silicon cells are mainly used for devices that require little power such as pocket calculators, watches and light detectors for televisions and cameras[27,28].

A completely different type of photovoltaic cell was reported by O'Regan and Graetzel[29], who fabricated a photoelectrochemical cell from a nanocrystalline titania electrode, sensitised by a ruthenium bipyridyl complex, bis(2,2′-bipyridine-4,4′-dicarboxylic acid)diisothiocyanato-ruthenium (see Fig. 1.1.4.2b). Light is absorbed by the transition metal complex and an electron is transferred to a nanocrystalline TiO_2 layer that ferries the electrons away to the electrode by a mechanism similar to that occurring during the photosynthesis of plants as shown in Fig. 1.1.4.2c. This type of cell can give high efficiencies of up to 10% in diffuse sunlight[30].

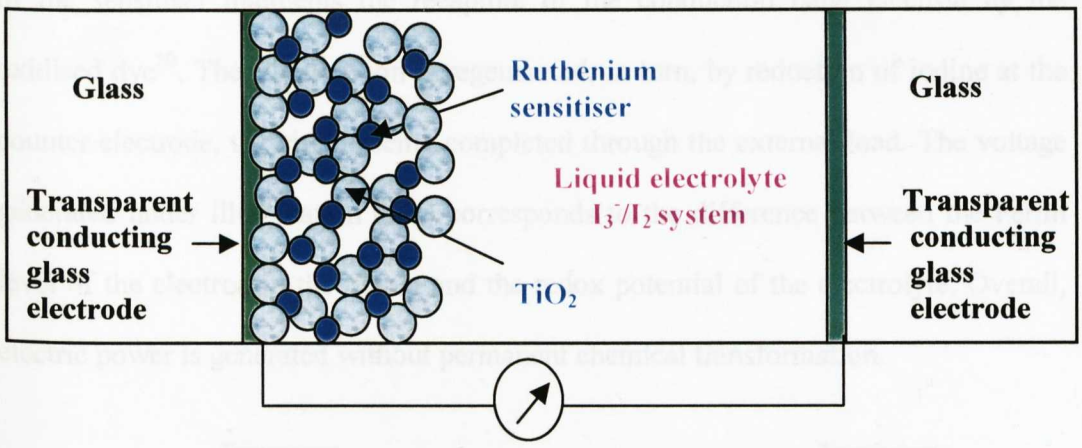

Fig. 1.1.4.2a: Schematic diagram of Graetzel cell

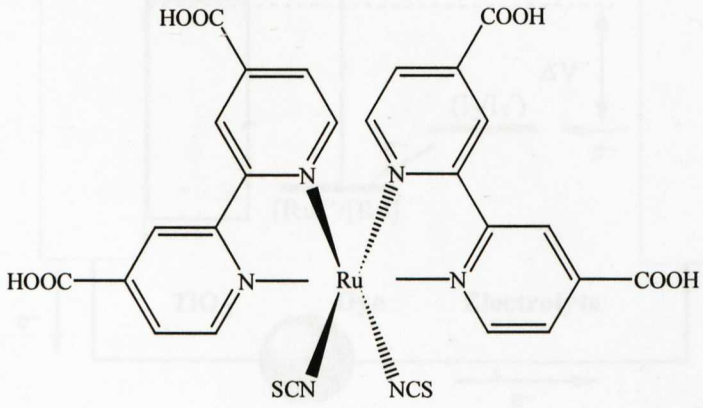

Fig. 1.1.4.2b: The chemical structure of the ruthenium bipyridyl complex.

The first Graetzel cell used a liquid electrolyte[31], usually an organic solvent containing the iodine/triiodide redox system, and gave an overall power conversion efficiency of 7.1%[27]. In these devices, photoexcitation of the dye results in the injection of an electron into the conduction band of the titania. The original state of the dye is subsequently restored by reduction by the triiodide ion. This regeneration

of the sensitiser intercepts the recapture of the conduction band electron by the oxidised dye[30]. The triiodide ion is regenerated, in turn, by reduction of iodine at the counter electrode, the circuit being completed through the external load. The voltage generated under illumination (ΔV) corresponds to the difference between the Fermi level of the electron in the titania and the redox potential of the electrolyte. Overall, electric power is generated without permanent chemical transformation.

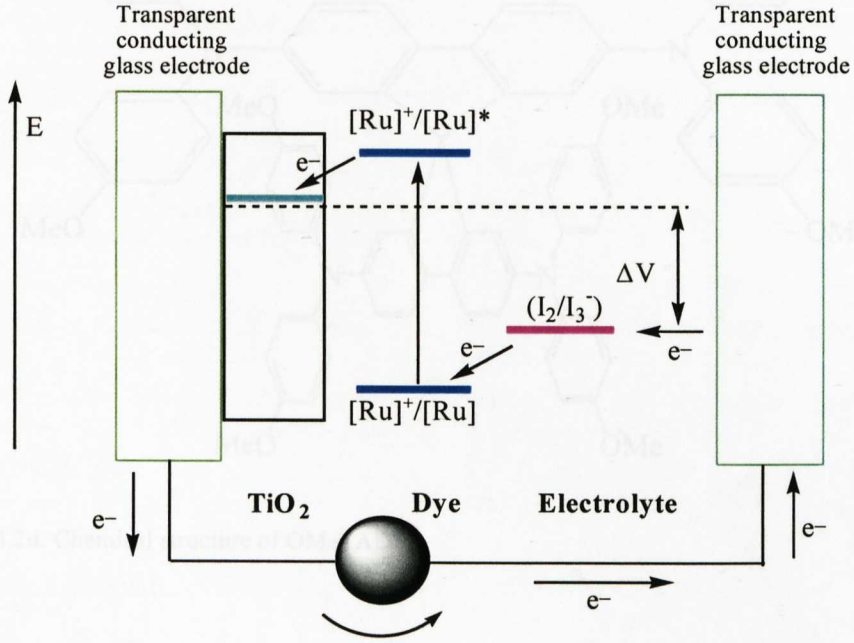

Fig. 1.1.4.2c: Energy level diagram of Graetzel cell

In 1998, a solid-state version of this type of cell, was published in which the liquid electrolyte was replaced with an amorphous organic hole transport material, OMeTAD (see Fig. 1.1.4.2d), as a solid hole transport material[32]. This solid-state cell based on an OMeTAD electrolyte was less efficient than the liquid electrolyte based

analogous by a factor of 2. More recently, the liquid electrolyte was replaced by a wide band gap inorganic p-type semiconductor, such as CuI[33] or CuSCN[34], where the excited dye injects electrons in the n-type oxide layer, and it is regenerated by hole injection in the p-type material[30].

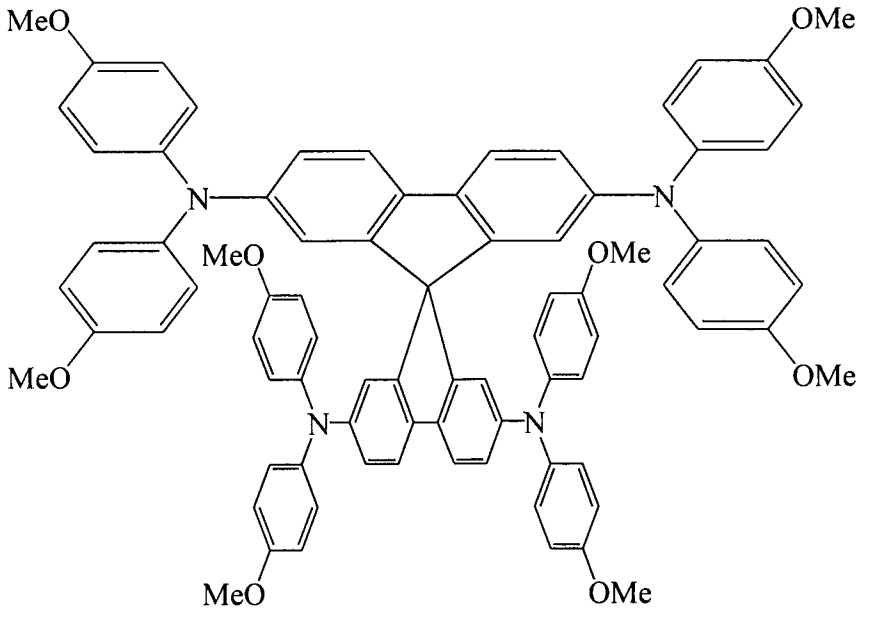

Fig. 1.1.4.2d: Chemical structure of OMeTAD

1.1.4.3 Applications of photovoltaics

Photovoltaic generated power offers advantages over diesel generators, primary batteries and even over conventional utility power. Photovoltaics are highly reliable, which makes them ideal for use in space, where repair is extremely expensive. They power the majority of the satellites in orbit as they operate reliably for long periods of

time. Photovoltaic arrays can also be constructed to any size based on the energy requirement[24].

Photovoltaics have low operating costs and require very little upkeep as they use the energy of sunlight to produce electricity, so there are no fuel costs. This makes them ideal for supplying power to communications stations on mountain tops, for navigational buoys and for remote sites, where fuel transport is problematic.

Photovoltaics are environmentally friendly as they burn no fuel and they contain no moving parts so they are clean and capable of contributing to solving the problems caused by the release of greenhouse gases. These benefits make photovoltaics the power of choice for more and more cases everyday.

The need for large area cells based on inexpensive materials, which can be easily processed with low-cost techniques urges the use of conjugated polymers in optoelectronic devices.

1.2 Conjugated polymers in optoelectronics

1.2.1 Methods for the synthesis of conjugated polymers

Poly(1,4-phenylenevinylene) is a bright yellow, highly fluorescent polymer with emission maxima at 551 nm and 520 nm for an energy gap of 2.25 eV and 2.4 eV respectively[10]. The polymer is insoluble, intractable, and infusible; hence any synthesis of PPV directly from a monomer produces an insoluble material, which cannot be easily processed. Solution processing of conjugated polymers by spin

coating is particularly desirable as high quality transparent thin films can be prepared for the production of polymer electroluminescent devices. The intractability of PPV is conveniently overcome by the use of a solution-processible precursor polymer. The sulfonium precursor route to PPV was introduced by Wessling and Zimmermann[35], and was subsequently modified and optimised by other groups[36,37].

The standard preparation of PPV was accomplished by the treatment of 1,4-bis(dichloromethyl)benzene (**1.1**) with tetrahydrothiophene to produce the bis-sulfonium salt (**1.2**), which is then polymerised by the addition of an equimolar amount of aqueous sodium hydroxide. The resulting precursor polymer (**1.3**) is then converted into PPV (**1.4**) by heating thin films (spin-coated with thickness of typically 100 nm) in the temperature range of 180-300°C for 12 hours under vacuum[38] (see Scheme 1.2.1a). Under these conditions, the by-products of the elimination (tetrahydrothiophene and hydrogen chloride) escape easily. It has been reported that traces of oxygen during the conversion step can cause the formation of undesired carbonyl groups that are believed to quench the luminescence of the resulting polymer[39,40]. The formation of such groups was suppressed by performing the conversion in a reducing atmosphere of hydrogen and nitrogen[39,41]. The conversion temperature could be reduced to 100°C by using the bromide instead of the chloride salt[37,42]. This enables processing of the precursor polymer on flexible foil substrates.

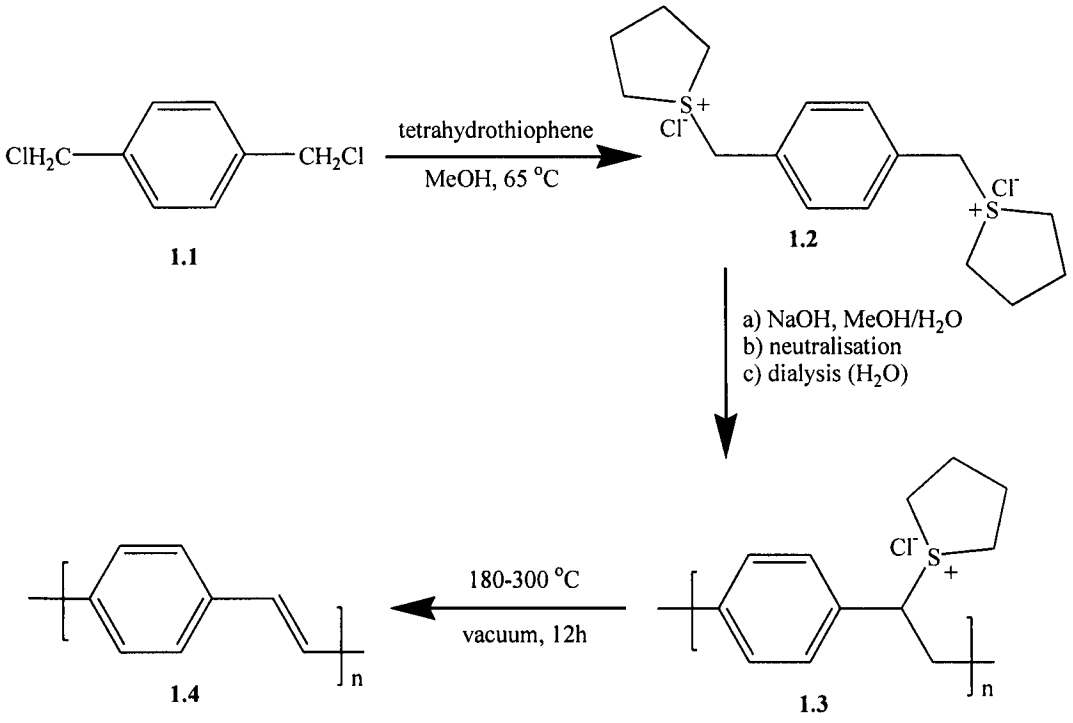

Scheme 1.2.1a: Synthesis of PPV through the sulfonium precursor route

Solution-processible substituted PPVs such as poly[(2,5-dialkoxy-1,4-phenylene)vinylenes] with at least one long, solubilising alkoxy side chain, can be also prepared by a sulfonium precursor route[38,43]. Such soluble polymers no longer require thermal treatment during processing, which is the drawback of the PPV precursor route, although they tend to have lower glass transition temperature. Although the Wessling route may be used to make soluble PPV derivatives, a dehydrohalogenation-condensation polymerisation, first developed by Gilch *et al*[44], is generally preferred, as seen in Scheme 1.2.1b. This reaction proceeds through dehydrobromination of 1,4-bis(bromomethyl)benzene (**1.5**) derivatives with a tenfold excess of potassium tert- butoxide in THF[45,46].

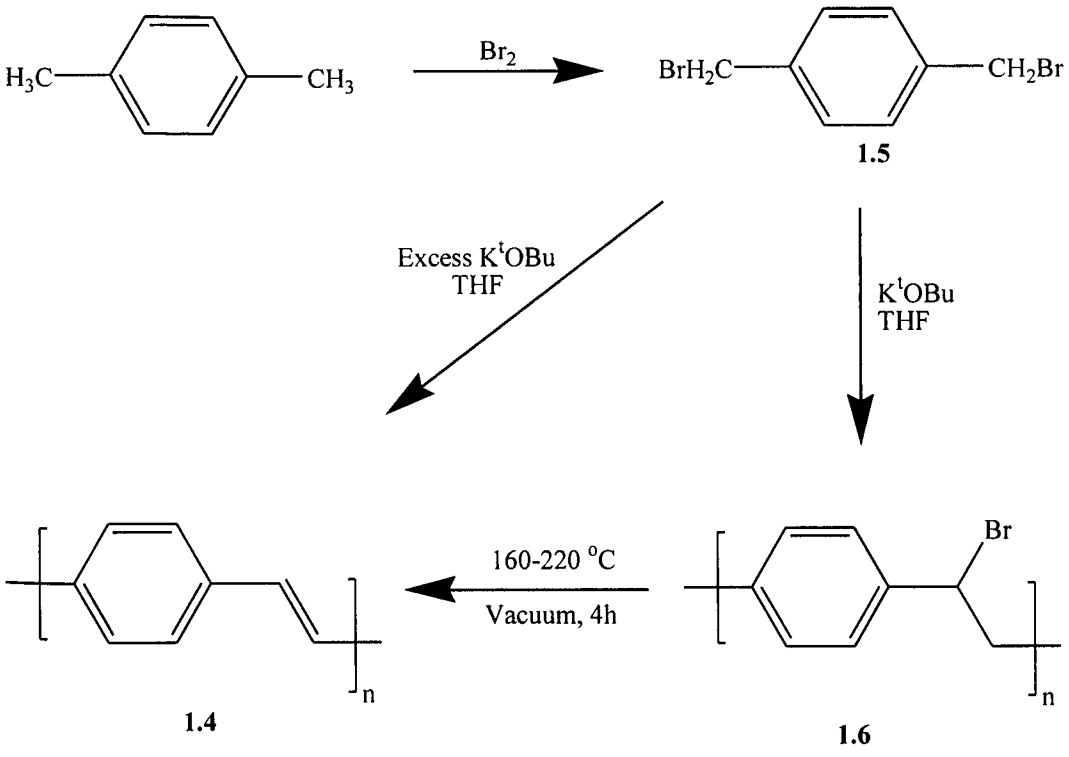

Scheme 1.2.1b: The halo-precursor route to substituted PPVs

Careful control of concentration is needed to avoid gelation. If less than one equivalent of base is used, soluble α-halo precursor polymers (**1.6**) can be obtained that can be converted into the desired polymer (**1.4**) by subsequent treatment with base or heating to high temperature[47].

Scheme 1.2.1c shows the synthesis of the most studied dialkoxy PPV, poly[2-methoxy-5-(2′-ethylhexyloxy)-1,4-phenylene-vinylene] (MEH-PPV) (**1.7**)[45,48]. The branched side chain in MEH-PPV has a favourable effect on the solubility of the polymer as branched side chains generally enhance solubility more than linear chains of identical length and composition by keeping the polymer backbones apart from

each other[10]. Indeed, MEH-PPV dissolves easily in solvents such as THF, chloroform and xylene.

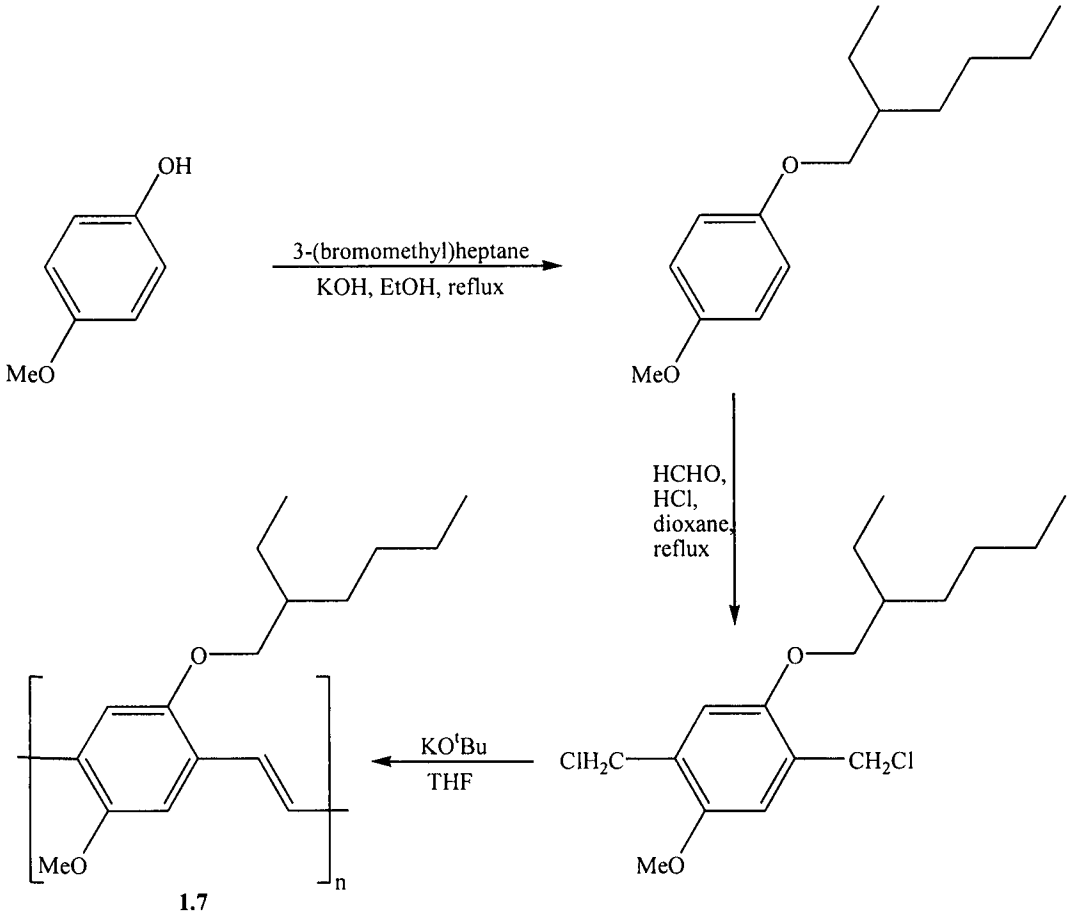

1.7

Scheme 1.2.1c: Preparation of poly[2-methoxy-5-(2'-ethylhexyloxy)-1,4-phenylene-vinylene] (MEH-PPV) (**1.7**)

Recently, palladium catalysed carbon-carbon coupling reactions have been extensively investigated to synthesise conjugated or other functional polymers. For example the Heck reaction[49] was successfully utilised to synthesise PPV and its derivatives, the Suzuki reaction was explored to synthesise poly(1,4-phenylene)

(PPP)[50] and polyfluorenes[51], and the Stille coupling reaction was applied to synthesise poly(phenylene-thiophene) (PPT)[52]. Attaining high molecular weight PPV derivatives by these methodologies has proved to be problematic. A phenyl-substituted PPV material (**1.9**) was synthesised by a Suzuki coupling[53] of 1,2-dibromoethene and bis-boronic acid (**1.8**) as shown in Scheme 1.2.1d.

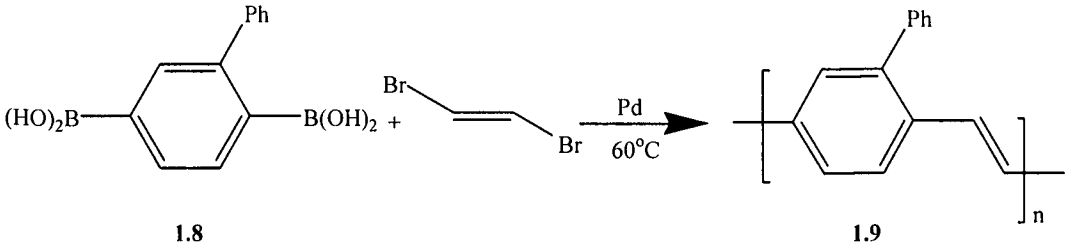

1.8 **1.9**

Scheme 1.2.1d: Synthesis of PPV by Suzuki coupling

The Heck reaction (Scheme 1.2.1e) involves the transition metal catalysed coupling of aryl halides with vinyl-substituted compounds[54]. The mechanism of Heck reaction proceeds via two main steps. The first step is the oxidative addition of the aryl halide to a Pd(0) complex to form the intermediate Ar-Pd(L_2)-X. This compound subsequently undergoes reaction with the vinyl compounds to give an alkyl halide palladium complex. Elimination of the Ar-vinyl product regenerates the Pd catalyst on reaction with a base.

The Stille reaction[51] involves the coupling of an aryl halide, triflate, or carbonyl chloride with an organotin compound, catalysed by a Pd catalyst. Polymerisation can be considered as a polycondensation reaction and proceeds by a similar mechanism to that of the Heck coupling reaction. The first step being an oxidative addition of the

aryl halide to the Pd catalyst, whereas the second step is a transmetalation reaction that produces Ar-R and Bu_3SnX, where R is usually a heterocycle or a vinyl unit.

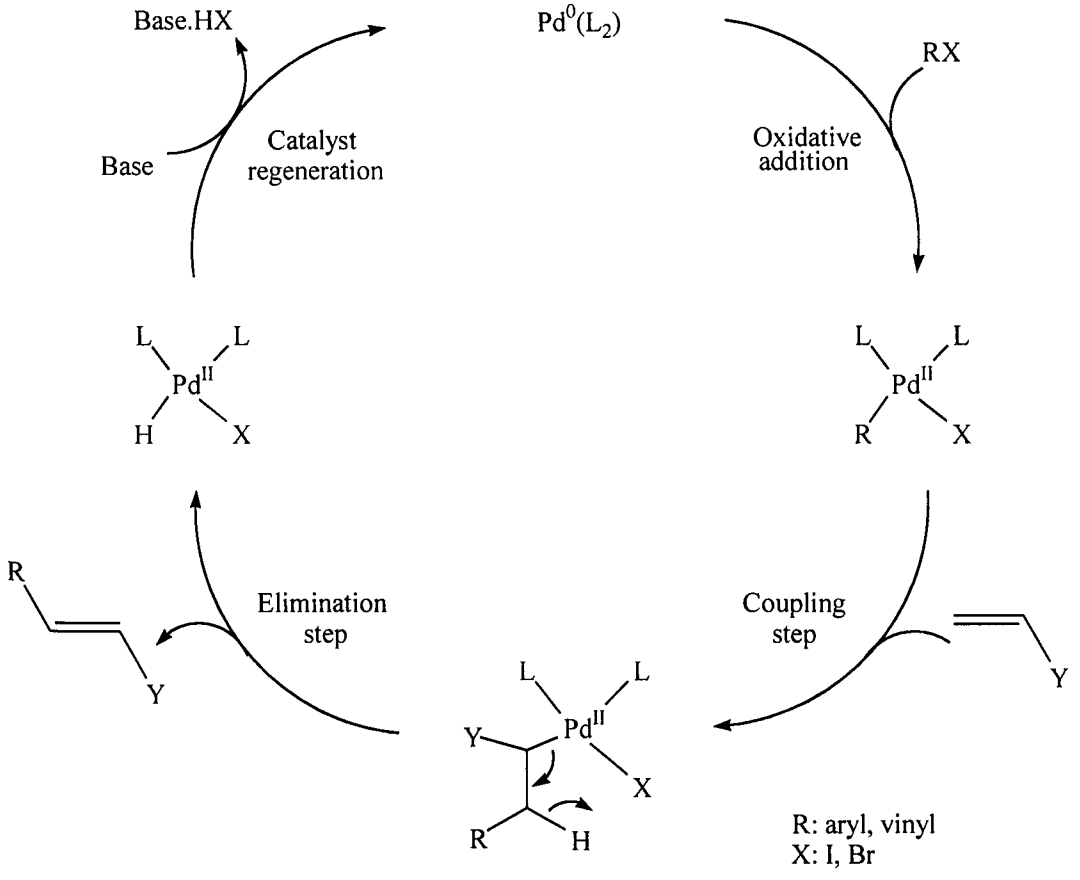

Scheme 1.2.1e: The Heck reaction mechanism[49]

The application of synthetic conjugated polymers requires the study of the physics of their optical and electrical properties.

1.2.2 Physics of conjugated polymers

The most common feature of phenylene-vinylene conjugated polymers is that they have a delocalised π – system, where the p_z orbitals on neighbouring carbon atoms overlap to form π molecular orbitals that are delocalised over the polymer chain. The lower-energy π orbitals form a pseudo-valence band, while the higher-energy π* orbitals form a pseudo-conduction band. The band gap between the HOMO and LUMO gives the polymer semiconducting behaviour[55].

A polymer must also satisfy two other conditions to function as a semiconductor. One is that the σ bonds should be strong enough to hold the molecule intact in the excited states, as excitation weakens the π bonds. The other requirement is that π orbitals on neighbouring polymer molecules should overlap with each other so that electrons and holes can move in three dimensions. Many conjugated polymers satisfy these three requirements[55].

Most conjugated polymers have semiconductor band gaps between 1.5-3 eV, which means that they can absorb or emit visible light between 400 nm and 700 nm. Phenylene-vinylene based conducting polymers such as MEH-PPV exhibit multiple absorption features extending well into the ultraviolet region of the spectrum. The maximum absorption band occurs at 2.2 eV which is due to the main delocalised π-π* transition. The corresponding photoluminescence occurs at 2.15 eV[56].

The colour of the emission from an electroluminescent polymer depends on the structural features of the macromolecule[10]. The energy gap in PPV has been

chemically modified, for example, by the partial elimination of precursor leaving groups, thereby providing an increase in the HOMO-LUMO gap by interrupting the conjugation along the chain[10]. Confinement of the effective conjugation has proved to be an efficient means for blue-shifting the emission spectrum. Confinement of the conjugation can also be achieved by other methods of tailoring the polymer structure such as; separating the emitting units by nonconjugated spacers as in conjugated-nonconjugated copolymers[57,58] (Scheme 1.2.2).

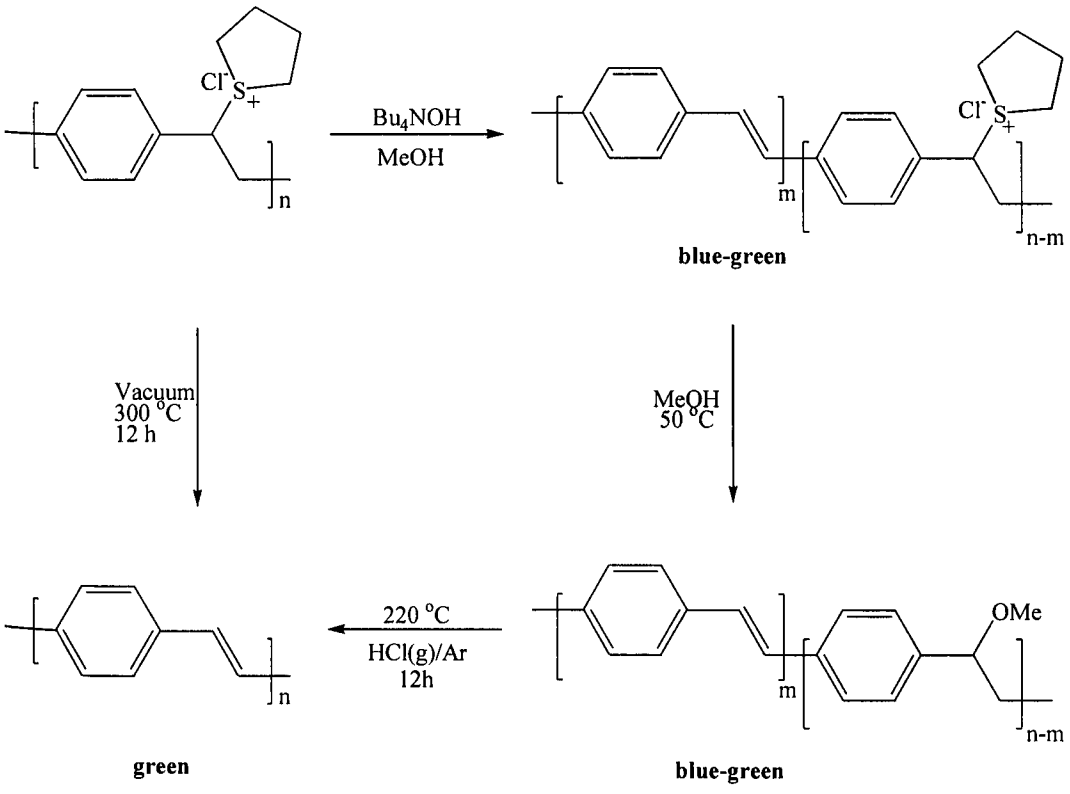

Scheme 1.2.2: Synthesis of partially conjugated PPV copolymer[10]

1.2.3 Light emitting diodes based on conjugated polymers

Electroluminescence from conjugated polymers was first reported in 1990[8], using poly(phenylenevinylene) as the semiconductor layer, sandwiched between two metallic electrodes. The device structure, as shown in Fig. 1.2.3a, consists of an ITO electrode, which is transparent and allows the light generated within the diode to leave the device. The top electrode is conveniently formed by the thermal evaporation of a metal. LED operation is achieved when the diode is biased sufficiently to achieve injection of positive and negative charge carriers from opposite electrodes. Capture of oppositely charged carriers within the region of the polymer layer can then result in photon emission[9].

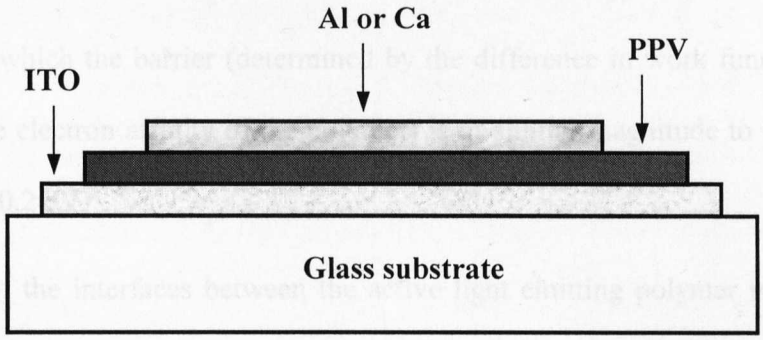

Fig. 1.2.3a: Schematic presentation of an LED device

The internal quantum efficiency of the device (η_{int}) is defined as the ratio of the number of photons produced within the device to the number of electrons flowing in the external circuit:

$$\eta_{int} = \gamma\, r_{st}\, q$$

Where γ is that ratio of the number of exciton formation events within the device to the number of electrons flowing in the external circuit, r_{st} is the fraction of excitons, which are formed as singlets and q is the efficiency of radiative decay of these singlet excitons[9].

Injection of charges from most electrode materials requires that charges tunnel through a barrier at the interface. This is expected on examination of the positions of the electrode metal work functions and the positions of the highest occupied molecular orbitals (HOMO) and the lowest unoccupied molecular orbitals (LUMO) in the polymer. For the case of PPV, ITO provides a relatively good match for hole injection, although there is a barrier of around 0.2 eV[59]. However, electron injection is difficult to achieve without the use of a low work function, reactive metal such as calcium, for which the barrier (determined by the difference in work function of the metal and the electron affinity of the polymer) is of similar magnitude to that of hole injection (ca 0.2 eV)[9].

The nature of the interfaces between the active light emitting polymer medium and the metal electrodes is of tremendous importance in determining device performance[60]. The chemistry that occurs at the metal-on-polymer interface varies with the identity of the metal, the polymer involved, and especially with the cleanliness of both the materials employed and the vacuum system used in the metallisation process[9]. ITO has been the usual choice of material for the anode, by virtue of its favourable transparency in the visible region of the spectrum. However, it

is not a well-controlled material as its work function depends greatly on how the material was prepared or treated[55].

In spite of the strong evidence for chemical interactions between the polymer and metal, there is clear evidence that the size of the barriers for electron and hole injection scales with the electrode work functions. This has been shown by measurements of the internal electric field in metal/polymer/metal devices structures[61].

The process of charge injection from the metal electrodes and charge transport within the polymer layer are difficult to disentangle from the device electrical characteristics, and the present literature can be confusing. For LEDs with large barriers for injection, the injection of charges, either by thermionic emission or by tunnelling, can limit the current flow[62,63]. However, for LEDs, which show good operating characteristics such as the low turn-on voltage, charge injection is not considered to limit current flow. Instead, current flow is bulk limited, principally through the build up of space charge. The space charge limited current regime is easily achieved in devices of these materials as the mobilities of charge carriers in relatively disordered molecular semiconductors are very low[64].

For recombination to occur in the bulk of the polymer layer, injection and transport of holes from the positive electrode into the bulk of the polymer must be matched by the injection and transport of electrons from the opposite electrode. Recent studies have shown that two-layer devices can effectively control injection rates of electrons and holes by either reducing barriers at the electrodes or introducing barriers for charge

transport at the heterojunction between the two semiconductor layers to obtain current balance[65,66,67]. Devices of this type have been most successfully fabricated using solution processible CN-PPV (**1.10**) (Fig. 1.2.3b), a derivative of PPV with nitrile groups attached to the vinylic carbons, complemented with hole-transporting PPVs. Under forward bias, injection of holes into the HOMO of the PPV layer results in transport of holes to the heterojunction, where they are confined by the potential barrier (created by the difference in energy between HOMO of PPV and CN-PPV). Similarly, electrons injected from the negative electrode into CN-PPV layer are confined at the heterojunction by the potential step required to progress into the LUMO of PPV. Tunnelling across the barrier allows electron-hole capture and electroluminescence.

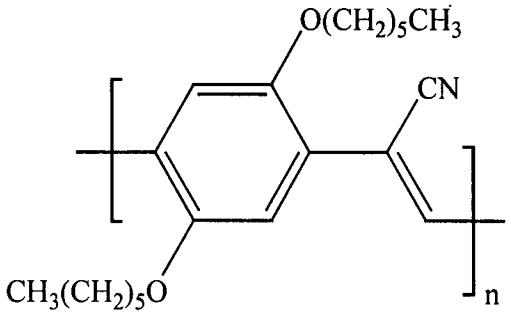

1.10

Fig. 1.2.3b: Chemical structure of CN-PPV

The process of electron-hole capture in these devices is crucial to device operation. In order to get efficient capture within the very thin polymer layers of ~100 nm, it is necessary that one or other charge carrier is of very low mobility so that the local

charge density is sufficiently high to ensure that the other charge carrier will pass within a collision capture radius of at least one charge. This can be enhanced in the heterostructure device discussed above, where confinement of charges at the heterojunction causes a build-up in charge density. Modelling of charge recombination in these devices has been studied by several groups[68,69,70].

Probably the most critical performance characteristics for polymer LEDs are their storage and operating lifetimes. Operating lifetimes in excess of 3,000 hours, and, generally, in excess of 10,000 hours, are required for most applications, and storage times of 5 years or more are required[9]. It is clear that all PPV materials, both polymeric and molecular are susceptible to photooxidation[71] in the presence of water and oxygen with the former found to play a very important role[72]. Devices must therefore be encapsulated against ingress of water and oxygen, and although this has been achieved for devices made on glass, there are unsolved problems in achieving adequate performance from flexible substrates[73] that are important to allow devices to be fabricated by reel-to-reel coating.

The performance of organic LEDs meets many of the targets necessary for applications in displays. Backlighting and segmented displays have been identified for early products by Philips[9]. Active matrix-addressed displays are attractive, as the device structure is relatively simple. Extension to a full colour graphic displays (computer monitor and video displays) is possible, not least because organic LEDs provide full viewing angle and video rate response times in contrast to current liquid crystal displays. Developments of full colour displays fabricated from organic

sublimed films have been reported and products are now available[74,75,76]. Solution processing of polymers offers new methods of colour patterning, among which there is particular interest in ink-jet printing[77,78], to place separated pixels of red, green and blue emitting polymers onto the prepared substrate[76]. Active-matrix transistor arrays, modified from those at present used for liquid crystal displays, can now provide sufficient current-driving capability to meet the requirements of organic LEDs. This is made possible by the improved properties of polycrystalline silicon compared to those of amorphous silicon, and demonstrator active matrix polymer displays using these materials have been made[76].

1.2.4 The Photovoltaic effect in conjugated polymers

There has been intense interest in the photovoltaic properties of molecular semiconductors over many years[79], but devices made with semiconductors of this type tend not to show useful efficiencies. There are several reasons for this, which include the difficulties associated with achieving efficient ionisation of the exciton initially created by photon absorption[80]. Ionisation of excitons that have binding energies significantly above kT can be achieved in the bulk, but this is often facilitated by the presence of a surface or interface. At a heterojunction between molecular semiconductors with different electronegativities, ionisation to place an electron in one layer and a hole in the other can be arranged to be energetically favoured[81]. This effect can be used to enhance the efficiency of photovoltaic devices fabricated from sublimed molecular films[80].

Generation of charged excited states can be observed by the measurement of photoconductivity[82]. For measurements of current flow within the plane of the polymer film, the steady-state photocurrent shows a sub-linear dependence on the light intensity, indicating that there is a recombination of positive and negative charges, which limits the quantum yield. The quantum yield is defined as the ratio of the measured short-circuit current to the estimated photon flux incident on the polymer film. The thickness of the polymer film strongly affects the photoresponse of the device. Reducing the polymer layer thickness increases the internal electric field in the polymer under short-circuit conditions, and this will increase the photoconductive gain[80].

Conjugated polymer based photovoltaic cells utilise semiconducting materials to absorb light of energies above the HOMO-LUMO gap to generate an exciton, these excitons are bound and at first sight, it would appear that conjugated polymers would not be suitable for use in photovoltaics. Exciton dissociation is known to be efficient at the interface between materials of different ionisation energy and electron affinity. This type of donor-acceptor combination, in which one polymer donates an electron and the other absorbs it, can be viewed as a semiconductor heterojunction[83].

Tremendous research effort was devoted to the development of photovoltaic cells during the late seventies and early eighties[19-23]. During this time significant interest was shown in organic semiconductors as they offer the advantage of low-cost and facile processing. Organic materials for use in photovoltaic devices require good chemical stability and a large optical absorption coefficient in the visible range. For

this purpose the first studied compounds were merocyanine[84] and phthalocyanine[85], which can readily be deposited as thin films on various substrates by vacuum evaporation. Power conversion efficiencies for such devices are about 1% for a small photovoltaic element.

It is intriguing to think of large photovoltaic elements based on a thin plastic film. In order to fulfil these low-cost and large area requirements, cheap production technologies for large-scale coating must be used together with a low cost material. Photovoltaic cells fabricated from polymers hold the potential for such low cost cells. The ability to chemically tailor the polymer properties, coupled with the cheap technology already well established for polymer thin film applications, meets the requirements for low cost photovoltaic device production.

Conjugated polymers were incorporated into photocells at an early stage, but the results were not very promising, with low open-circuit voltages and low overall efficiencies. Initial efforts concentrated on polyacetylene[86,87] and some of the polythiophenes[88,89]. The breakthrough to higher efficiencies was achieved by switching to different classes of conjugated polymers, such as polyphenylenevinylenes (PPV) and their derivatives and by mixing them with suitable electron acceptors[90].

The long term photostability of conjugated polymers is also important for the application of these materials. Protection from air and humidity is absolutely necessary to achieve a shelf lifetime of several years and operational lifetime of tens of thousands of hours[71,72].

Fullerene (C_{60}) has been widely used as an electron acceptor in conjunction with conjugated polymers in double-layer photovoltaic cell structures[91]. In a similar manner, some organic pigments such as perylene have been used as electron acceptors[92].

Recent research work has shown that interpenetrating donor-acceptor heterojunctions, such as polymer/C_{60} composites[93], polymers/CdSe nanoparticle composites[94] and interpenetrating conjugated polymer networks can substantially improve the photoconductivity, and therefore quantum efficiency of polymer-based photovoltaics. In these devices, an exciton is photogenerated in the active material, diffuses towards the donor-acceptor interface, and dissociates via charge transfer across the interface. An internal electric field is set by the difference between the contact electrode energy levels, whereas the donor-acceptor morphology controls the quantum efficiency of the cell.

Several approaches towards solid-state organic semiconductor photovoltaic cells have been recently published. A research group at the university of Osaka[95], has reported a solid state dye-sensitised solar cell fabricated by using polypyrrole as a hole transport layer to replace the liquid electrolyte in a Graetzel cell. The conductivity of polypyrrole was improved by immersion of the polymer into 0.2 M $LiClO_4$ acetonitrile solution. The overall energy conversion efficiency of that cell was ca 0.1%.

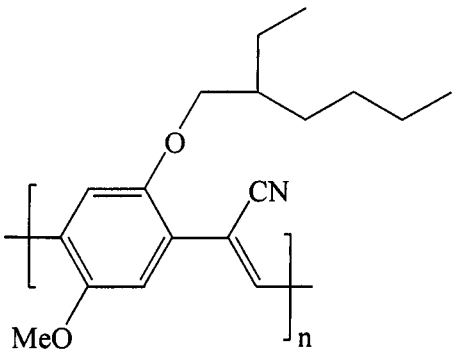

1.11

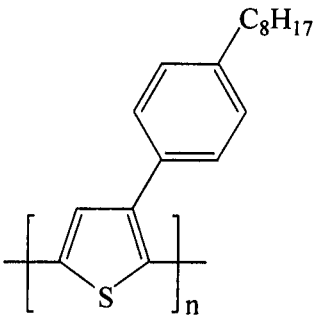

1.12

A laminated structure of polymeric photovoltaic diodes has been introduced by the Cavendish Laboratory in Cambridge[96]. Two-layer polymer diodes were fabricated by a lamination technique followed by controlled annealing. The two layers are blends of donor and acceptor semiconducting polymers, which helps to optimise the charge separation at the donor-acceptor heterojunction. The electron acceptor layer is composed of 95% MEH-CN-PPV (**1.11**) and 5% POPT (**1.12**), whereas the electron donor layer is composed of 5% MEH-CN-PPV (**1.11**) and 95% POPT (**1.12**). This structure produced an overall power conversion efficiency of 1.9% with simulated solar light (AM1.5).

The use of TiO_2 as the electron-acceptor layer for conjugated polymer sensitised photovoltaic cells was recently published (Fig. 1.2.4), where the TiO_2 layer was produced by either CVD technique[97] or the sol-gel route[98]. In these devices the internal electric field is set by the difference between the energy levels of the polymer and TiO_2 and the morphology of the interface controls the quantum efficiency of the cell.

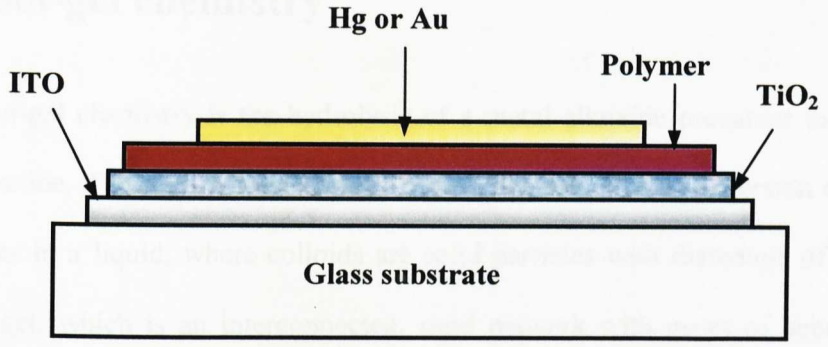

Fig. 1.2.4: Schematic diagram of a PPV/TiO_2 based photovoltaic device.

Goossens[99] has recently reported the fabrication of photovoltaic devices using TiO_2 as the electron acceptor layer sensitised by a PPV derivative. In these devices, thin films (80 nm) of anatase TiO_2 were deposited on an ITO electrode using chemical vapour deposition (CVD). Onto these substrates, films of MEH-PPV were applied by spin coating from a $CHCl_3$ solution. A counter contact was provided by a mercury droplet. The open circuit voltage measured was 0.92 V with a fill factor of 0.52 and the overall energy conversion efficiency of that cell was ca 0.14% under simulated solar light AM1.5. The sol-gel technique has been reported to prepare TiO_2 substrates for use in photovoltaic devices of similar structure as described above but using gold as the counter electrode[100]. In these devices, the open circuit voltage recorded was 0.7 V with a fill factor of 0.43 and the quantum efficiency reported was below 4% under illumination by a halogen lamp source with intensity of 2 mW/cm^2.

Due to the application of the sol-gel process in preparing TiO_2 substrates, the chemistry of the sol-gel process will be discussed in more details in the next section

1.3 Sol-gel chemistry

The Sol-gel chemistry is the hydrolysis of a metal alkoxide precursor to generate a metal oxide. The term sol-gel derives from a sol, which is a dispersion of colloidal particles in a liquid, where colloids are solid particles with diameters of 1-100 nm, and a gel, which is an interconnected, rigid network with pores of submicrometer dimensions and polymeric chains whose average length is greater than a micrometer[101]. The term "gel" embraces a diversity of combinations of substances that can be classified in four categories as discussed by Flory[102]: (1) well-ordered lamellar structures; (2) covalent polymeric networks, completely disordered; (3) polymer networks formed through physical aggregation, predominantly disordered; (4) particular disordered structures.

Three general approaches have been reported to prepare sol-gel monoliths and thin films: (1) gelation of a solution of colloidal powders; (2) hydrolysis and polycondensation of alkoxides or nitrate precursors followed by hypercritical drying of gels; (3) hydrolysis and polycondensation of alkoxide precursors, followed by ageing and drying under ambient atmospheres[103].

In the sol-gel process, the precursors (starting compounds) for preparation of a colloid sol consist of a metal or metalloid element bound by various ligands[104]. For instance, common precursors for aluminium oxide include inorganic salts such as $Al(NO_3)_3$ and organic compounds, metal alkoxides, such as $Al(OC_4H_9)_3$. Alkoxides are the most widely used precursors used in sol-gel research[104].

Metal alkoxides are popular precursors because they react readily with water. The most thoroughly studied example is the hydrolysis of silicon tetraethyl orthosilicate, $Si(OC_2H_5)_4$ (TEOS) to silicon dioxide.

$$Si(OEt)_4 + 2\ H_2O \rightleftharpoons SiO_2 + 4\ EtOH$$

Depending on the amount of water and the nature of the catalyst present, hydrolysis may go to completion so that all OR groups are replaced by OH groups, or stop while the TEOS is only partially hydrolysed[104].

Hydrolysed molecules can link together in a condensation reaction with elimination of either water or an alcohol:

$$Si\text{-}OH + Si\text{-}OH \rightleftharpoons Si\text{-}O\text{-}Si + H_2O \qquad \text{(oxolation)}$$

$$Si\text{-}OR + Si\text{-}OH \rightleftharpoons Si\text{-}OH + ROH \qquad \text{(alkoxolation)}$$

This type of reaction can continue to build larger networks depending on the degree of polymerisation. If the metal alkoxide has three or more labile groups then linear chains can be joined by crosslinks to form a three-dimensional structure and eventually a metal oxide.

1.3.1 Chemistry of metal alkoxide precursors

Transition metal alkoxides, $M(OR)_n$, especially those of the d^0 transition metals (Ti, Zr), are widely used as molecular precursors to glasses and ceramics[105]. Transition metal alkoxides are in general very reactive due to the presence of highly

electronegative ligands that stabilise the metal in its highest oxidation state and render it very susceptible to nucleophilic attack.

Several factors distinguish transition metal alkoxides from silicon alkoxides. These include the lower electronegativity of transition metals, this causes them to be more electrophilic and thus less stable towards hydrolysis, condensation, and reactions with nucleophiles[104]. The greater reactivity of transition metals often requires that they are processed with stricter control of moisture and conditions of hydrolysis in order to prepare homogeneous sols rather than precipitates. Transition metals often exhibit several stable coordination numbers, and when coordinatively unsaturated can expand their coordination sphere via alkoxides bridges or other nucleophilic association mechanisms[104].

1.3.1.1 Mechanisms of hydrolysis and condensation of metal alkoxides

Yoldas reported that the hydrolysis and condensation reactions in sol-gel chemistry are not separated in time but take place simultaneously[106]. For coordinatively saturated metals in the absence of a catalyst, hydrolysis and condensation occur by mechanisms involving nucleophilic addition (A_N) followed by proton transfer from the attacking molecule to an alkoxide or hydroxide ligand within the transition state, followed by removal of the protonated species as either alcohol (alcoxolation) or water (oxolation).

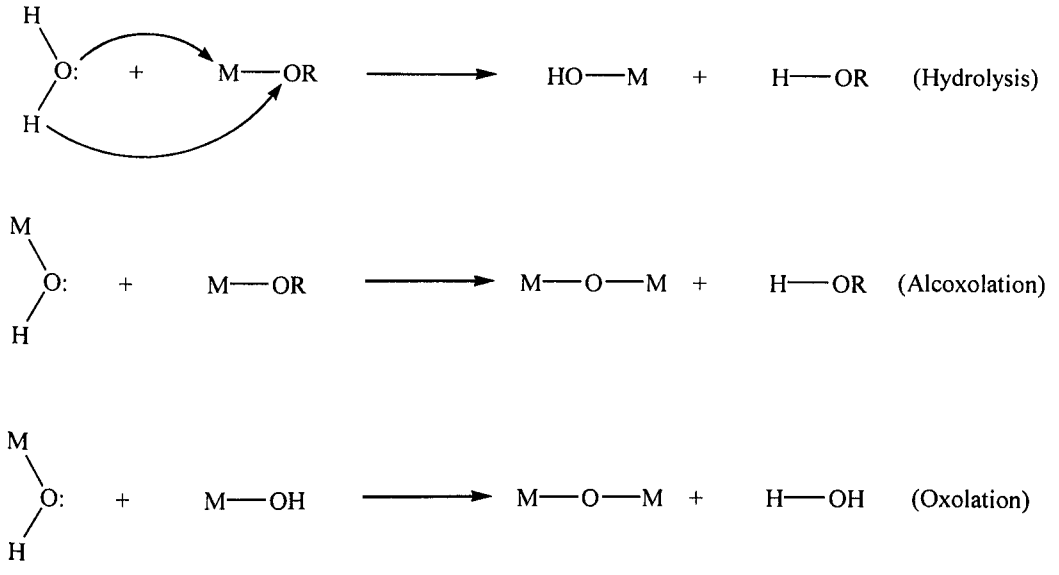

Scheme 1.3.1.1: Mechanisms of hydrolysis and condensation

As discussed by Orcel *et al*[107,108,109], Hench[110], Klemperer *et al*[111], Scherer and Brinker[104], and Artaki *et al*[112], many factors influence the kinetics of the hydrolysis and condensation reactions. The variables of major importance are temperature, nature and concentration of the catalyst, nature of the solvent and type of the alkoxide precursor.

The nature of the alkoxy groups in the alkoxide precursor influences the hydrolysis rate constant. As a general rule, the longer and the bulkier the alkoxide group, the slower the rate constant[113]. For example, in the case of the hydrolysis of $Si(OR)_4$, the rate of hydrolysis, when R is C_2H_5, is 17 times faster than that when R is $(CH_3)_2CH(CH_2)_3CH(CH_3)CH_2$.

1.3.1.2 The role of the catalyst

Acid or base catalysts can influence both the hydrolysis and condensation rates and the structure of the condensed product. Acids serve to protonate alkoxide ligands, enhancing the reaction kinetics by producing good leaving groups, and eliminating the requirement for proton transfer within the transition state[104].

Alkaline conditions produce strong nucleophiles via deprotonation of hydroxide ligands that are produced during the hydrolysis, thus condensation kinetics are systematically enhanced under basic conditions. Base catalysed condensation reactions are rapid, leading to more compact, highly branched species.

Both catalysts increase the rate of hydrolysis and condensation over the uncatalysed process but the base catalysis increases the rate of condensation more than the acid system and the acid catalysis increases the rate of hydrolysis more than the base system as it has been well established that the presence of H_3O^+ in the solution increases the rate of the hydrolysis reaction, whereas OH^- ions increase the rate of the condensation reaction[114].

1.3.1.3 Structure of condensed products

Orcel *et al* studies showed that the structure of condensed products from $Si(OEt)_4$ depends on the relative values of the rate constants of hydrolysis and polycondensation[108]. Fast hydrolysis and slow condensation favour formation of linear polymers, on the other hand, slow hydrolysis and fast condensation result in larger, bulkier and more ramified polymers[115]. The contribution of each of these

reactions depends in turn on internal parameters such as the nature of the metal atom and alkoxy group, water/metal ratio in the alkoxide and the molecular complexity as well as external parameters such as the choice of catalyst, concentration, solvent and temperature.

Unfortunately, due to the fast kinetics of the hydrolysis and condensation reactions of transition metal alkoxides compared to the silicon system, relatively little information is available concerning progressive structure evaluation in transition metal oxide systems[104].

1.3.2 Techniques for preparing TiO_2 thin films for use in photovoltaics

In 1990, Graetzel reported the preparation of transparent titanium dioxide membranes (thickness 2.7 μm) by sintering of 8-nm colloidal anatase particles on a conducting glass support[116]. The procedure applied was similar to that used for the preparation of unsupported films[117]. The procedure involved hydrolysis of titanium isopropoxide in deionised distilled water under a stream of dry nitrogen. The mixture was vigorously stirred. Nitric acid was then added to the formed white precipitate. The mixture was then stirred for 8 hours at 80 °C without reflux to produce a stable sol. The size of the colloidal particles was ~ 8 nm and X-ray diffraction analysis showed them to consist of anatase. Crystallisation was shown to occur during the reflux, as the initial TiO_2 precipitate was X-ray amorphous. The stable TiO_2 colloidal sol was concentrated under vacuum to reach a visibly viscous state. The sol was then spun onto a

conducting glass substrate. The spun TiO_2 layers were then fired directly in a 400 °C heated oven. Membranes thinner than 500 nm did not crack when fired directly at 400 °C. Membranes up to 4 μm thick were formed by multiple application and firing of ~ 0.4 μm layers. After a final firing at 400 °C for one hour, the membranes were heated at 550 °C under dried argon.

In 1991, Graetzel introduced a slight modification to this preparation[27], where the hydrolysis of titanium isopropoxide in deionised distilled water was followed by autoclaving for 12 hours at 200 °C. To form films, the sol was concentrated by evaporation of water in vacuum at 25 °C until a viscous liquid was obtained. Carbowax M-20,000 (40% by weight of TiO_2) was added and the viscous dispersion (TiO_2 content 20% by weight) was spread on the conducting glass support (Asahi glass, fluorine doped SnO_2 overlayer, transmission 85% in the visible light region) to give a membrane of 10 μm thickness. This was heated under air for 30 minutes at 450 °C. High-resolution scanning electron microscope revealed TiO_2 films were found to be composed of a three-dimensional network of interconnected nanoscale particles[116].

In addition to sol-gel processing, high-cost and relatively high-energy deposition methodologies have also been used to prepare anatase titania thin films, such as chemical vapour deposition (CVD)[118] and sputtering[119].

Carter *et al*[98] at the University of California produced sintered nanocrystalline TiO_2 layers by coating an indium-tin-oxide (ITO) coated glass substrate with a viscous TiO_2 water solution that is spread onto the substrate and annealed for 30 min at 500 °C to fuse the nanoparticles. The opaque TiO_2 layers are typically 400-600 nm thick

films and strongly adhere to the substrate. An atomic force microscope (AFM) image of the surface of a micron thick TiO_2 film reveals an average particle size of 80 nm with estimated pore diameters above 20 nm. Thin films (± 80 nm) of anatase TiO_2 were produced by Goossens *et al*[99] by deposition on ITO (30 Ω / square, glastron) using chemical vapour deposition (CVD) yielding very smooth and transparent layers.

1.4 References

[1] H. Shirakawa, E. J. Louis, A. G. MacDiarmaid, C. K. Chiang, A. J. Heeger, *Chem. Comm.* **1977**, 578

[2] T. Ohnishi, T. Noguchi, T. Nakano, M. Hirooka, I. Murase, *Synth. Met.* **1991**, *41*, 309-312

[3] J. L. Bredas, D. Beljonne, Shuaiz, J. M. Toussaint, *Synth. Met.* **1991**, 43, 3743-3746

[4] M. Esteghamatian, G. Xu, *Synth. Met.* **1994**, *63*, 195-197

[5] M. Ahlskog, M. Reghu, T. Noguchi, T. Ohnishi, *Synth. Met.* **1997**, 89, 11-15

[6] M. M. Murray, A. B. Holmes, *Semiconducting Polymers*, Wiley-VCH, Weinheim, **2000**

[7] S. Roth, W. Graupner, *Synth. Met.* **1993**, *55*, 3623

[8] J. H. Burroughes, D. D. C. Bradley, A. R. Brown, R. N. Marks, K. MacKay, R. H. Friend, P. L. Burn, A. B. Holmes, *Nature*, **1990**, *347*, 539

[9] R. H. Friend, R. W. Gymer, A. B. Holmes, J. H. Burroughes, R. N. Marks, C. Taliani, D. D. C. Bradley, D. A. Dos Santos, J. L. Bredas, M. Loegdlund, W. R. Salaneck, *Nature*, **1999**, *397*, 121

[10] A. Kraft, A. C. Grimsdale, A. B. Holmes, *Angew. Chem. Int. Ed.* **1998**, *37*, 402-428

[11] T. Geelhaar, *Liquid Crystals*, **1998**, *24*, 91-98

[12] M. Pope, H. Kallmann, *J. Chem. Phys.* **1963**, *38*, 2042

[13] W. Helfrich, W. G. Schneider, *Phys. Rev. Lett.* **1965**, *14*, 229

[14] R. H. Bube, *Photoelectronic Properties of Semiconductors*, **1992**, Cambridge University Press

[15] M. Pope, C. E. Swenberg, *Electronic Processes in Organic Crystals*, **1982**, Clarendon Press, Oxford

[16] C. W. Tang, *Appl. Phys. Lett.* **1986**, *48*, 183

[17] D. M. Chapin, C. S. Fuller, G. L. Pearson, *J. Appl. Phys.* **1954**, *25*, 676

[18] D. C. Raynolds, G. Leies, L. L. Antes, R. E. Marburger, *Phys, Rev.* **1954**, *96*, 533

[19] H. J. Hovel, *Semiconductors and Semimetals*, Academic Press, New York, **1975**

[20] C. E. Backus, *Solar Cells*, IEEE Press, New York, **1976**

[21] D. L. Pulfrey, *Photovoltaic Power Generation*, Van Nostrand Reinhold, New York, **1978**

[22] W. D. Johnston, *Solar Voltaic Cells*, Dekker, New York, **1980**

[23] K. J. Bachmann, *Current Topics in Material Science*, North-Holland, Amsterdam, **1979**

[24] V. M. Andreev, V. D. Rumyantsev, *Solar Energy Materials and Solar Cells*, **1996**, *44*, 319-332

[25] G. Johnson, M. E. Hunt, W. R. Determan, P. A. Hosang, J. Ivanenok, M. Schuller, *IEEE Aerospace and Electronic Systems Magazine*, **1997**, *12*, 33-40

[26] J. J. M. Halls, C. A. Walsh, N. C. Greenham, E. A. Marsegilia, R. H. Friend, S. C. Moratti, A. B. Holmes, *Nature*, **1995**, *376*, 498

[27] K. C. Lin, W. J. Sah, S. C. Lee, *IEEE Transactions On Electron Devices*, **1994**, *41*, 666-670

[28] P. Rieve, M. Sommer, M. Wagner, K. Seibel, M. Bohm, *J. Non-Cryst. Solids*, **2000**, *266*,1168-1172

[29] B. O'Regan, M. Graetzel, *Nature*, **1991**, *353*, 737-739

[30] A. Hagfeldt, M. Graetzel, *Acc. Chem. Res.* **2000**, *33*, 269-277

[31] M. K. Nazeeruddin, M. Graetzel, *J. Am. Chem.* Soc. **1993**, *115*, 6382

[32] U. Bach, D. Lupo, P. Comte, J. E. Moser, F. Weissoertel, J. Saalbeck, H. Spreitzer, M. Graetzel, *Nature*, **1998**, *395*, 583

[33] K. Tennakone, G. R. R. A. Kumara, A. R. Kumarasinghe, K. G. U. Wijayantha, P. M. Sirimanne, *Semicond. Sci. Technol.* **1995**, *10*, 1689

[34] B. O'Regan, D. T. Schwarz, *J. Appl. Phys.* **1996**, *80*, 4749-4754

[35] R. A. Wessling, *J. Polym. Sci. Symp.* **1985**, *72*, 55-66

[36] R. W. Lenz, C. C. Han, J. Stenger-Smith, F. E. Karasz, *J. Polym. Sci. Polym. Chem.* **1988**, *26*, 3241-3249

[37] R. O. Garay, U. Baier, C. Bubeck, K. Mullen, *Adv. Mater.* **1993**, *5*, 561-564

[38] P. L. Burn, D. D. C. Bradley, R. H. Friend, D. A. Halliday, R. W. Jackson, A. Kraft, *J. Chem. Soc. Perkin Trans. 1* **1992**, 3225-3231

[39] F. Papadimitrakopoulos, K. Konstadinis, T. M. Miller, R. Opila, E. A. Chandross, M. E. Galvin, *Chem. Mater.* **1994**, *6*, 1563-1568

[40] V. H. Tran, V. Massardier, T. P. Nguyen, J. Davenas, *Polymer*, **1996**, *37*, 2061-2065

[41] F. Papadimitrakopoulos, M. Yan, L. J. Rothberg, H. E. Katz, E. A. Chandross, M. E. Galvin, *Mol. Cryst. Liq. Cryst.* **1994**, *256*, 663-669

[42] A. Beerden, D. Vanderzande, J, Gelan, *Synth. Met.* **1992**, *52*, 387-394

[43] I. Murase, T. Ohnishi, T. Noguchi, M. Hirooka, *Synth. Met.* **1987**, *17*, 639-644

[44] H. G. Gilch, W. L. Wheelwright, *J. Polym. Sci. A1* **1966**, *4*, 1337-1349

[45] A. J. Heeger, D. Braun (UNIAX), WO-B 92/16023, **1992** [*Chem. Abstr.* **1993**, *118*, 157401j]

[46] G. J. Sarnecki, P. L. Burn, A. Kraft, R. H. Friend, A. B. Holmes, *Synth. Met.* **1993**, *55*, 914-917

[47] B. R. Hsieh, H. Antoniadis, D. C. Bland, W. A. Feld, *Adv. Mat.* **1995**, *7*, 36-38

[48] F. Wudl, P. M. Allemand, G. Srdanov, Z. Ni, D. McBranch, *ACS Symp. Ser.* **1991**, *455*, 683: F. Wudl (University of California), US-B 5189136, **1990** [*Chem. Abstr.* **1993**, *118*, 255575p]

[49] W. Cabri, I. Candiani, *Acc. Chem. Res.* **1995**, *28*, 2-7

[50] Z. Bao, Y. Chen, R. Cai, L. Yu, *Macromolecules*, **1993**, *26*, 5281

[51] B. Liu, W. L. Yu, Y. H. Lai, W. Huang, *Chem. Comm.* **2000**, *7*, 551-552; Q. Pei, Y. Yang, *J. Am. Chem. Soc.* **1996**, *118*, 7416

[52] Z. Bao, W. K. Chan, L. Yu, *J. Am. Chem. Soc.* **1995**, *117*, 12426

[53] F. Koch, W. Heitz, *Macromol. Chem. Phys.* **1997**, *198*, 1531

[54] R. F. Heck, *Org. React.* **1982**, *27*, 345

[55] R. H. Friend, J. Burroughes, T. Shimoda, *Physics World*, **1999**, *June*, 35-40

[56] D. Braun, A. J. Heeger, *Appl. Phys. Lett.* **1991**, *58*, 1982

[57] P. L. Burn, A. B. Holmes, A. Kraft, D. D. C. Bradley, A. R. Brown, R. H. Friend, *Chem. Comm.* **1992**, 32-34

[58] A. R. Brown, P. L. Burn, D. D. C. Bradley, R. H. Friend, A. Kraft, A. B. Holmes, *Mol. Cryst. Liq. Cryst.* **1992**, *216*, 111-116

[59] A. R. Brown, *Appl. Phys. Lett.* **1992**, *61*, 2793-2795

[60] W. R. Salaneck, J. L. Bredas, *Adv. Mat.* **1996**, *8*, 48-52

[61] H. I. Campell, T. W. Hagler, D. L. Smith, J. P. Ferraris, *Phys. Rev. Lett.* **1996**, *76*, 1900-1903

[62] R. N. Marks, D. D. C. Bradley, R. W. Jackson, P. L. Burn, A. B. Holmes, *Synth. Met.* **1993**, *57*, 4128-4233

[63] I. D. Parker, *J. Appl. Phys.* **1994**, *75*, 1656-1666

[64] P. W. M. Bolm, M. J. M. De Jong, J. J. M. Vleggaar, *Appl. Phys. Lett.* **1996**, *68*, 3308-3310

[65] C. W. Tang, S. A. Van Slyke, *Appl. Phys. Lett.* **1987**, *51*, 913-915

[66] C. W. Tang, S. A. Van Slyke, *J. Appl. Phys.* **1989**, *65*, 3610-3616

[67] M. J. Shi, C. W. Tang, *Appl. Phys. Lett.* **1997**, *70*, 1665-1667

[68] H. Bassler, *Polym. Adv. Technol.* **1998**, *9*, 402-418

[69] P. W. M. Bolm, M. J. M. De Jong, S. Breedijk, *Appl. Phys. Lett.* **1997**, *71*, 930-932

[70] J. C. Scott, S. Karg, S. A. Carter, *J. Appl. Phys.* **1997**, *82*, 1454-1460

[71] R. D. Scurlock, B. J. Wang, P. R. Ogilby, J. R. Sheats, R. L. Clough, *J. Am. Chem. Soc.* **1995**, *117*, 10194-10202

[72] K. Z. Xing, *Adv. Mat.* **1996**, *8*, 971-974

[73] G. Gustafsson, Y. Gao, G. M. Treacy, F. Klavetter, N. Colaneri, A. J. Heeger, *Nature* **1992**, *357*, 477

[74] C. Hosokawa, *Synth. Met.* **1997**, *91*, 3-7

[75] S. Miyaguchi, 9th international workshop on inorganic and organic electroluminescence, Oregeon, Bend, USA, **1998**

[76] D. Lacey, 9th international workshop on inorganic and organic electroluminescence, Oregeon, Bend, USA, **1998**

[77] T. R. Hebner, C. C. Wu, D. Marcy, M. H. Lu, J. C. Sturm, *Appl. Phys. Lett.* **1998**, *72*, 519-521

[78] J. Bharathan, Y. Yang, *Appl. Phys. Lett.* **1998**, *72*, 2660-2662

[79] L. Smilowitz, A. Hays, A. J. Heeger, *J. Chem. Phys. Lett.* **1993**, *62*, 2827

[80] R. N. Marks, J. J. M. Halls, D. D. C. Bradley, R. H. Friend, A. B. Holmes, *J. Phys. Condens. Matter.* **1994**, *6*, 1379-1394

[81] C. W. Tang, *Appl. Phys. Lett.* **1986**, *48*, 183

[82] K. Pichler, D. Holliday, D. D. C. Bradley, A. B. Holmes, *J. Phys. Condens. Matter.* **1993**, *5*, 7155

[83] C. J. Barbec, N. Sariciftci, *Semiconducting polymers, Semiconducting Polymers*, Wiley-VCH, Weinheim, **2000**

[84] G. A. Chamberlain, *Solar Cells*, **1983**, *8*, 47

[85] J. Simon, J. Andre, *Molecular Semiconductors*, Springer-Verlag, Berlin, **1985**

[86] B. R. Weinberger, M. Akhtar, S. C. Gau, *Synth. Met.* **1984**, *4*, 187

[87] J. Kanicki, in T. A. Skotheim (Ed.) *Handbook of conducting polymers*, Vol. 1, Marcel Dekker, New York **1985**, p 544

[88] S. Glenis, G. Tourillon, F. Garnier, *Thin Solid Films* **1986**, *139*, 221

[89] G. Horovitz, *Adv. Mater.* **1989**, *2*, 287

[90] N. S. Sariciftci, L. Smilowitz, A. J. Heeger, F. Wudl, *Science*, **1992**, *258*, 1474

[91] N. S. Sariciftci, A. J. Heeger, F. Wudl, *Appl. Phys. Lett.* **1993**, *62*, 585

[92] J. J. M. Halls, R. H. Friend, *Synth. Met.* **1997**, *85*, 1307-1308

[93] G. Yu, A. J. Heeger, *J. Phys.* **1995**, 87, 2685

[94] N. C. Greenham, X. Peng, A. P. Alivisatos, *Phys. Rev. B* **1996**, *54*, 17628

[95] K. Murakoshi, R. Kogure, Y. Wada, S. Yanagida, *Chem. Lett.* **1997**, 471-472

[96] M. Granstroem, K. Petritsch, A. C. Arias, A. Lux, M. R. Andersson, R. H. Friend, *Nature*, **1998**, *395*, 257

[97] G. K. Boschloo, A. Goossens, J. Schoonman, *J. Electrochem. Soc.* **1997**, *144*, 1311

[98] S. A. Carter, J. C. Scott, P. J. Brock, *Appl. Phys. Lett.* **1998**, *71*, 1145

[99] T. J. Savenjie, J. M. Warman, A. Goossens, *Chem. Phys. Lett.* **1998**, *287*, 148-153

[100] S. A. Carter, J. C. Scott, P. J. Brock, *Appl. Phys. Lett.* **1999**, *74*, 1698

[101] J. T. Davis, E. K. Rideal, *Interfacial Phenomena*, Academic Press, New York, **1963**

[102] J. P. Flory, *Principles of Polymer Chemistry*, Cornell University Press, Ithaca, NY, **1953**, Chapter IX

[103] L. L. Hench, J. K. West, *Chem. Rev.* **1990**, *90*, 33

[104] C. J. Brinker, G. W. Scherer, *Sol-Gel Science: The Physics and Chemistry of Sol-Gel Processing*, Academic Press, London, **1990**

[105] L. L. Hench, *Bibliography on Ceramics and Glass*, Wiley, New York, **1976**

[106] B. E. Yoldas, *J. Non-Cryst. Solids*, **1984**, *63*, 145

[107] G. Orcel, PhD Dissertation, University of Florida, **1987**

[108] G. Orcel, L. L. Hench, I. Artaki, J. Jones, T. W. Zerda, *J. Non-Cryst. Solids* **1988**, *105*, 223

[109] G. Orcel, L. L. Hench, *Science of Ceramic Chemical Processing*, Wiley, New York, **1986**, p 224

[110] L. L. Hench, G. Orcel, *J. Non-Cryst. Solids* **1986**, *82*, 1

[111] W. G. Klemperer, S. D. Ramamurthi, *Better Ceramics Through Chemistry III*, Material Research Society, Pittsburgh, **1988**, *121*, 1

[112] I. Artaki, M. Bradley, T. W. Zerda, J. Jonas, G. Orcel, L. L. Hench, *Science of Ceramic Chemical Processing*, Wiley, New York, **1986**, p 73

[113] H. Schmidt, A. Kaiser, *Glastechn. Ber.* **1981**, *54*, 338

[114] M. Prassas, L. L. Hench, *Ultrastructure Processing of Ceramics, Glasses and Composites*, Wiley, New York, **1984**, p 100

[115] C. J. Brinker, K. D. Keefer, D. W. Schaefer, C. S. Ashley, *J. Non-Cryst. Solids*, **1982**, *48*, 47

[116] B. O'Regan, J. Moser, M. Anderson, M. Graetzel, *J. Phys. Chem.* **1990**, *94*, 8720-8726

[117] M. A. Anderson, M. J. Gieselmann, Q. Xu, *J. Membrane Sci.* **1988**, *43*, 392

[118] W. A. Badawy, *J. Mater. Sci.* **1997**, *32*, 4979-4984

[119] H. Tang, K. Prasad, R. Sanjines, P. E. Schmidt, F. Levy, *J. Appl. Phys.* **1994**, *75*, 2042-2047

Chapter 2: Experimental-Synthesis

All reactions were carried out under an inert atmosphere of dry nitrogen using freshly distilled solvents. All ^{1}H and ^{13}C NMR spectra were recorded using a Bruker AC 250 spectrometer, mass spectra were recorded using a Fisons VG Pro Spec 3000 machine and IR spectra were run on a Perkin-Elmer Paragon 1000 FTIR spectrometer. The molecular weight of polymers was estimated by GPC relative to polystyrene. All the spectroscopic characterisation data of synthesised starting materials were consistent with those reported in the literature. Preparation of tributyl-vinyl-stannane[1], tetrakis(triphenylphosphine)palladium(0)[2], palladacycle[3,4] (Fig. 2) [*trans*-di(*μ*-acetato)-bis[*o*-(di-*o*-tolylphosphino)benzyl]dipalladium(II)], 1,4-diethynylbenzene[5] and 1,4-divinylbenzene[6] was carried out according to literature procedures.

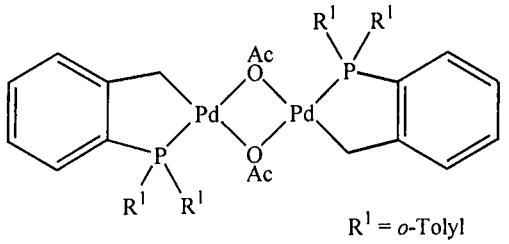

Fig. 2: Chemical structure of palladacycle catalyst

2.1 Synthesis of substituted divinylbenzenes via the Stille reaction

2.1.1 Preparation of 1,4-didodecyloxybenzene[7] (3.2a)

Hydroquinone (27.53 g, 0.25 mol) was dissolved in DMF and heated to 80°C, potassium carbonate (71.86 g, 0.52 mol) was added as one portion. The reaction

mixture was stirred for 1 hour, 1-bromododecane (124.86 ml, 0.52 mol) was added and the mixture was left to stir for 16 hours, after which time the colour of the solution had turned dark red. The reaction mixture was then poured into 1 litre of water, shaken and filtered. The precipitate was washed with acidic water (5% HCl), and then with 10% NaOH solution. The product was redissolved in DCM, dried over $MgSO_4$ and finally recrystallised from ethanol to give 67% yield of 1,4-didodecyloxybenzene.

^1H NMR ($CDCl_3$): δ = 6.75 (s, 4H, arom), 3.83 (t, 4H, J = 6 Hz, α-OCH_2), 1.67 (qt, 4H, J = 6 Hz, -OCH_2-CH_2), 1.5-1.2 (m, 36H, aliph), 0.8 ppm (t, 6H, J = 7 Hz, -CH_3).

2.1.2 Preparation of 1,4-didodecyloxy-2,5-diiodobenzene[7] (3.3a)

A 250 ml flask was charged with iodine (1.14 g, 4.5 mmol), 1,4-didodecyloxy-benzene (2.23 g, 5 mmol), iodic acid (0.527 g, 3 mmol), CCl_4 (4 ml), glacial acetic acid (18 ml), H_2SO_4 (0.65 ml) and deionised water (3 ml). The resulting mixture was heated to 75 °C and held at this temperature for 3 hours. After this time a solution of sodium thiosulfate was added to remove any unreacted iodine. The solution was extracted with DCM and washed three times with 5% NaOH solution, followed by washing three times with water. The organic layer was dried over $MgSO_4$ and the solvent removed under reduced pressure. The product, 1,4-diiodo-2,5-didodecyloxy benzene, was isolated by two recrystallisation steps from ethanol to give an overall yield of 60%.

^{1}H NMR ($CDCl_3$): δ = 7.17 (s, 2H, arom), 3.92 (t, 4H, J = 6 Hz, α-OCH_2), 1.78 (qt, 4H, J = 6 Hz, -OCH_2-CH_2), 1.5-1.2 (m, 36H, aliph), 0.8 ppm (t, 6H, J = 7 Hz, -CH_3).

2.1.3 Preparation of 1-dodecyloxy-4-methoxybenzene (3.2b)

4-Methoxyphenol (22.02 g, 0.2 mol) was dissolved in 250 ml of DMF and heated to 80°C. Potassium carbonate (29 g, 0.21 mol) was added as one portion. The reaction mixture was stirred for 1 hour, 1-bromododecane (50.05 ml, 0.21 mol) was added and the mixture was left to stir for 16 hours, after which time the colour had turned dark red. The reaction mixture was then poured into 1 litre of water, shaken and filtered. The precipitate was washed with water to remove K_2CO_3 and HBr, followed by washing with 10% NaOH solution. The product was redissolved in DCM, dried over $MgSO_4$ and finally recrystallised from ethanol to give 65% yield of 1-dodecyloxy-4-methoxybenzene.

^{1}H NMR ($CDCl_3$): δ = 6.82 (s, 4H, arom), 3.87 (t, 2H, J = 6 Hz, α-OCH_2), 3.77 (s, 3H, -OCH_3), 1.67 (qt, 2H, J = 6 Hz, -OCH_2-CH_2), 1.5-1.2 (m, 18H, aliph), 0.8 ppm (t, 3H, J = 7 Hz, -CH_3).

2.1.4 Preparation of 1-dodecyloxy-4-methoxy-2,5-diiodobenzene (3.3b)

A 250 ml flask was charged with iodine (4.57 g, 18 mmol), 1-dodecyloxy-4-methoxy-benzene (5.84 g, 20 mmol), iodic acid (2.11 g, 12 mmol), CCl_4 (20 ml), glacial acetic

acid (50 ml), H_2SO_4 (1 ml) and H_2O (4.6 ml). The reaction mixture was heated to 75°C for 3 hours. A solution of sodium thiosulfate was then added to remove any unreacted iodine. The product was extracted with DCM and washed 3 times with 5% NaOH solution, followed by washing 3 times with water. The organic layer was dried over $MgSO_4$ and solvent was removed. The product, 1-dodecyloxy-4-methoxy-2,5-diiodobenzene, was recrystallised twice from ethanol to give a yield of 50%.

^1H NMR ($CDCl_3$): δ = 7.18 (d, 2H, arom), 3.93 (t, 2H, J = 6 Hz, α-OCH_2), 3.82 (s, 3H, -OCH_3), 1.79 (qt, 2H, J = 6 Hz, -OCH_2-CH_2), 1.5-1.2 (m, 18H, aliph), 0.8 ppm (t, 6H, J = 7 Hz, -CH_3).

2.1.5 Synthesis of 1,4-didodecyloxy-2,5-divinylbenzene (3.4a)

Two mole equivalents of tributyl-vinyl-stannane (0.6 ml, 1.93 mmol) were added to a solution of 1,4-didodecyloxy-2,5-diiodo-benzene (0.64 g, 0.92 mmol) in 50 ml of toluene. To this, 0.1 g of the catalyst, [tetrakis(triphenylphosphine)palladium(0)], was added. The reaction mixture was stirred at 90°C for 3 hours and after this time an additional amount (0.1 g) of the catalyst was added and the mixture heated at 90°C for 36 hours. The reaction mixture was allowed to cool to room temperature and a solution of potassium fluoride and ether was added and stirred for 3 hours. The resulting solution was filtered through Celite to remove solid tributyltinfluoride and the catalyst residues. The solvents were removed under reduced pressure and the crude product was purified by column chromatography on silica gel using

hexane/DCM 6:1 as the eluent. Recrystallisation of the product from cold ethanol gave 0.25 g (55% yield) of 1,4-didodecyloxy-2,5-divinylbenzene.

State : yellow crystals

Molecular formula : $C_{34}H_{58}O_2$

Molecular weight : 498

Stability : stable to air and moisture

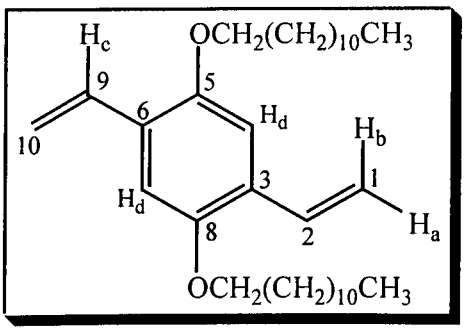

^{1}H NMR

Chemical shift (δ)	Integration ratio	Multiplicity	Correspondence
0.8	6	m	-CH_3(alkoxy group)
1.25-1.45	36	broad multiplet	-CH_2(alkoxy group)
1.8	4	qt (J = 6)	-OCH_2CH_2(alkoxy)
3.9	4	t (J = 6)	-OCH_2(alkoxy group)
5.2	2	d,d (J = 11, 1)	H_a(vinyl group)
5.65	2	d,d (J = 18, 1)	H_b(vinyl group)
6.9	2	m	H_c(vinyl group)
7	2	s	H_d

^{13}C NMR

Chemical shift (δ)	Correspondence
13	-CH_3(alkoxy group)
23-30	-CH_2(alkoxy group)
32	-OCH_2CH_2(alkoxy group)
69	-OCH_2(alkoxy group)
56	-OCH_3(methoxy)
110	$C_{2,9}$(vinyl group)
113	$C_{1,10}$(vinyl group)
126.5	CH_d
127	$C_3 + C_6$
131	$C_5 + C_8$

Elemental Analysis

Element	% Expected	% Found
C	81.86	81.64
H	11.72	11.94

Mass spectroscopy (EI)

m/z	Species	Intensity %
498	M^+	100

2.1.6 Synthesis of 1-dodecyloxy-4-methoxy-2,5-divinylbenzene (3.4b)

Prepared in a similar procedure to that described in section 2.1.5 and the starting materials used were: tributylvinyltin (3.3 ml, 11.4 mmol), 1-dodecyloxy-4-methoxy-2,5-diiodo-benzene (2.95 g, 5.42 mmol), toluene (150 ml) and tetrakis(triphenylphosphine)palladium(0) (0.15 g). Recrystallisation of the product from cold ethanol gave 1 g (55%) of 1-dodecyloxy-4-methoxy-2,5-divinylbenzene.

State : yellow crystals

Molecular formula : $C_{23}H_{36}O_2$

Molecular weight : 344

Stability : stable to air and moisture

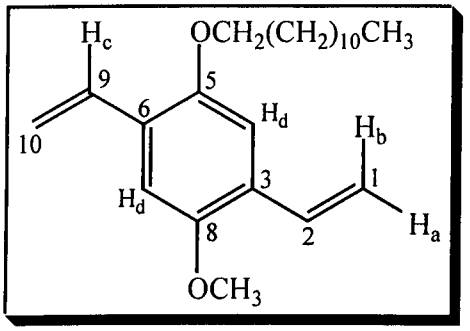

^{1}H NMR

Chemical shift (δ)	Integration ratio	Multiplicity	Correspondence
0.8	3	t (J = 7)	-C**H**3(alkoxy group)
1.25-1.45	18	broad multiplet	-C**H**2(alkoxy group)
1.8	2	qt (J = 6)	-OCH2C**H**2(alkoxy)
3.75	3	s	-OC**H**3(methoxy)

3.9	2	t (J = 6)	-OCH_2(alkoxy group)
5.25	2	d,d (J = 11, 1)	H_a(vinyl group)
5.6	2	d,d (J = 18, 1)	H_b(vinyl group)
7.0	2	m	H_c(vinyl group)
7.2	2	s	H_d

^{13}C NMR

Chemical shift (δ)	Correspondence
13	-CH_3(alkoxy group)
23-30	-CH_2(alkoxy group)
32	-OCH_2CH_2(alkoxy group)
69	-OCH_2(alkoxy group)
56	-OCH_3(methoxy)
108	C_9(vinyl group)
110	C_2(vinyl group)
113.5	C_{10}(vinyl group)
114	C_1(vinyl group)
126	CH_d
151, 151.5	$C_3 + C_6$
131	$C_5 + C_8$

Elemental Analysis

Element	% Expected	% Found
C	80.23	79.34
H	10.46	10.51

Mass spectroscopy (EI)

m/z	Species	Intensity %
344	M^+	100

2.1.7 Synthesis of 1,4-dihexadecyloxy-2,5-divinylbenzene (3.4c)

Prepared in a similar procedure to that described in section 2.1.5 and the starting materials used were: tributylvinyltin (2.25 ml, 7.72 mmol), 1-dihexadecyloxy-2,5-diiodobenzene (2.5 g, 3.87 mmol), toluene (150 ml) and

tetrakis(triphenylphosphine)palladium(0) (0.15 g). Recrystallisation of the product from cold ethanol gave 0.9 g (55%) of 1,4-dihexadecyloxy-2,5-divinylbenzene.

State : yellow crystals

Molecular formula : $C_{42}H_{74}O_2$

Molecular weight : 610

Stability : stable to air and moisture

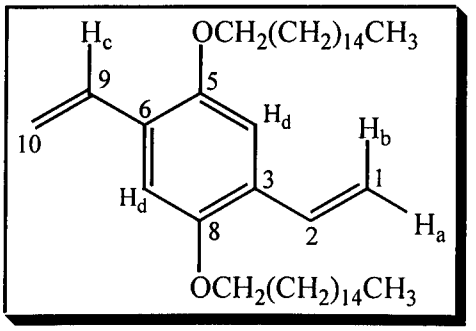

^{1}H NMR

Chemical shift (δ)	Integration ratio	Multiplicity	Correspondence
0.8	6	t (J = 7)	-CH_3(alkoxy group)
1.2-1.5	52	broad multiplet	-CH_2(alkoxy group)
1.8	4	qt (J = 6)	-OCH_2CH_2(alkoxy)
2.5	4	t (J = 6)	-OCH_2(alkoxy group)
5.2	2	d,d (J = 15, 2)	H_a(vinyl group)
5.6	2	d,d (J = 18, 2)	H_b(vinyl group)
6.9	2	m	H_c(vinyl group)
7.2	2	s	H_d

^{13}C NMR

Chemical shift (δ)	Correspondence
13	-CH_3(alkoxy group)
23-30	-CH_2(alkoxy group)
32	-OCH_2CH_2(alkoxy group)
69	-OCH_2(alkoxy group)
56	-OCH_3(methoxy)
110	$C_{2,9}$(vinyl group)
113	$C_{1,10}$(vinyl group)
126.5	CH_d
127	$C_3 + C_6$
131	$C_5 + C_8$

Elemental analysis

Element	% Expected	% Found
C	82.62	81.97
H	12.13	12.55

Mass spectroscopy (EI)

m/z	Species	Intensity %
610	M^+	100

2.1.8 Synthesis of 2,5-divinylthiophene[8]

Two mole equivalents of tributyl-vinyl-stannane (2.6 ml, 8.8 mmol) were added to a solution of 2,5-dibromothiophene (0.5 ml, 4.2 mmol) in 150 ml of toluene. To this, 50 mg of the catalyst, tetrakis(triphenylphosphine)palladium(0), was added. The reaction mixture was stirred at 90°C for 3 hours and after this time an additional amount (50 mg) of the catalyst was added and the mixture heated at 90°C for 36 hours. The reaction mixture was allowed to cool to room temperature and a solution of potassium fluoride and ether was added and stirred for 3 hours. The resulting solution was filtered through Celite to remove solid tributyltinfluoride and the catalyst residues. The solvents were removed under reduced pressure to give a 50% yield of 2,5-divinythiophene as identified by ^{1}H NMR spectroscopy. Attempts towards isolating the product by distillation were not successful, as the product appears to undergo polymerisation when heated.

^{1}H NMR ($CDCl_3$): δ = 6.71 (s, 2H, arom), 6.63 (dd, 2H, -C*H*=CH_2), 5.45 (dd, 2H, $^{trans}J$ = 17 Hz, ^{gem}J = 1 Hz, *trans*-CH=CH_2), 5.05 (dd, 2H, ^{cis}J = 11 Hz, ^{gem}J = 1 Hz, *cis*- CH=CH_2).

2.2 Synthesis of diethynyl substituted benzenes and heteroaromatic compounds

2.2.1 Preparation of 1,4-bis(3-methyl-3-hydroxy-but-1-ynyl)benzene (3.6)

1,4-Diiodobenzene (9.9 g, 30 mmol) was dissolved in 150 ml of triethylamine and 2-methyl-3-butyn-2-ol (6.6 ml, 66 mmol) was added. The flask was then flushed with N_2 before addition of CuI (0.1 g) and tetrakis(triphenyphosphine)palladium(0) (0.2 g). The resulting mixture was stirred for 1 hour at 50°C. A white solid was formed which was dissolved in DCM, washed 3 times with water and then dried over $MgSO_4$. The organic phase was filtered through Celite to remove the catalyst. The solvents were then removed and the crude product was recrystallised twice from toluene to give 4.3 g (60%) of 1,4-bis(3-methyl-3-hydroxy-but-1-ynyl)benzene

^1H NMR ($CDCl_3$): δ = 7.24 (s, 4H, arom), 1.6 ppm (s, 12H, -C*H*3).

2.2.2 Preparation of 1,4-diethynylbenzene (3.7)

1,4-Bis-(3-methyl-3-hydroxy-but-1-ynyl)benzene (2.42 g, 10 mmol) was added to a solution of one equivalent of NaOH (0.4 g, 10 mmol) in isopropyl alcohol, which was heated to reflux. The mixture was stirred at reflux for 4 hours and then poured into 500 ml of ice water. A yellow solid precipitated and was filtered off, this solid was

extracted in petroleum ether (40-60) and then dried over $MgSO_4$. The solvent was removed to give a low yield (10%) of 1,4-diethynylbenzene.

^1H NMR ($CDCl_3$): δ = 7.18 (s, 4H, arom), 3.32 ppm (s, 2H, *acetylenic-CH*).

2.2.3 Attempted preparation of 2,5-diethynylthiophene

2,5-Dibromothiophene (2 ml, 17.8 mmol) was dissolved in 50 ml of triethylamine and 2-methyl-3-butyn-2-ol (4 ml, 37 mmol) was added. The flask was then flushed with N_2 and the following compounds added: tetrakis(triphenylphosphine)palladium(0) (0.2 g), CuI (0.1 g), triphenylphosphine (0.1 g) plus a few crystals of LiCl. The reaction mixture was stirred for 14 hours at 60°C. The product was then extracted into DCM, washed three times with water and dried over $MgSO_4$. The organic phase was filtered through Celite to remove the catalyst. The solvents were then removed and the crude product was added directly to a refluxing solution of one equivalent of NaOH in isopropyl alcohol. The mixture was stirred for 4 hours and then washed with water. The product was extracted into petroleum ether and dried over $MgSO_4$. The solvent was removed to give a dark red oil. Unfortunately, attempted distillation at 40°C and 0.1 mm/Hg resulted in decomposition of the product.

2.2.4 Attempted preparation of 2,5-diethynylpyridine

2,5-Dibromopyridine (2.85 g, 12 mmol) was dissolved in toluene (20 ml) and triethylamine (50 ml) and 2-methyl-3-butyn-2-ol (3 ml, 30 mmol) was added. The flask was then flushed with N_2 and the catalytic system was added in the following

order; CuI (0.15 g), tetrakis(triphenylphosphine)palladium(0) (0.25 g), triphenylphosphine (0.1 g) plus a few crystals of LiCl. The reaction mixture was stirred for 14 hours at 60°C. The product was then extracted into DCM, washed three times with water and dried over $MgSO_4$. The organic phase was filtered through Celite to remove the catalyst. The solvents were then removed and the crude product was added directly to a refluxing solution of one equivalent of NaOH in ethanol. The mixture was stirred for 4 hours and then washed with water. The product was extracted in petroleum ether and then dried over $MgSO_4$. The solvent was removed to give a brown oil. Unfortunately, the deprotection step yielded a mixture of compounds, which were not possible to separate.

2.3 Synthesis of diethynyl substituted benzenes via trimethylsilylacetylene

2.3.1 Synthesis of 1,4-didodecyloxy-2,5-bis[(trimethylsilyl)ethynyl]-benzene (3.8)

1,4-Didodecyloxy-2,5-diiodobenzene (4 g, 5.72 mmol) was dissolved in 30 ml of toluene and 70 ml of triethylamine. Trimethylsilylacetylene (2 ml, 14.3 mmol) was then added and the reaction flask was flushed with N_2. A small amount (0.2 mol%, 0.11 mmol) of the catalyst system [CuI (20 mg), PPh_3 (40 mg) and tetrakis(triphenylphosphine)palladium(0) (122 mg)] was then added. The reaction mixture was stirred at 80°C for 3 hours and then washed with water, dried over

$MgSO_4$, filtered through Celite and the solvent removed under reduced pressure. The resulting solid was recrystallised from acetone to give 2.6g (74% yield) of a yellow powder. This was identified by NMR spectroscopy as 1,4-didodecyloxyl-2,5-bis[(trimethylsilyl)ethynyl]-benzene.

^1H NMR ($CDCl_3$): δ = 6.87 (s, 2H, arom), 3.93 (t, 4H, J = 6 Hz, α-OCH_2), 1.68 (qt, 4H, J = 6 Hz, -OCH_2-CH_2), 1.5-1.2 (m, 36H, aliph), 0.8 (t, 6H, J = 7 Hz, *aliphatic*-CH_3), 0.5 ppm [t, 18H, J = 5 Hz, -Si(CH_3)$_3$].

2.3.2 Synthesis of 1,4-didodecyloxy-2,5-diethynylbenzene (3.9)

1,4-Didodecyloxyl-2,5-bis[(trimethylsilyl)ethynyl]-benzene (2.36 g, 3.86 mmol) was dissolved in a mixture of methanol (25 ml) and DCM (75 ml). To this solution, K_2CO_3 (0.65 g, 4.65 mmol) was added. The reaction mixture was then stirred at room temperature for 14 hours. The solvents were removed and the product was redissolved in DCM, washed twice with sodium bicarbonate solution and then twice with water. The organic phase was dried over $MgSO_4$ and solvent removed. The product was recrystallised from cold acetone to give 1.55 g (81% yield) of yellow crystalline needles of 1,4-didodecyloxyl-2,5-diethynylbenzene.

State : yellow orange crystals

Molecular formula : $C_{34}H_{54}O_2$

Molecular weight : 494

Stability : stable to air and moisture

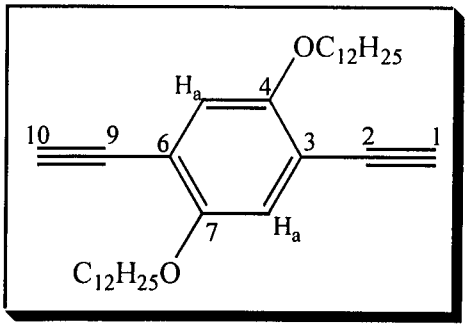

^{1}H NMR

Chemical shift (δ)	Integration ratio	Multiplicity	Correspondence
0.75	6	t (J = 7)	-CH_3(alkoxy group)
1.2-1.5	36	broad multiplet	-CH_2(alkoxy group)
1.8	4	qt (J = 6)	-OCH_2CH_2(alkoxy)
3.9	4	t (J = 7)	-OCH_2(alkoxy group)
3.25	2	s	-CH(acetylenic)
6.9	2	s	H_a

^{13}C NMR

Chemical shift (δ)	Correspondence
14.2	-CH_3(alkoxy group)
23-30	-CH_2(alkoxy group)
32	-OCH_2CH_2(alkoxy group)
69	-OCH_2(alkoxy group)
79	$C_{1,10}$(acetylenic)
82	$C_{2,9}$(acetylenic)
153	$C_3 + C_6$
131	$C_5 + C_8$
113	$C_4 + C_7$
118	CH_a

Elemental analysis

Element	% Expected	% Found
C	81.59	81.72
H	10.93	10.91

Mass spectroscopy (EI)

m/z	Species	Intensity %
495	MH^+	45

2.4 Synthesis of bis-halomethyl substituted benzenes

2.4.1 Synthesis of 1-(2-ethylhexyloxy)-4-methoxybenzene (3.10)

4-Methoxyphenol (10 g, 80.5 mmol) was dissolved in 250 ml of DMF under N_2 and heated to 80°C. Potassium carbonate (12.25 g, 88.6 mmol) was added as one portion. The reaction mixture was stirred for 1 hour, 3-bromomethylheptane (17.1 g, 88.6 mmol) was added and the mixture was left to stir for 16 hours, after which time the colour had turned light brown. The reaction mixture was allowed to cool down, DCM (50 ml) was added and the organic phase was washed against HCl solution (5%) and water. The organic phase was dried over $MgSO_4$, the solvent was evaporated and the product purified by column chromatography using hexane/DCM as the eluent to yield 8 g (50%) of 1-(2-ethylhexyloxy)-4-methoxy benzene.

^1H NMR ($CDCl_3$): δ = 6.82 (s, 4H, arom), 3.79 (s, 3H, -OC*H*$_3$), 3.77 (d, 2H, J = 3 Hz, α-OC*H*2), 1.67 (qt, 1H, J = 6 Hz, -OCH$_2$-C*H*), 1.5-1.2 (m, 18H, aliph), 0.8 ppm (m, 6H, -C*H*$_3$).

2.4.2 Synthesis of 1,4-bis-chloromethyl-2(2-ethylhexyloxy)-5-methoxy benzene (3.11a)

A mixture of 1-(2-ethylhexyloxy)-4-methoxy benzene (5 g, 21.15 mmol), KCl (12.62 g, 169.2 mmol) and paraformaldehyde (10.15 g, 338.4 mmol) was dissolved in 200 ml of acetic acid under N_2. The solution was heated to 80°C and stirred for 30

minutes. A solution of acetic acid (40 ml) and H_2SO_4 (7 ml) was added dropwise to this solution over a period of 30 minutes, and the white emulsion turned clear as HCl gas was evolved. The mixture was stirred for 16 hours at 80°C and then poured into 500 ml of H_2O. The product was extracted with DCM and washed twice against HCl/NaCl solution and three times against NaOH (5%) and then dried over $MgSO_4$. The solvent was removed and the product purified by column chromatography using hexane/DCM as the eluent to yield 2 g (30%) of 1,4-bis-chloromethyl-2(2-ethylhexyloxy)-5-methoxy benzene.

State : white powder

Molecular formula : $C_{17}H_{26}O_2Cl_2$

Molecular weight : 333

Stability : stable to air and moisture

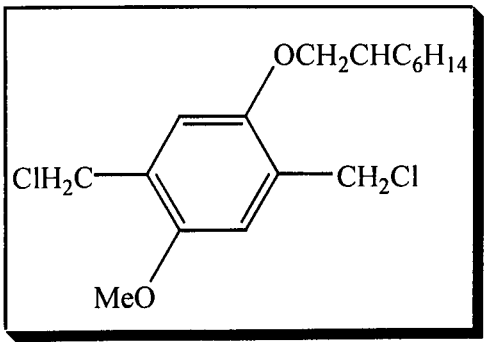

^{1}H NMR

Chemical shift (δ)	Integration ratio	Multiplicity	Correspondence
0.9	3	t (J = 6)	-CH_3(alkoxy group)
1.2-1.5	11	broad multiplet	-CH_2(alkoxy group)
1.75	1	qt (J = 6)	-OCH_2CH(alkoxy)
3.85	2	m	-OCH_2(alkoxy group)
3.9	3	s	-OCH_3
4.6	4	s	-CH_2Cl
6.9	2	s	H(phenyl group)

Further characterisation is in agreement with values reported in literature[9,10,11]

2.4.3 Synthesis of 1,4-bis-chloromethyl-2-dodecyloxy-5-methoxy benzene (3.11b)

A mixture of 1-dodecyloxy-4-methoxy benzene (6.18 g, 21.15 mmol), KCl (12.62 g, 169.2 mmol) and paraformaldehyde (10.15 g, 338.4 mmol) was dissolved in 100 ml of acetic acid under N_2, heated to 60°C and stirred for 30 minutes. To this, a solution of acetic acid (40 ml) and H_2SO_4 (7 ml) was added dropwise over a period of 30 minutes, and the white emulsion turned clear as HCl gas was evolved. The mixture was stirred for 16 hours at 80°C and then poured into 500 ml of H_2O. The product was extracted with DCM and washed twice against NaOH/NaCl solution and then dried over $MgSO_4$. The solvent was removed and the product purified by column chromatography using hexane/DCM as the eluent to yield 860 mg (10%) of 1,4-bis-chloromethyl-2-dodecyloxy-5-methoxybenzene.

State : white powder

Molecular formula : $C_{21}H_{34}O_2Cl_2$

Molecular weight : 387

Stability : stable to air and moisture

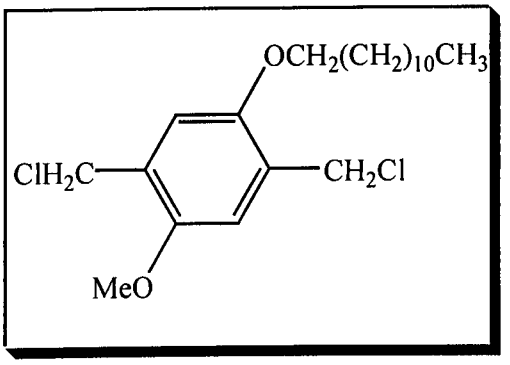

^{1}H NMR

Chemical shift (δ)	Integration ratio	Multiplicity	Correspondence
0.9	3	t (J = 6)	-CH_3(alkoxy group)
1.25-1.5	18	broad multiplet	-CH_2(alkoxy group)
1.8	2	qt (J = 6)	-OCH_2CH_2(alkoxy)

3.95	2	t (J = 6)	-OCH_2(alkoxy group)
3.85	3	s	-OCH_3
4.6	4	s	-CH_2Cl
6.9	2	s	H(phenyl group)

Further characterisation is in agreement with values reported in literature[9,10,11]

2.5 Polymerisation

2.5.1 Synthesis of poly(1,4-phenylene-ethynylenes)

2.5.1.1 Synthesis of poly[1,4-(2,5-didodecyloxy)phenylene-ethynylene-co-(1,4-phenylene-ethynylene)] (PPE-1)

1,4-Didodecyloxy-2,5-diiodobenzene (1.36 g, 2 mmol) was dissolved in a mixture of THF (30 ml) and triethylamine (30 ml). To this solution, 1,4-diethynylbenzene (246 mg, 2 mmol) was added. The reaction flask was then flushed with N_2. This was followed by the addition of a catalytic amount of PPh_3 (0.2 mol%) and tetrakis(triphenylphosphine)palladium(0) (0.2 mol%). The reaction mixture was stirred at 40°C for 14 hours. No reaction was detected, so the temperature was raised to reflux and the mixture was stirred for a further 36 hours. The reaction mixture was allowed to cool, then poured into water and extracted with DCM. The organic phase was washed twice with water, dried over $MgSO_4$ and filtered through Celite. The solvent was then removed to give an orange red solid which was redissolved in the minimum amount of DCM and precipitated twice into methanol and once into

petroleum ether to yield 515 mg (47% yield) of poly[1,4-(2,5-didodecyloxy)phenylene-ethynylene-co-(1,4-phenylene-ethynylene)].

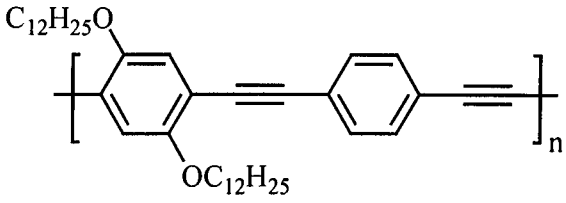

State : yellow green solid

Absorption maximum : 406 nm

^{1}H NMR

Chemical shift (δ)	Integration ratio	Multiplicity	Correspondence
0.75	6	broad triplet	-CH_3(alkoxy group)
1.25-1.6	36	broad multiplet	-CH_2(alkoxy group)
1.85	4	broad quintet	-OCH_2CH_2(alkoxy)
3.9	4	broad triplet	-OCH_2(alkoxy group)
6.95	2	broad singlet	**H**(dialkoxy ring)
7.16	4	broad singlet	**H**(benzene ring)

It proved impossible to record ^{13}C NMR with adequate signal to noise even using a large number of scans.

Elemental Analysis

Element	% Expected	% Found
C	74.07	74.71
H	8.64	8.82

GPC

Mn	Mp	Mw	Polydispersity
3128	2845	3715	1.19

2.5.1.2 Synthesis of poly[1,4-(2,5-didodecyloxy)phenylene-ethynylene-co-(2,5-thienylene-ethynylene)] (PPET)

1,4-Didodecyloxy-2,5-diethynylbenzene (0.5 g, 1.012 mmol) was dissolved in a mixture of DMA (35 ml) and triethylamine (30 ml). To this solution, 2,5-dibromothiophene (245 mg, 1.012 mmol) was added and the reaction flask was then flushed with N_2. This was followed by the addition of a catalytic amount of PPh_3 (0.2 mol%) and tetrakis(triphenyphosphine)palladium(0) (0.2 mol%). The reaction mixture was stirred at 80°C for 3 hours. The mixture was allowed to cool down, then poured into water and extracted with DCM. The organic phase was washed twice with water, dried over $MgSO_4$ and filtered through Celite. The solvent was then removed to give an orange red solid, which was redissolved in the minimum amount of hot toluene, and precipitated twice into acetone and then stirred for 3 hours in acetone to yield 350 mg (60%) of poly[1,4-(2,5-didodecyloxy)phenylene-ethynylene-co-(2,5-thienylene-ethynylene)].

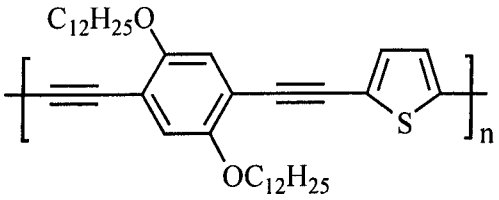

State : yellow orange solid

Absorption maximum : 451 nm

^{1}H NMR

Chemical shift (δ)	Integration ratio	Multiplicity	Correspondence
0.75	6	broad triplet	-CH_3(alkoxy group)
1.25-1.6	36	broad multiplet	-CH_2(alkoxy group)
1.85	4	broad quintet	-OCH_2CH_2(alkoxy)
4.03	4	broad triplet	-OCH_2(alkoxy group)
6.98	2	broad singlet	H(dialkoxy ring)
7.16	2	broad singlet	H(thiophene ring)

It proved impossible to record ^{13}C NMR with adequate signal to noise even using a large number of scans.

Elemental Analysis

Element	% Expected	% Found
C	78.53	76.79
H	9.81	9.35
S	5.83	7.1

GPC

Mn	Mp	Mw	Polydispersity
61633	92464	221713	3.6

2.5.1.3 Synthesis of poly[1,4-(2,5-didodecyloxy)phenylene-ethynylene-co-1,4-(2-nitro-phenylene-ethynylene)] (PPE-NO_2)

1,4-Didodecyloxy-2,5-diethynylbenzene (0.5 g, 1.012 mmol) was dissolved in a mixture of DMA (35 ml) and triethylamine (30 ml). To this solution, 1,4-dibromo-2-nitrobenzene (284 mg, 1.012 mmol) was added and the reaction flask was then flushed with N_2. This was followed by the addition of a catalytic amount of PPh_3 (0.2 mol%) and tetrakis(triphenyphosphine)palladium(0) (0.2 mol%). The reaction mixture was heated to 100°C and stirred at this temperature for 16 hours. The product was extracted with toluene, washed twice with brine, dried over $MgSO_4$ and filtered

through Celite. The solvent was removed to give a deep red solid, which was redissolved, in the minimum amount of hot toluene, and precipitated twice into a mixture of methanol and acetone to yield 400 mg (63%) of poly[1,4-(2,5-didodecyloxy)phenylene-ethynylene-co-1,4-(2-nitro-phenylene-ethynylene)].

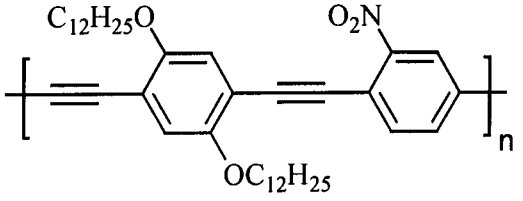

State : brown red solid

Absorption maximum : 448 nm

^{1}H NMR

Chemical shift (δ)	Integration ratio	Multiplicity	Correspondence
0.8	6	broad triplet	-C**H**$_3$(alkoxy group)
1.2-1.6	36	broad multiplet	-C**H**$_2$(alkoxy group)
1.85	4	broad quintet	-OCH$_2$C**H**$_2$(alkoxy)
3.9	4	broad	-OC**H**$_2$(alkoxy group)
7.0	2	broad single	**H**(dialkoxy ring)
7.2, 7.6, 8.2	1, 1, 1	broad	**H**(nitrobenzene ring)

It proved impossible to record ^{13}C NMR with adequate signal to noise even using a large number of scans.

Elemental Analysis

Element	% Expected	% Found
C	74.38	72.78
H	8.97	8.92
N	2.26	1.95

GPC

Mn	Mp	Mw	Polydispersity
12154	19699	43545	3.6

2.5.2 Synthesis of poly (1,4-phenylene-vinylenes)

2.5.2.1 Synthesis of poly[1,4-(2-dodecyloxy-5-methoxy)phenylene-vinylene-co-(1,4-phenylene-vinylene)] via Heck reaction (PPV12-1)[7]

A mixture of 1-dodecyloxy-4-methoxy-2,5-diiodo-benzene (97.7 mg, 0.75 mmol) and 1,4-divinylbenzene (405 mg, 0.75 mmol) was dissolved under N_2 in a mixture of DMA (50 ml) and triethylamine (10 ml). This was followed by the addition of a catalytic amount (0.2 mol%) of tetrakis(triphenylphosphine)palladium(0). The mixture was heated to 100 °C and stirred at this temperature for 14 hours. The product was extracted with toluene, washed twice with brine, dried over $MgSO_4$ and filtered through Celite. The solvent was removed to give an orange red solid, which was redissolved in the minimum amount of hot toluene, precipitated twice into a mixture of methanol and acetone to yield 185 mg (45%) poly[1,4-(2-dodecyloxy-5-methoxy)phenylene-vinylene-co-(1,4-phenylene-vinylene)].

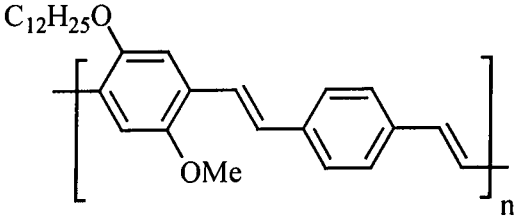

State : orange solid

Absorption maximum: 448 nm

^{1}H NMR

Chemical shift (δ)	Integration ratio	Multiplicity	Correspondence
0.85	3	broad triplet	-CH_3(alkoxy group)
1.25-1.6	18	broad multiplet	-CH_2(alkoxy group)
1.85	4	broad quintet	-OCH_2CH_2(alkoxy)
4.05	2	broad triplet	-OCH_2(alkoxy group)
3.9	3	broad singlet	-OCH_3
7.1	4	broad	**H**(vinylene)
7.15	2	broad	**H**(dialkoxy ring)
7.5	4	broad	**H**(unsubstituted ring)

It proved impossible to record ^{13}C NMR with adequate signal to noise even using a large number of scans.

Elemental Analysis

Element	% Expected	% Found
C	83.25	80.67
H	9.1	8.52

GPC

Mn	Mp	Mw	Polydispersity
6083	8592	11400	1.8

2.5.2.2 Synthesis of poly[1,4-(2-dodecyloxy-5-methoxy)phenylene-vinylene] via Heck reaction (PPV12-1/12-1)

A mixture of 1-dodecyloxy-4-methoxy-2,5-diiodo-benzene (474 mg, 0.872 mmol) and 1-dodecyloxy-4-methoxy-2,5-divinylbenzene (300 mg, 0.872 mmol) was dissolved under N_2 in a mixture of DMA (50 ml) and triethylamine (10 ml). This was followed by the addition of a catalytic amount (0.2 mol%) of *trans*-di(*μ*-acetato)-bis[*o*-(di-*o*-tolylphosphino)benzyl]dipalladium(II). The mixture was heated to 80 °C

for 3 hours. The reaction temperature was raised to 120 °C and the mixture stirred for 14 hours. Toluene (15 ml) was added to dissolve the precipitated polymer and the reaction mixture heated at reflux for a further 24 hours. The product was extracted with toluene, washed twice with 5% HCl and H_2O, and filtered through Celite. The solvent was removed to give deep dark red solid, which was redissolved in the minimum amount of hot toluene, precipitated twice into a mixture of methanol and acetone to yield 250 mg (45%) of poly[1,4-(2-dodecyloxy-5-methoxy)phenylene-vinylene].

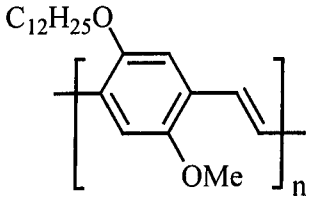

State : red solid

Absorption maximum: 458 nm

^{1}H NMR

Chemical shift (δ)	Integration ratio	Multiplicity	Correspondence
0.8	3	broad triplet	-CH_3(alkoxy group)
1.25-1.6	18	broad multiplet	-CH_2(alkoxy group)
1.85	4	broad quintet	-OCH_2CH_2(alkoxy)
4	2	broad	-OCH_2(alkoxy group)
3.9	3	broad singlet	-OCH_3
7.1	2	broad	**H**(vinylene)
7.45	2	broad	**H**(phenylene)

It proved impossible to record ^{13}C NMR with adequate signal to noise even using a large number of scans.

Elemental Analysis

Element	% Expected	% Found
C	79.74	74.91
H	10.12	9.22

GPC

Mn	Mp	Mw	Polydispersity
6625	10293	13221	1.9

2.5.2.3 Synthesis of poly[1,4-(2-dodecyloxy-5-methoxy)phenylene-vinylene] via Gilch reaction (GPPV12-1)

In a 250 ml flask, potassium tert-butoxide (0.522 g, 4.651 mmol) was dissolved in THF (100 ml) under argon and the solution was stirred for 15 minutes. A solution of 1,4-bis(chloromethyl)-2-dodecyloxy-5-methoxy-benzene (300 mg, 0.775 mmol) in THF (40 ml) was added dropwise over a period of 10 minutes at room temperature. During that time, the colour of the mixture changed from colourless to yellow to orange and the viscosity of the mixture increased. The reaction was allowed to proceed for 16 hours and the solvent was then removed. The residue was redissolved in the minimum amount of toluene and precipitated once in methanol. The collected polymer was precipitated twice in acetone and washed three times with water and stirred in acetone for 14 hours. The solvent was then removed and the product dried to yield 110 mg (45%) poly[1,4-(2-dodecyloxy-5-methoxy) phenylene-vinylene].

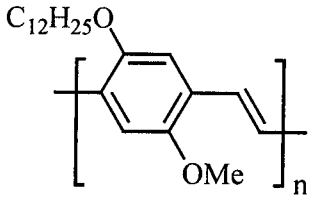

State : red solid

Absorption maximum: 500 nm

^{1}H NMR

Chemical shift (δ)	Integration ratio	Multiplicity	Correspondence
0.9	3	broad triplet	-CH_3(alkoxy group)
1.25-1.6	18	broad multiplet	-CH_2(alkoxy group)
1.85	4	broad quintet	-OCH_2CH_2(alkoxy)
4.1	2	broad	-OCH_2(alkoxy group)
3.95	3	broad	-OCH_3
7.12	2	broad	H(vinylene)
7.5	2	broad	H(phenylene)

It proved impossible to record ^{13}C NMR with adequate signal to noise even using a large number of scans.

Elemental Analysis

Element	% Expected	% Found
C	79.74	75.23
H	10.12	9.77

GPC

Mn	Mp	Mw	Polydispersity
153687	1054288	1164495	7.5

2.5.2.4 Synthesis of poly[1,4-(2-dodecyloxy-5-methoxy)phenylene-vinylene-co-(1,4-(2,5-dihexadecyloxy)phenylene-vinylene] via Heck reaction (PPV12-1/16-16)

A mixture of 1-dodecyloxy-4-methoxy-2,5-diiodo-benzene (133 mg, 0.246 mmol) and 1,4-dihexadecyloxy-2,5-divinylbenzene (150 mg, 0.246 mmol) was dissolved under N_2 in a mixture of DMF (50 ml) and triethylamine (10 ml). This was followed by the addition of a catalytic amount (0.2 mol%) of *trans*-di(*μ*-acetato)-bis[*o*-(di-*o*-tolylphosphino)benzyl]dipalladium(II), palladacycle. The mixture was heated to 120 °C and stirred for 14 hours. The product was extracted with toluene, washed twice with 5% HCl and H_2O, and filtered through Celite. The solvent was removed to give a dark red solid, which was redissolved in the minimum amount of hot toluene and precipitated twice into methanol to yield 120 mg (55%) of poly[1,4-(2-dodecyloxy-5-methoxy)phenylene-vinylene-co-(1,4-(2,5-dihexadecyloxy)phenylene-vinylene].

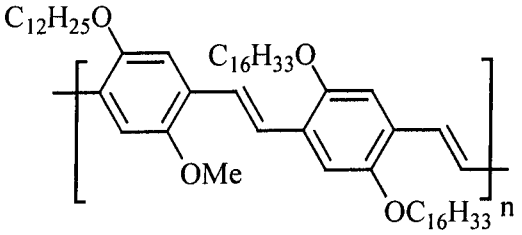

State : red solid

Absorption maximum: 446 nm

^{1}H NMR

Chemical shift (δ)	Integration ratio	Multiplicity	Correspondence
0.8	9	broad triplet	-CH_3(alkoxy group)

1.25-1.6	70	broad multiplet	-CH_2(alkoxy group)
1.85	6	broad quintet	-OCH_2CH_2(alkoxy)
4	6	broad	-OCH_2(alkoxy groups)
3.85	3	broad singlet	-OCH_3
7.1	4	broad	H(vinylene)
7.45	4	broad	H(phenylene)

It proved impossible to record ^{13}C NMR with adequate signal to noise even using a large number of scans.

Elemental Analysis

Element	% Expected	% Found
C	78.66	76.42
H	13.11	11.89

GPC

Mn	Mp	Mw	Polydispersity
5045	5029	6659	1.3

2.5.2.5 Synthesis of poly[1,4-{2-methoxy-5(2'-ethylhexyloxy)}phenylene-vinylene] via Gilch reaction (MEH-PPV)

In a 250 ml flask, potassium tert-butoxide (1.32 g, 11.8 mmol) was dissolved in THF (100 ml) under argon and the solution stirred for 15 minutes. A solution of 1,4-bis(chloromethyl)-2-methoxy-5-(2-ethylhexyloxy)-benzene (600 mg, 1.8 mmol) in THF (40 ml) was added dropwise over a period of 10 minutes at room temperature. During that time, the colour of the mixture changed from colourless to yellow to orange and the viscosity of the mixture increased. The reaction was stirred for 22 hours and after this time the volume of the reaction mixture was reduced to 50% and

the mixture was poured into MeOH to precipitate the polymer. The polymer was redissolved in toluene and washed with brine and twice with water. The polymer solution was concentrated and reprecipitated three times in acetone to yield 240 mg (51%) of poly[1,4-{2-methoxy-5(2′-ethylhexyloxy)}phenylene-vinylene].

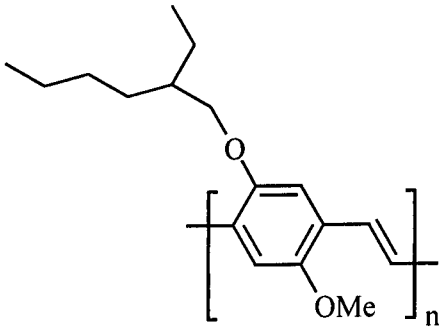

State : red solid

Absorption maximum: 500 nm

^{1}H NMR

Chemical shift (δ)	Integration ratio	Multiplicity	Correspondence
0.9	3	broad	-CH_3(alkoxy group)
1.25-1.6	52	broad multiplet	-CH_2(alkoxy group)
1.85	4	broad quintet	-OCH_2CH_2(alkoxy)
3.8	1	broad	-OCH(alkoxy group)
3.95	3	broad	-OCH_3
7.2	2	broad	H(vinylene)
7.5	2	broad	H(phenylene)

It proved impossible to record ^{13}C NMR with adequate signal to noise even using a large number of scans.

Elemental Analysis

Element	% Expected	% Found
C	78.46	78.26
H	9.23	10.14

GPC

Mn	Mp	Mw	Polydispersity
702995	1498385	1711824	2.4

2.6 References

1 D. Seyferth, F. G. A. Stone, *J. Am. Chem. Soc.* **1957**, *79*, 515

2 D. R. Coulson, *Inorg. Synth.*, **1972**, *13*, 121

3 W. A. Herrmann, C. Brossmer, H. Fischer, *Angew. Chem. Int. Ed. Engl.* **1995**, *34*, 1844.

4 W. A. Hermann, C. Reisinger, K. Oelfe, C. Brossmer, M. Beller, H. Fischer, *J. Mol. Catalysis*, **1996**, *108*, 51-56

5 A. S. Hay, *J. Org. Chem.* **1960**, *189*, 541

6 R. Broos, M. Anteunis, *Synth. Commun.* **1976**, *6*, 53-57

7 Philip Bentley, PhD Thesis, University of Sheffield, **1999**

8 J. Lim, M. Suzuki, T. Masato, *Polym. Bull.*, **1993**, *31*, 651

9 D. Braun, A. J. Heeger, *Appl. Phys. Lett.* **1991**, *58*, 1982

10 G. Gustafsson, Y. Gao, G. M. Treacy, F. Klavetter, N. Colaneri, A. J. Heeger, *Nature* **1992**, *357*, 477

11 G. J. Sarnecki, P. L. Burn, A. Kraft, R. H. Friend, A. B. Holmes, *Synth. Met.* **1993**, *55*, 914

Chapter 3: Results and Discussion-Synthesis

This Chapter describes the synthesis of soluble conjugated polymers for use in low-cost photovoltaic cells. Polymers of particular interest are those that can absorb within the most intense region of the solar spectrum i.e. between 400 and 700 nm.

For the preparation of suitable phenylene monomers, we first investigated the Stille coupling reaction to prepare divinyl monomers using tributylvinyltin as a reagent. We also prepared diethynyl monomers using 2-methyl-3-butyn-2-ol or trimethylsilylacetylene as a source of the alkyne followed by deprotection hydrolysis to produce diethynyl benzenes. Chloromethyl substituted monomers were prepared by one-step chloromethylation reaction using paraformaldehyde and KCl/H_2SO_4 as the source of HCl.

For the polymerisation, we applied the Heck reaction, which involves a palladium-catalysed coupling between vinyl or ethynyl substituted aryl monomers with aryl halides and the Gilch reaction involving dehydrochlorination of chloromethyl substituted aryl monomers.

3.1 Preparation of monomers

3.1.1 Synthesis of divinyl substituted benzenes via the Stille reaction

The preparation of divinyl-substituted benzenes is a three-step reaction as shown in Fig. 3.1.1. The synthetic procedure started from hydroquinone (**3.1**) and as the reaction between hydroquinone and bromododecane proceeds, the colour of the solution turns to dark red. This reaction mixture required mechanical stirring at above

80°C for 14 hours to assure the efficient distribution of the potassium carbonate. The first recrystallisation provided pure product (**3.2**) according to ^{1}H NMR spectroscopy.

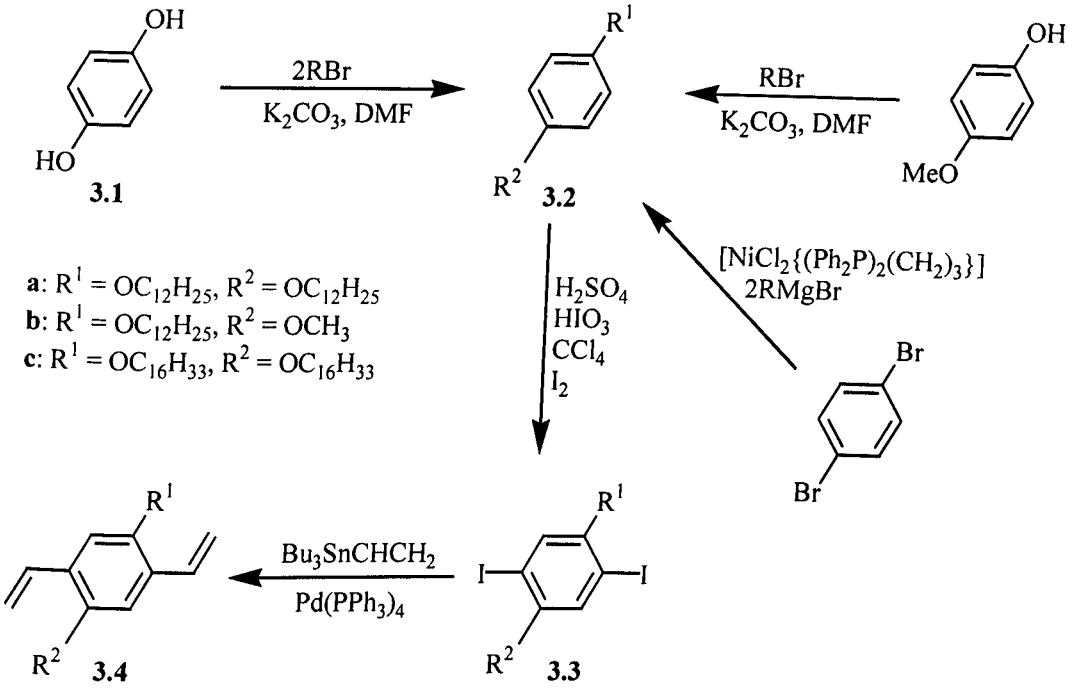

Fig 3.1.1 Preparation of divinyl substituted benzenes via the Stille reaction

Subsequent iodination of **3.2** requires the presence of an oxidising agent, H_2SO_4, and an acidic medium such as acetic acid. Purification of the product (**3.3**) is very tedious and it must be recrystallised at least three times from ethanol, as each time a small amount of immiscible oily material remains at the bottom of the flask. This immiscible material must be removed completely as although it cannot be detected in the ^{1}H NMR spectrum it has been found to cause problems in the subsequent coupling reaction.

Stille reaction

The cross coupling of tributyl-vinyl-stannane with various aryl halides in the presence of a palladium catalyst has been demonstrated by Stille[1] and others[2,3,4] to be a highly efficient method for the preparation of styrene derivatives. This methodology has been employed to develop an efficient synthesis of 1,4-dialkyl and 1,4-dialkoxy substituted 2,5-divinylbenzenes.

Reaction of **3.3** with tributyl-vinyl-stannane in the presence of a palladium catalyst required high temperatures (>80 °C) and extended reaction times. The products, 1,4-dialkyl and 1,4-dialkoxy substituted 2,5-divinylbenzenes, **3.4**, were isolated (55%) in the necessary purity for polymerisation reactions by column chromatography and a recrystallisation. To ensure that the products are free of any organotiniodide impurities it was necessary to treat the reaction mixture with potassium fluoride to precipitate insoluble tributyltinfluoride, which may be removed by filtration through Celite.

A range of reaction conditions was employed to optimise the yield of **3.4**. The best conversions were obtained using a palladacycle catalyst, **3.5**, prepared by reaction of palladium acetate and tri(*o*-tolyl)phosphine, in toluene at a temperature below reflux.

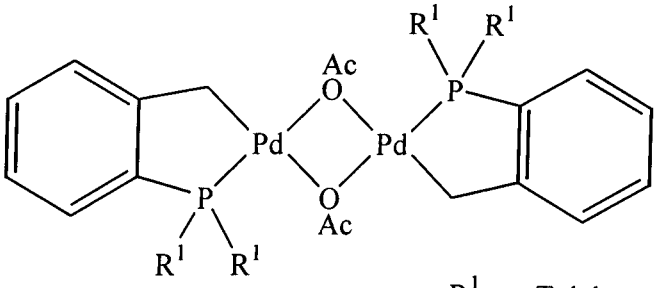

3.5

This palladacycle catalyst, **3.5**, was found to be more stable at high temperatures than tetrakis(triphenylphosphine)palladium. No reaction was detected at reaction temperatures below 80 °C and at temperatures close to toluene reflux (110 °C) the reaction time was much reduced but the isolated yield was very low (25%). The highest isolated yield (55%) of pure product was obtained after 40 hours at 90 °C. The cross coupling of tributyl-vinyl-stannane with the analogous substituted dibromobenzenes was also possible. However, a higher reaction temperature (100 °C) was required to achieve complete conversion and it was necessary to add an extra equivalent of the catalyst after 40 hours in order to isolate 45% of the coupled product after 90 hours.

3.1.2 Synthesis of diethynyl-substituted benzenes using 2-methyl-3-butyn-2-ol[5]

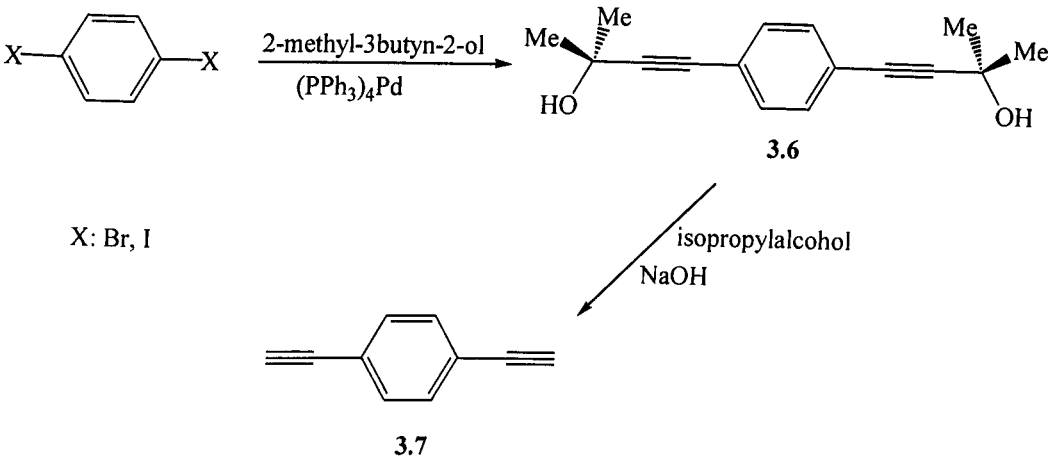

Fig 3.1.2 Preparation of diethynyl-substituted aryls from 2-methyl-3-butyn-2-ol

1,4-Dibromobenzene reacts rapidly with 2-methyl-3-butyn-2-ol at room temperature in the presence of PPh_3 and $CuI/Pd(PPh_3)_4$. Yellow needles of the product (**3.6**) were isolated by recrystallisation in toluene. Analogous reaction of 2,5-dibromopyridine gave a quantitative yield of the disubstituted product as indicated by TLC and ^1H NMR spectroscopy, but unfortunately it proved impossible to isolate the product. Reaction with 2,5-dibromothiophene tended to give a mixture of the mono- and diethynylated thiophene regardless of reaction time, temperature and the amount of added catalyst.

Hydrolysis of the product (**3.6**) was attempted in a variety of solvents (1-butanol, isopropyl alcohol, ethanol) using several different bases (KOH, NaOH, NaH and

K_2CO_3). The best results were obtained using isopropyl alcohol and one equivalent of NaOH at the reflux temperature for 2 hours. The hydrolysis proceeds much faster in 1-butanol as it has a higher boiling point, but reaction in this solvent led to decomposition of the product (**3.7**). Due to the high temperature required for the hydrolysis that led to decomposition of the product and hence low yield, it was decided to try a different route to synthesise diethynylbenzenes using trimethylsilylacetylene (TMSA).

3.1.3 Synthesis of alkoxy substituted diethynylbenzenes using TMSA

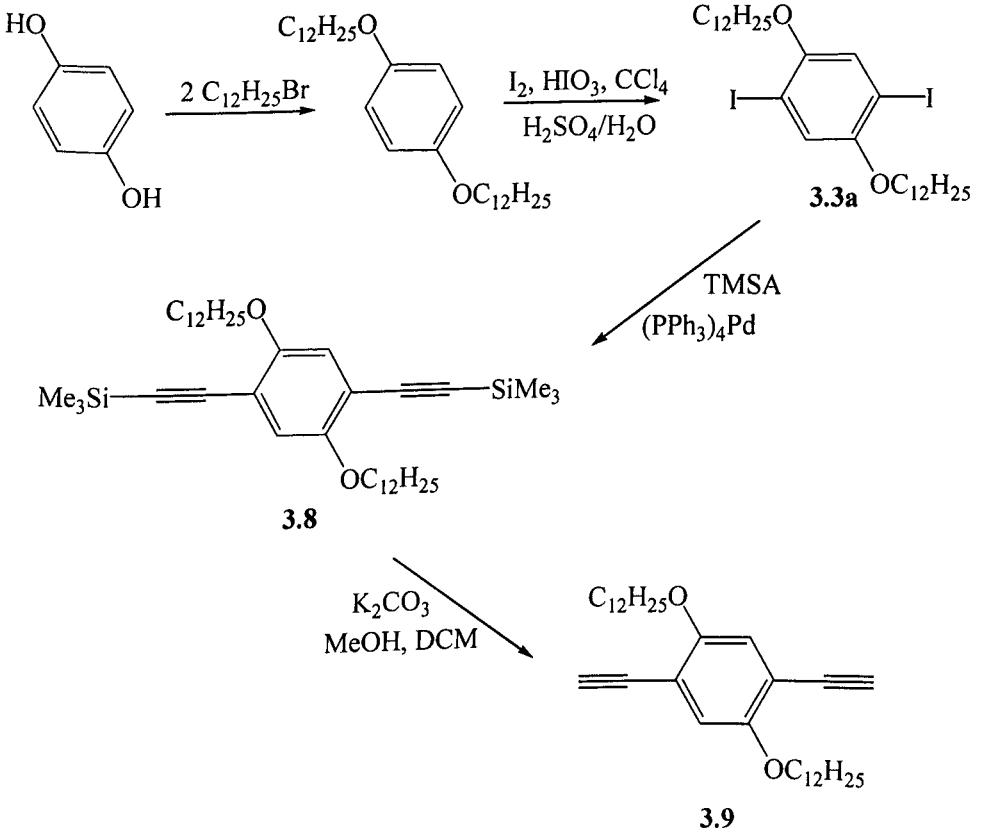

Fig 3.1.3 Preparation of alkoxy-substituted diethynylbenzenes using TMSA

Coupling of trimethylsilylacetylene with 1,4-didodecyloxy-2,5-diiodobenzene (**3.3a**) used the same catalytic system as for ethynylation with 2-methyl-3-butyn-2-ol, but the reaction was carried out at higher temperature (80°C)[6]. The intermediate product (**3.8**), 1,4-didodecyloxy-2,5-bis(trimethylsilylethynyl)benzene, could be recrystallised from cold ethanol or acetone in about 75%. The trimethylsilyl group can be easily removed under very mild conditions[7], i.e. DCM/methanol as the solvent and K_2CO_3 as the base at room temperature. A single recrystallisation from acetone gave a pure product (**3.9**) as yellow-orange crystals in a yield of about 80%.

3.1.4 Synthesis of bis(chloromethyl)-dialkoxybenzenes

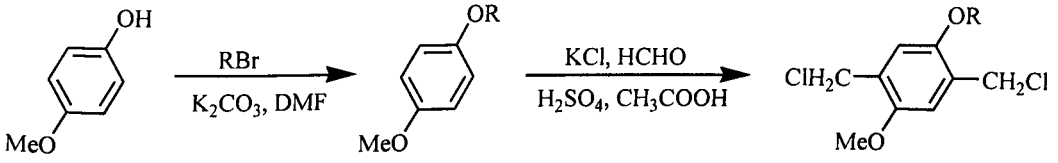

3.10: R = 2-ethylhexyl
3.2b: R = dodecyl group

3.11a: R = 2-ethylhexyl
3.11b: R = dodecyl group

Fig 3.1.4 Preparation of bis(chloromethyl)-dialkoxybenzenes

The chloromethylation of dialkoxy-substituted benzenes has been reported[8,9,10]. The procedure reported was carried out in presence of paraformaldehyde and under a flow of HCl gas stream for 72 hours. In order to avoid the harmful hazards of HCl gas, we used KCl and H_2SO_4 to evolve HCl gas *in situ*.

Several reaction temperatures were applied, the best conversion was obtained at a temperature of 80°C for the preparation of 2,5-*bis*-chloromethyl-1-(2-ethyl-

hexyloxy)-4-methoxy benzene (**3.11a**) and 60°C for the preparation of 2,5-*bis*-chloromethyl-l-dodecyloxy-4-methoxybenzene (**3.11b**). The low yield (10%) obtained for the preparation of 2,5-bis-chloromethy-l-dodecyloxy-4-methoxybenzene was attributed to the poor solubility of l-dodecyloxy-4-methoxy benzene in acetic acid. Column chromatography purification was needed to obtain high purity products, which are essential for reproducible polymerisation chemistry.

3.2 Polymerisation

Recently, synthetic methods employing transition metal catalysed C-C bond forming reactions such as the Heck reaction have been exploited in the synthesis of substituted soluble conjugated polymers[11,12,13]. This methodology involves two main steps. The first step is the oxidative addition of the aryl halide to a Pd(0) complex to form the intermediate Ar-Pd(L_2)-X. This compound subsequently undergoes reaction with the vinyl compounds to give an alkyl halide palladium complex. Elimination of the Ar-vinyl product regenerates the Pd catalyst on reaction with a base[14,15].

Palladium-catalysed polymerisation allows for the fine-tuning of the polymer chemical structure to match the required application. This can be achieved by the coupling of monomers that carry various substituents such as the electron-donating alkoxy groups that increase the solubility of the resulting polymer and also enhance the conjugation along the polymer chain and hence lower the polymer band gap energy.

In synthetic organic chemistry only a small variety of palladium complexes are employed as catalyst precursors[16]. These complexes are generally stabilised by phosphine ligands. Examples of complexes used in this work are tetrakis(triphenylphosphine)palladium(0) and the palladacycle (**3.5**). This catalyst has shown advantage over tetrakis(triphenylphosphine)palladium(0), which is attributed to the presence of carbon-metal bond[17]. The main advantage of this moisture and air stable catalyst is the long lifetime, even under severe reaction conditions, with negligible precipitation of palladium black during catalysis. Tetrakis(triphenylphosphine)palladium(0) catalyst works well for the synthesis of poly(1,4-phenylene-ethynylene), but not for the synthesis of poly(1,4-phenylene-vinylene) as it decomposed at high temperatures that are required for these reactions.

3.2.1 Synthesis of poly(1,4-phenylene-ethynylenes)

The palladium catalysed coupling of aryl iodides and bromides with terminal acetylenes is a well-established synthetic method as reported independently by L. Cassar[18] and R. F. Heck[19]. Poly(phenylene-ethynylene) has been prepared previously by Sonogashira coupling of diethynylbenzenes and dihalobenzenes[20,21]. The synthesis of soluble alkoxy-substituted poly(arylene-ethynylenes) has recently been introduced by R. Giesa[6,22] who also employed a Heck cross-coupling using $(PPh_3)_2PdCl_2$ as a catalyst, CuI as a cocatalyst and triethylamine as a base in the synthesis of poly[1,4-(2,5-dialkoxy)phenylene-ethynylene]. Despite the long alkoxy groups (hexyloxy,

decyloxy and heptadecyloxy) used in his synthesis the solubility of these polymers was poor.

3.2.1.1 Synthesis of poly[1,4-(2,5-didodecyloxy)phenylene-ethynylene-co-(1,4-phenylene-ethynylene)] (PPE-1)

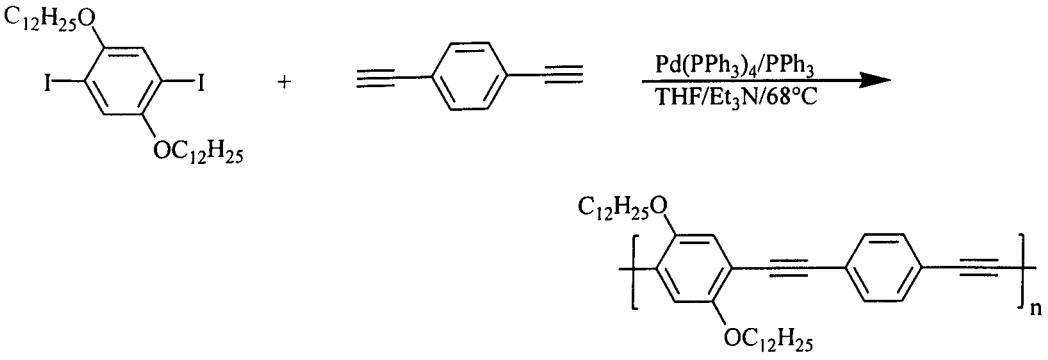

PPE-1

The polymerisation proceeded very slowly in refluxing THF and resulted in a low molecular weight polymer, PPE-1, (about 3,000 according to GPC) (Mn) as the reaction temperature (68°C) presumably was too low. This reaction was not repeated at higher temperatures as the starting material, 1,4-diethynylbenzene, was difficult to handle at high temperatures. It was found that for such low molecular weight polymers, petroleum ether is a good reprecipitation medium.

^{1}H NMR spectroscopy showed broad peaks at 6.95 and 7.16 ppm for the substituted and unsubstituted phenylene protons respectively, which were slightly shifted downfield to the corresponding peaks of the starting materials. No signal was observed for the acetylenic CH protons of the starting material.

3.2.1.2 Synthesis of poly[1,4-(2,5-didodecyloxy)phenylene-ethynylene-co-(2,5-thienylene-ethynylene)] (PPET)

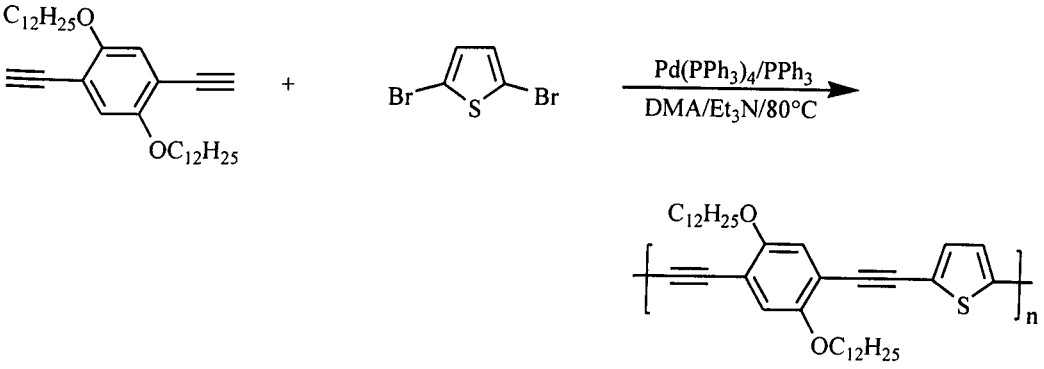

PPET

The polymerisation was carried out in DMA to increase the reaction temperature and hence accelerate the oxidative addition step to favour the formation of high molecular weight chains. Commercial 2,5-dibromothiophene is supplied in 95% purity, the main impurities are other isomeric structures as 2,3- and 3,4-dibromothiophene. The 2,5-dibromothiophene used in this polymerisation was redistilled in a spinning band distillation column to remove these traces of other isomers. The polymerisation reaction was completed in only 3 hours to yield high molecular weight polymer, PPET, (about 60,000 as estimated by GPC). The high molecular weight is suggested to be due to the extremely high purity of 2,5-dibromothiophene and the diethynyl monomers.

The polymer was poorly soluble in DCM but dissolves readily in hot toluene. The polymer was precipitated three times into acetone.

^{1}H NMR spectroscopy showed broad peaks at 4.03, 6.98 and 7.16 ppm for the OCH_2 (alkoxy group), phenylene and thienylene protons respectively, which were ~ 0.1 ppm downfield of the corresponding peaks of the starting materials. The acetylenic CH signal of the alkyne proton of the starting material at 3.25 ppm had completely disappeared.

3.2.1.3 Synthesis of poly[1,4-(2,5-didodecyloxy)phenylene-ethynylene-co-1,4-(2-nitro-phenylene-ethynylene)] (PPE-NO_2)

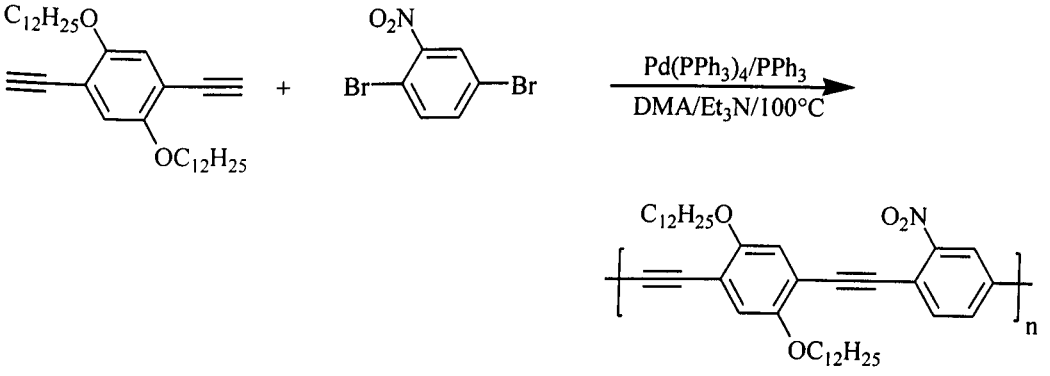

PPE-NO_2

This polymerisation was carried out in a mixture of DMA and toluene at 100°C for 16 hours. At the end of the reaction a suspension was formed, which indicated that the high molecular weight polymer was not soluble in a hot DMA/toluene mixture. The resulting polymer (PPE-NO_2) was redissolved in hot toluene and precipitated into a mixture of methanol and acetone.

The GPC estimated molecular weight (Mn) is 12,000. The low molecular weight is attributed to the poor solubility of the polymer in DMA/toluene mixture.

^{1}H NMR spectroscopy showed broad peaks at 7.0, 7.6 and 8.2 ppm for the phenylene and nitrophenylene protons respectively compared to 6.9, 7.5 and 8.1 for the starting materials. The 0.1 ppm chemical shift downfield is presumably due to the enhanced conjugation in the polymer chain and also to the pull-push system introduced by the NO_2 and OR substituents. The acetylenic CH signal of the alkyne proton of the starting material was not detected.

The complete disappearance of the acetylenic CH signal of the alkyne proton of the starting material at 3.25 ppm in all poly(1,4-phenylene-ethynylenes) indicates that the end groups were assumed to be mostly bromine and iodine substituents. This is in agreement with the characterisation of previously synthesised alkoxy-substituted poly(1,4-phenylene-ethynylene), recently reviewed by Bunz[23].

3.2.2 Synthesis of poly(1,4-phenylene-vinylenes)

Palladium catalysed coupling reactions have been used by various groups to produce conjugated polymers such as poly(1,4-phenylene) (PPP), polyfluorenes, poly(phenylene-vinylene) (PPV) and poly(phenylene-ethynylene)[24,25,26]. Wegner *et al.*[24,27,28,29] studied the synthesis of PPPs using the palladium catalysed Suzuki reaction[30,31], where an aromatic diboronic acid ester and an aromatic dibromide are coupled to give regioregular polymers of greater than 50 repeating units.

W. Heitz *et al*[32] used palladium coupling in the form of the Heck reaction to synthesise substituted PPVs. The coupling of ethylene with dibromobenzenes described by Heitz opens up a very flexible route to the synthesis of substituted PPV.

Unfortunately, the materials made by this route are, up to now, of low molecular weight and of indeterminate regioregularity.

L. Yu *et al*[33,34,35] have synthesised substituted PPP, poly(phenylene-thienylene) (PPT) and PPV using the palladium catalysed Stille[1] coupling reaction, where distannyl benzenes/thiophenes or distannyl ethylene are coupled with diiodo benzenes.

We have employed the Heck reaction to prepare PPV polymers using alkoxy-substituted divinyl monomers prepared by the Stille reaction.

3.2.2.1 Synthesis of poly(1,4-phenylene-vinylenes) by transition metal catalysed polymerisation

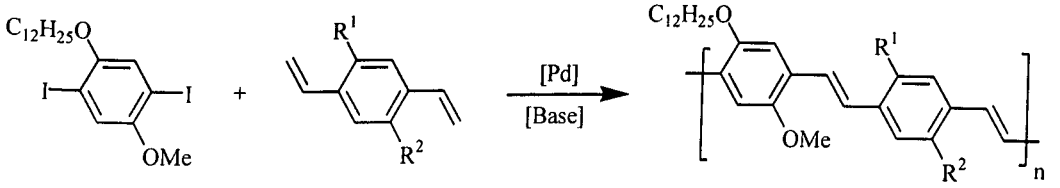

PPV12-1: $R^1 = H, R^2 = H$
PPV12-1/12-1: $R^1 = OC_{12}H_{25}, R^2 = OCH_3$
PPV12-1/16-16: $R^1 = OC_{16}H_{33}, R^2 = OC_{16}H_{33}$

Fig. 3.2.2.1: Preparation of PPV by transition metal catalysed polymerisation

The synthetic method involved the initial synthesis of the required dialkoxybenzenes with a subsequent iodination of these materials. Previous work at the University of Sheffield, carried out by Philip Bentley[36], showed that the Heck reaction of dibromobenzenes with divinyl benzenes required a reaction temperature greater than 125 °C and extended reaction times to proceed and the resulting polymers were found

to have very low molecular weight. A possible reason for the low molecular weight and extended reaction times required could be that the rate-determining step for the Heck reaction is the oxidative addition of the aryl-halogen bond at Pd. The palladium catalysts are electron rich species and therefore the oxidative addition step is more favourable when the aryl ring is electron deficient. Dialkoxybenzenes are electron rich moieties and therefore the oxidative addition is disfavoured. The use of more labile iodide improved the rate of the oxidative addition step. The Heck reaction with analogous diiodo compounds proceeded at ~ 100 °C in less than 2 hours.

One problem encountered with the Heck reaction was its irreproducibility. The reaction would work fine for one diiodo material and then would fail completely for a very similar reagent. If the reaction did not work, the solution would become brown and work up of the reaction mixture would yield only the starting materials with no trace of conjugated material. This irreproducibility was apparent even after the solvent and base were rigorously purified in addition to the starting divinyl and the diiodobenzenes. Unsubstituted divinylbenzene was routinely purified by sublimation, dialkoxy substituted divinylbenzenes were purified by column chromatography and the diiodobenzenes were recrystallised until HPLC gave a purity of greater than 99%.

After extensive investigations, the problem with the polymerisation reaction was traced to the diiodobenzenes, if the dialkoxybenzene is iodinated at too higher temperature or for too long, then on recrystallisation a yellow oily precipitate was observed in small quantities. This material was nearly insoluble in the recrystallisation solvent unless heated for prolonged periods. When this impurity was

added to a test Heck reaction, even in very small quantities, it appeared to poison the catalyst and release molecular iodine.

A test was devised by Philip Bentley[36] to check that the diiodo compounds were pure enough for polymerisation. This test involved heating the precursor (substituted diiodobenzene) in DMF with dry sodium acetate. If the mixture turned a clear sky blue then the Heck reaction would not work and the diiodo material would need further purification. To be totally sure a drop of styrene would be added to the mixture along with a small amount of catalyst and heated again. If fluorescence was observed when irradiated with light of wavelength 354 nm then the substituted diiodobenzene would undergo the Heck reaction.

Recent results from workers at Sheffield suggests that the problem with the purity of diiodobenzenes is inclusion of elemental sulphur with the diiodo materials. It seems that sulphur readily crystallises with the diiodo materials and is very difficult to totally remove from the products. The source of this sulphur at this point seems to be the sodium thiosulphate work up.

Unfortunately, several attempts at incorporating thiophene and bithiophene units into the polymer chain were unsuccessful. The monomers used were dibromothiophene, diiodothiophene and diiodobithiophene. The failure of these reactions was attributed to the high temperature required for the oxidative addition of these monomers and also due to the instability of the thienylene-vinylene moieties. However, when 2,5-dibromo-3,4-dinitrothiophene was employed, insoluble material was obtained and the 1,4-dialkoxy-2,5-divinylbenzene was recovered unchanged after 16 hours of reaction

time at 110°C. This observation suggested that the self-polymerisation of the 2,5-dibromo-3,4-dinitrothiophene was occurring.

Characterisation of the polymers by NMR spectroscopy

The polymers were characterised by ^{13}C, ^{31}P and ^{1}H NMR spectroscopy using 15 mg of sample in 0.5 ml of $CDCl_3$. The ^{31}P NMR spectra were used to check for the presence of residual catalyst and no signals were observed in any of the spectra. This proved that a single Celite filtration of a toluene solution of the isolated polymer was adequate to filter off any catalyst residuals.

A common feature of the ^{1}H NMR spectra of the Heck polymers is the presence of the peaks corresponding to vinyl endgroups at 5.2, 5.7 and 6.95 ppm. Integration of these peaks in the ^{1}H NMR spectrum of PPV12-1, assuming that the polymer has two vinyl endgroups per polymer molecule, gives a degree of polymerisation of 14 repeating units, which is in agreement with the GPC estimated molecular weight value (6,083). Analysis of the vinyl endgroups for PPV12-1/16-16 shows that it has only 6 repeating units, which agrees well with the GPC estimated molecular weight (5,045). The low degree of polymerisation is due to the poorer solubility of this polymer. Although the inclusion of long alkoxy groups should result in an increase of the solubility of the resulting polymer, it was found that polymerisation of monomers that are symmetrically substituted with long alkoxy groups (C_8 and above) resulted in polymers with poor solubility. Analysis of the ^{1}H NMR spectrum of PPV12-1/12-1 shows that the polymer has 10 repeating units that is also in agreement with the GPC estimated molecular weight (6,625).

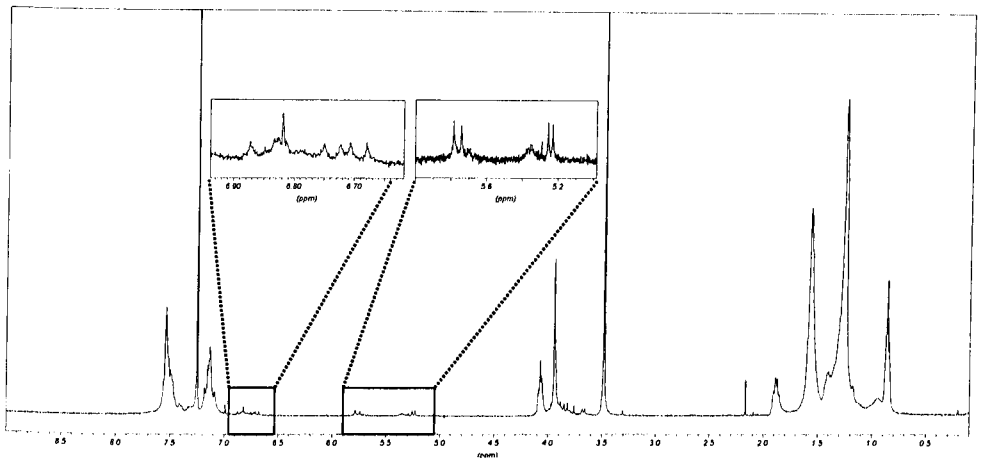

Fig. 3.2.2.1a: ^{1}H NMR spectrum of PPV12-1, showing expansions of the signals associated with the 1,1 links and the cis-olefinic links

Another common observation for all of the polymers synthesised by the Heck reaction that is only visible using high field ^{1}H NMR spectroscopy is the presence of two broad doublets at 5.36 and 5.71 ppm (Fig. 3.2.2.1a). These signals are due to 1,1 links (Fig. 3.2.2.1b) introduced into the polymer chain. Integration of these peaks against the methoxy protons signals gives a proportion of ~ 2 % of 1,1 links in the polymer backbone.

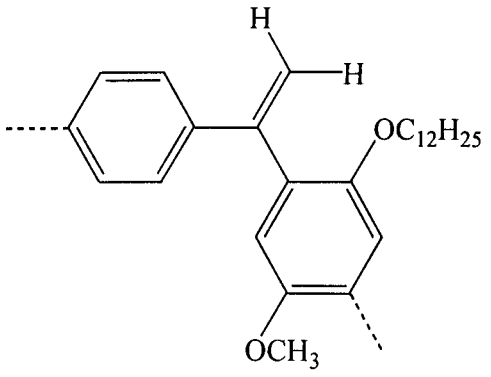

Fig. 3.2.2.1b: Schematic drawing of the proposed 1,1 link

In addition, several signals are observed between 6.68 and 6.88 ppm, which can be assigned to cis-olefinic protons (Fig. 3.2.2.1c). These peaks are too small for an accurate integration, suggesting that the cis-olefinic links occur at below 1%.

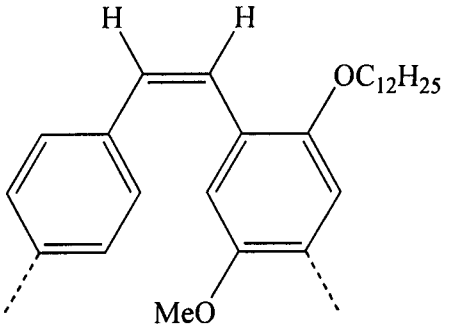

Fig. 3.2.2.1c: Schematic drawing of the proposed cis-olefinic link

^{13}C NMR spectra were very difficult to interpret for these polymers as it proved impossible to achieve adequate signal to noise even with large number of scans at high field.

3.2.2.2 Synthesis of poly(1,4-phenylene-vinylenes) by dehydrohalogenation

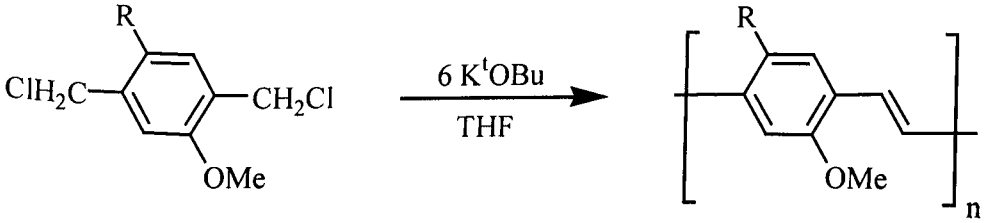

MEH-PPV: R = 2-ethylhexyloxy group
GPPV12-1: R = dodecyloxy group

Fig. 3.2.2.2: Preparation of PPV by dehydrochlorination polymerisation

The Gilch reaction is a well-established route for the synthesis of soluble 1,4-phenylene-vinylenes polymers via dehydrohalogenation of bis-halomethylbenzenes[8,37,38]. One problem encountered with the Gilch reaction is that gelation always occurs during the polymerisation process, especially when the polymer is prepared from the bis-bromomethyl monomer through the Gilch route. Control of the gelation and polydispersity has recently been improved by the use of a benzylic halide compound as a terminator[39]. The length of the chain and the chemical structure of the solubilising alkoxy side chains play a crucial role in determining the solubility of the resulting polymer.

The synthesis of the much-studied poly[2-methoxy-5(2'-ethylhexyloxy)-1,4-phenylene-vinylene], MEH-PPV, as shown in Fig. 3.2.2.2, was reported by Heeger *et al*[8,40]. A related polymer **3.12** with a 3,7-dimethyloctyloxy side chain has been the subject of investigation by workers at Philips[41] and Hoechst[42].

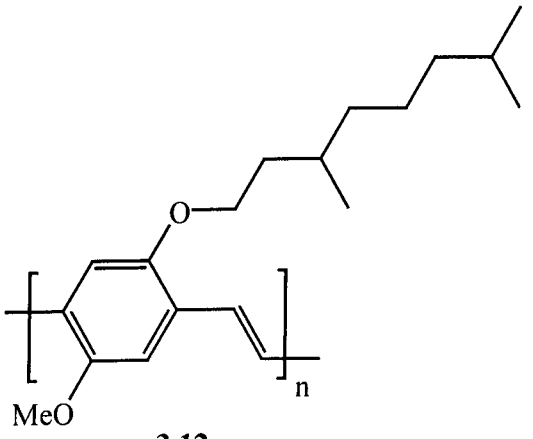

3.12

The Gilch reaction was found to be extremely efficient in achieving high molecular weight, soluble, homopolymers (MEH-PPV and GPPV12-1). Copolymerisation of

dialkoxy-substituted 1,4-bis(chloromethyl)benzenes with 2,5-bis(chloromethyl)-thiophene with different molar ratios of the two monomers (1:1, 2:1, 5:1 respectively) resulted in insoluble material with a metallic appearance. This suggests that the dehydrochlorination of 2,5-bis(chloromethyl)-thiophene occurred faster than that of the dialkoxy-substituted 1,4-bis(chloromethyl)benzenes resulting in the formation of insoluble unsubstituted poly(thienylene-vinylene).

Dehydrochlorination polymerisation of symmetrically substituted 1,4-bis(chloromethyl)-benzenes, such as 2,5-dioctyloxy-1,4-bis(chloromethyl)benzene and 2,5-didodecyloxy-1,4-bis(chloromethyl)benzene, resulted in polymers that have poor solubility in commonly used organic solvents such as THF, toluene and xylene.

In these reactions, the molar ratio of the base used is also important to ensure complete dehydrohalogenation into a fully conjugated polymer. In this work, six molar equivalents of potassium tert-butoxide were found to be sufficient to ensure complete dehydrohalogenation of the monomers.

The solubility of MEH-PPV is believed to be enhanced by the branched nature of the ethylhexyloxy side-chain. It was found that poly[2-methoxy-5-dodecyloxy-1,4-phenylene-vinylene], GPPV12-1, is less soluble than MEH-PPV in THF.

The estimated GPC molecular weight (Mn) was 700,000 for MEH-PPV and 150,000 for polymer GPPV12-1. This is attributed to the solubility difference of both polymers in THF, which is used as solvent for the dehydrohalogenation polymerisation reaction. In comparison to the molecular weight of previously

discussed polymers prepared by transition metal catalysed coupling reactions, MEH-PPV and GPPV12-1 showed a great increase in the molecular weight. This shows that the dehydrohalogenation chain-growth polymerisation is much more efficient in the synthesis of conjugated polymers than the step-growth condensation reactions in terms of molecular weight of the resulting polymers.

Characterisation of the polymers by NMR spectroscopy

Due to the high molecular weight of these polymers, NMR samples were prepared using a maximum amount of 5 mg in 0.5 ml of $CDCl_3$.

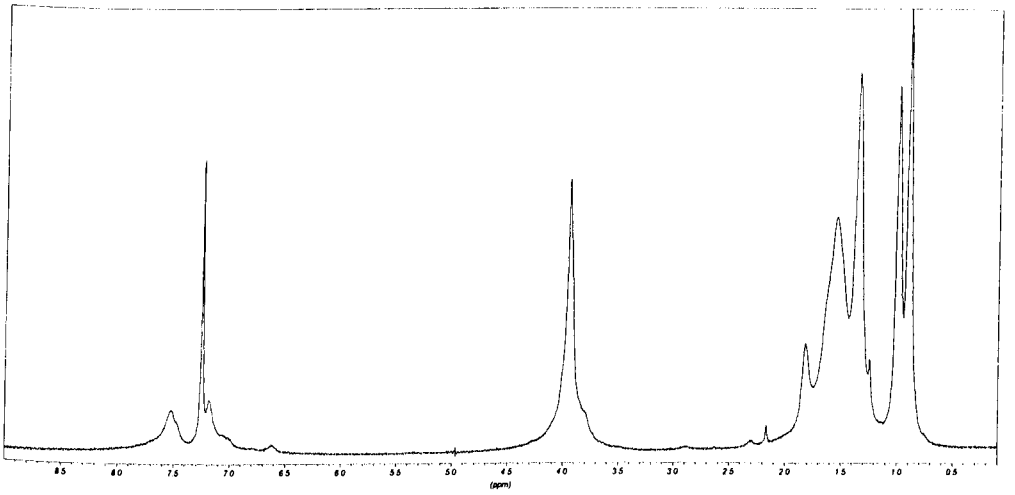

Fig. 3.2.2.2a: ^1H NMR spectrum of MEH-PPV, showing the absence of signals associated with the vinyl endgroups and the 1,1 and cis-olefinic links

One of the characteristics features of the ^1H NMR spectra of all polymers synthesised by the Gilch reaction is the absence of peaks related to 1,1 links and cis-olefinic links (Fig. 3.2.2.2a) that were observed in all polymers prepared by the Heck polymers. This suggests that polymers synthesised by the Gilch reaction are regioregular and

free of the 1,1 and cis-olefinic links defects that are common in polymers prepared by the Heck reaction.

Another common observation of the Gilch polymers is the disappearance of peaks at 4.6 ppm related to the chloromethyl endgroups. This might be due to the high molecular weight of these polymers.

3.3 Optical properties of synthesised polymers

3.3.1 Solution absorption and photoluminescence

The solution UV-Vis absorption and photoluminescence spectra were measured in dilute DCM solution.

3.3.1.1 Poly(1,4-phenylene-ethynylene)

Absorption spectroscopy showed that PPE-1 absorbs at 406 nm. The blue shift from PPV polymers was suggested to be due to exciton confinement that is attributed to the shortened conjugation length, which is realised by introduction of C-C triple bonds in the main chain of conjugated polymers[43]. This effect of C-C triple bonds was suppressed by the introduction of an electron-rich moiety such as thiophene, which increased the effective conjugation length, and hence red shifts the absorption of PPET that occurred at 450 nm. The red shift in the absorption of PPE-NO_2, which occurred at 448 nm, is attributed to the pull-push system of the electron-withdrawing nitro group and the electron-donating alkoxy group.

	GPC (Mn)	Absorption (nm)	Photoluminescence (nm)
PPE-1	3,128	406.7	448
PPET	61,633	451.2	489
PPE-NO_2	12,154	448.6	Quenched

Table 3.3.1.1: Solution UV-Vis absorption and photoluminescence data for PPE polymers

3.3.1.2 Poly(1,4-phenylene-vinylene) via Heck

	GPC (Mn)	Absorption (nm)	Photoluminescence (nm)
PPV12-1	6,083	457.6	515.8
PPV12-1/16-16	5,045	445.6	537.2
PPV12-1/12-1	6,625	448.6	524

Table 3.3.1.2: Solution UV-Vis absorption and photoluminescence data for Heck PPV polymers

Both the absorption and photoluminescence data are very similar, which is expected to be the case as the chromophore (the polymer backbone) should be exactly the same in all materials. Although PPV12-1/12-1 and PPV12-1/16-16 have four electro-donating groups per repeating unit, they absorb at shorter wavelengths than that of PPV12-1 that has only two alkoxy substituents per repeating unit. This is difficult to

account for, as the conjugation of PPV12-1/12-1 and PPV12-1/16-16 should be enhanced by the increase of the number of the electron-donating groups and as such they should be red-shifted. A possible answer for this is that PPV12-1 has slightly better conjugation because there is only one long alkoxy chain that can sterically hinder coplanarity.

Absorption occurs in all parts of all chains simultaneously, as all chromophores will absorb a certain part of the incident radiation. The absorption of radiation generates an excited state (exciton) that has a certain lifetime. This exciton can move up and down along the polymer chain as long as it always moves onto segments with lower exciton energies, within this lifetime. Segments with all trans regioregularity will have lower exciton energies and thus excitons will tend to migrate to these areas before decaying to the ground state, emitting a photon characteristic of the energy of that segment. From the photoluminescence data (Table 3.3.1.2), it seems that PPV12-1/16-16, due to the presence of three long alkoxy chains, fluoresces at longer wavelengths. One possible reason for this could be that the defect density in PPV12-1/16-16 is less than in PPV12-1 and PPV12-1/12-1 and hence this polymer has regions of more extended conjugation.

3.3.1.3 Poly(1,4-phenylene-vinylene) via Gilch

	GPC (Mn)	Absorption (nm)	Photoluminescence (nm)
MEH-PPV	702,995	504	555
GPPV12-1	153,687	500	549

Table 3.3.1.3: Solution UV-Vis absorption and photoluminescence data for Gilch PPV polymers

As can be seen from Table 3.3.1.3, the absorption and photoluminescence spectra are extremely similar for these polymers. This similarity is due to the similar structure and the regioregularity of these polymers. The UV-Vis absorption spectra of Gilch PPV polymers are red-shifted by 40-50 nm from those PPV polymers prepared by the Heck reaction. This is attributed to the higher molecular weight and hence more extended length of effective conjugation and the higher regioregularity of Gilch polymers.

3.3.2 Solid-state absorption and photoluminescence

Polymers were spin coated from toluene solution (5 mg/ml) onto spectrosil B quartz disks to produce thin films. Absorption measurements were recorded using an ATI Unicam UV-Vis spectrometer. Photoluminescence measurements were recorded using a gallium nitride LED to excite the sample and emission was detected using a CCD detector (Instaspec IV), via a spectrograph (Oriel Bi UV 836).

3.3.2.1 Poly(1,4-phenylene-ethynylene)

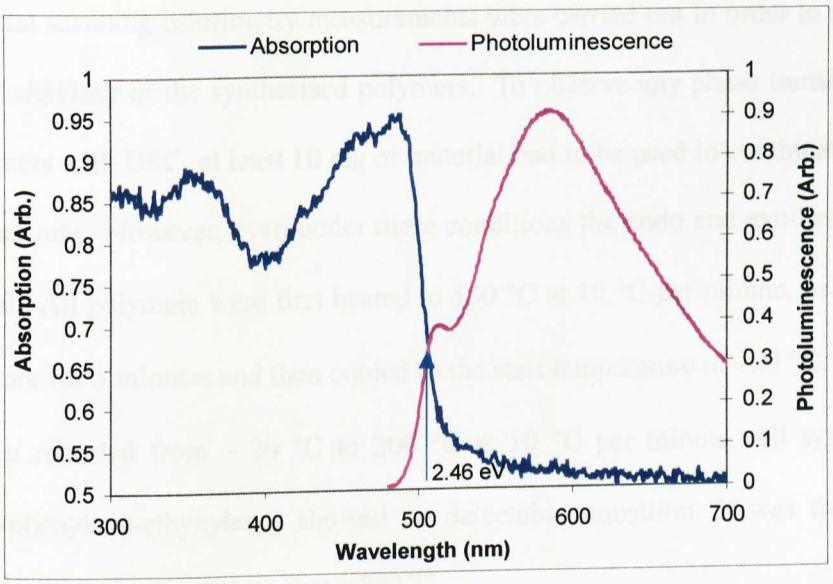

Fig. 3.3.2.1a: Absorption and photoluminescence spectra of PPET

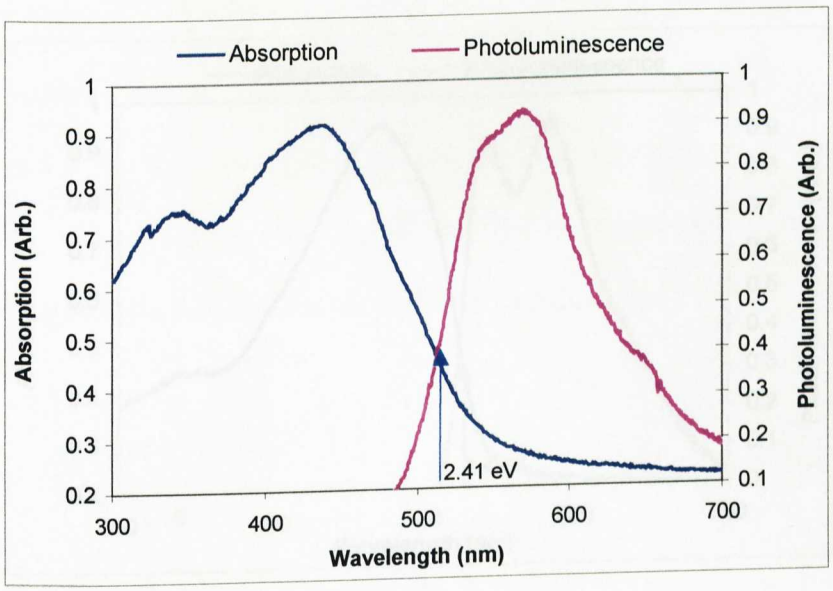

Fig.: 3.3.2.1b: Absorption and photoluminescence spectra of PPE-NO_2

Thermal Behaviour of the polymers

Differential scanning calorimetry measurements were carried out in order to study the thermal behaviour of the synthesised polymers. To observe any phase transitions for the polymers with DSC, at least 10 mg of material had to be used in combination with a fast scan rate. However, even under these conditions the endo and exotherms were very small. All polymers were first heated to 150 °C at 10 °C per minute, held at this temperature for 5 minutes and then cooled to the start temperature of –20 °C. Samples were then reheated from – 20 °C to 200 °C at 10 °C per minute. All synthesised poly(1,4-phenylene-ethynylene) showed no detectable transition. It was found that they decompose at temperature above 200°C.

3.3.2.2 Poly(1,4-phenylene-vinylene) via Heck

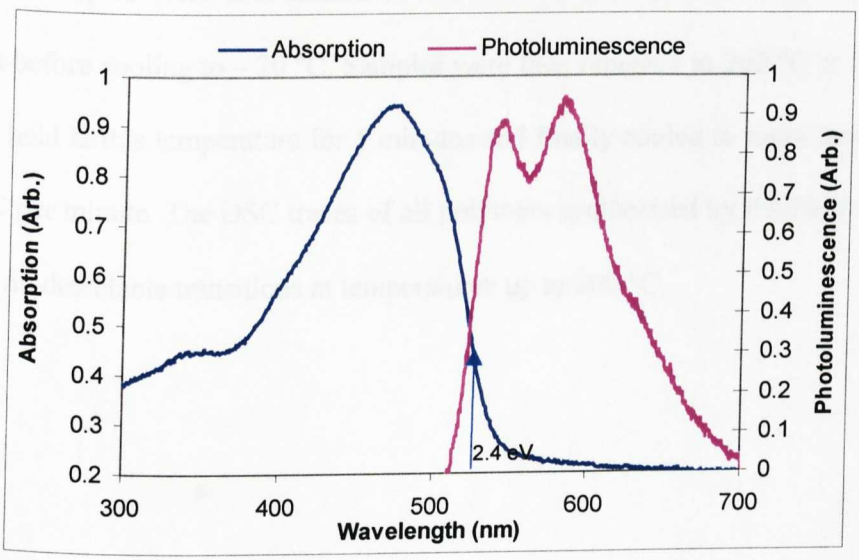

Fig. 3.3.2.2a: Absorption and photoluminescence spectra of PPV12-1

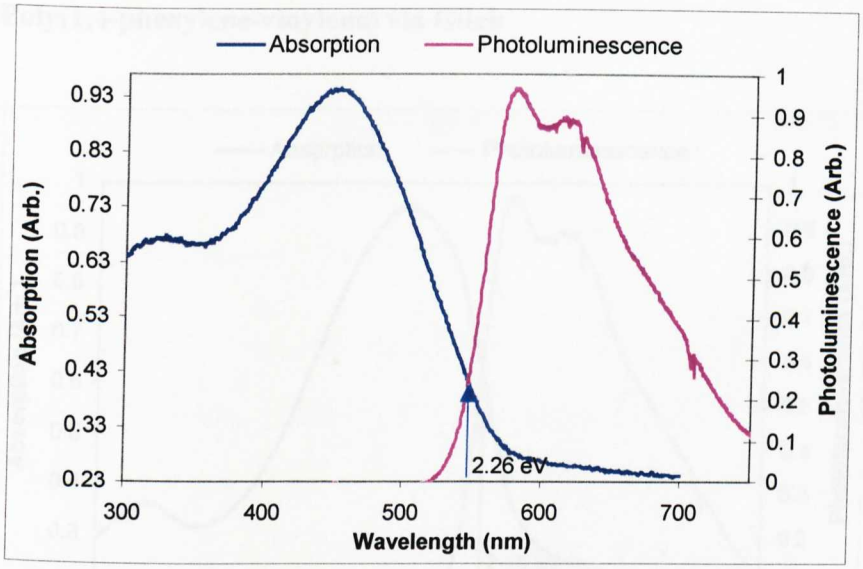

Fig. 3.3.2.2b: Absorption and photoluminescence spectra of PPV12-1/16-16

Thermal Behaviour of the polymers

Polymers samples were first heated to 150 °C and held at this temperature for 5 minutes before cooling to – 20 °C. Samples were then reheated to 200 °C at 10 °C per minute, held at this temperature for 5 minutes and finally cooled to room temperature at 10 °C per minute. The DSC traces of all polymers synthesised by the Heck reaction showed no detectable transitions at temperatures up to 200 °C.

3.3.2.3 Poly(1,4-phenylene-vinylene) via Gilch

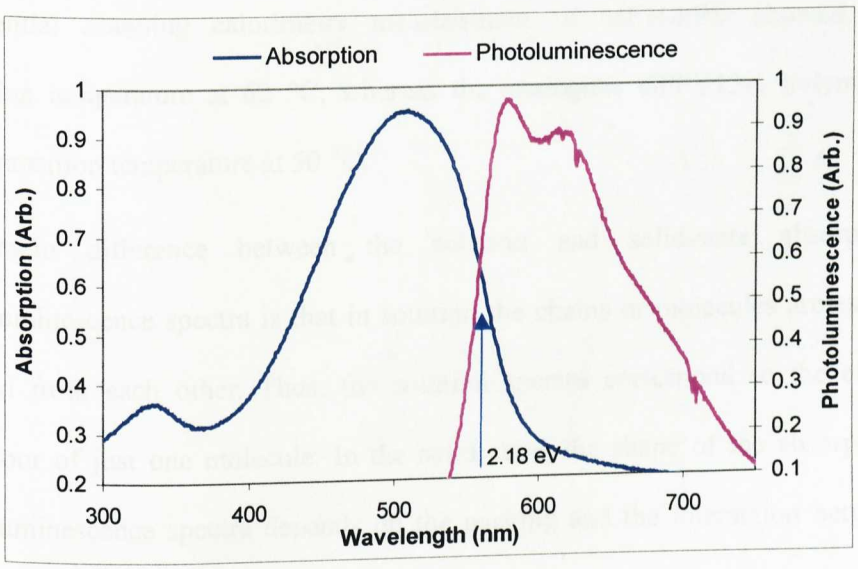

Fig. 3.3.2.3a: Absorption and photoluminescence spectra of MEH-PPV

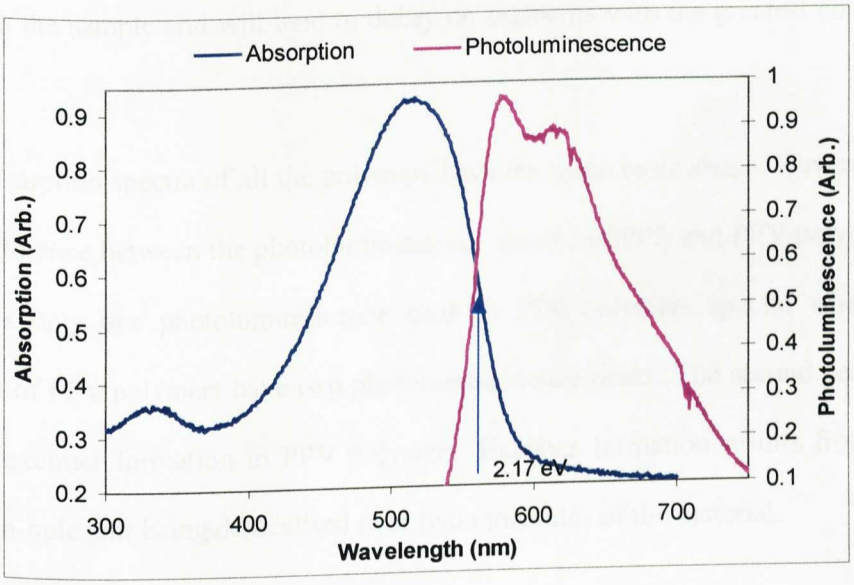

Fig. 3.3.2.3b: Absorption and photoluminescence spectra of GPPV12-1

Thermal Behaviour of the polymers

Differential scanning calorimetry measurement of MEH-PPV showed a glass transition temperature at 62 °C, whereas the analogous GPPV12-1 polymer has a glass transition temperature at 50 °C.

The main difference between the solution and solid-state absorption or photoluminescence spectra is that in solution the chains or molecules are essentially isolated from each other. Thus, the solution spectra correspond to the electronic behaviour of just one molecule. In the solid state, the shape of the absorption and photoluminescence spectra depends on the packing and the interaction between the molecules or chains. The photoluminescence spectra gives information about the most highly conjugated segments with the lowest energy, as the formed exciton can migrate through the sample and will tend to decay on segments with the greatest conjugation length.

The absorption spectra of all the polymers have the same basic shape. However, there is a difference between the photoluminescence spectra of PPE and PPV polymers that there is only one photoluminescence peak in PPE polymers spectra whereas the spectra of PPV polymers have two photoluminescence peaks. The second peak is due to the excimer formation in PPV polymers. Excimer formation results from bound electron-hole pair being delocalised over two molecules of the material.

	Abs solid-state (nm)	Pl solid-state (nm)	Band Gap (eV)
PPET	485	585	2.46
PPE-NO_2	475	520	2.41
PPV12-1	470	528	2.4
PPV12-1/16-16	490	578	2.26
MEH-PPV	510	595	2.18
GPPV12-1	518	596	2.17

Table 3.3.2: Solid-state UV-Vis absorption and photoluminescence data for all synthesised polymers

One of the methods used to estimate the band gap energy of organic semiconductors is by plotting the normalised absorption and photoluminescence spectra on the same wavelength axis. The wavelength at which the two curves meet is taken as the band gap energy.

From Table 3.3.2, it can be seen that the band gap energies of PPV polymers are lower than those of PPE polymers as a result of the longer effective conjugation length. It is also clear that the band gap energies of PPV polymers synthesised by the Gilch reaction are lower than those of Heck polymers due to the higher molecular weight and the regioregularity of Gilch polymers.

3.4 References

[1] D. R. McKean,, G. A. Parrinello, F. Renaldo, J. K. Stille, *J. Org. Chem.* **1987**, *52*, 422.

[2] B. Gómez-Lor, A. M. Echavarren, A. Santos, *Tet. Lett.* **1997**, *38*, 5347.

[3] J. N. G. Pillow, P. L. Burn, I. D. W. Samuel, M. Halim, *Synth. Met.* **1999**, *102*, 1468.

[4] A. F. Littke, G. C. Fu, *Angew. Chem. Int. Ed. Engl.* **1999**, *38*, 2411.

[5] E. T. Sabourin, A. Onopechenko, *J. Org. Chem.* **1983**, *48*, 5135

[6] R. Giesa, R. C. Schulz, *Makromol. Chem. Phys.* **1990**, *191*, 857

[7] A. William, B. Norman, L. Kreisler, *J. Org. Chem.* **1981**, *46*, 2280

[8] D. Braun, A. J. Heeger, *Appl. Phys. Lett.* **1991**, *58*, 1982

[9] G. Gustafsson, Y. Gao, G. M. Treacy, F. Klavetter, N. Colaneri, A. J. Heeger, *Nature* **1992**, *357*, 477

[10] G. J. Sarnecki, P. L. Burn, A. Kraft, R. H. Friend, A. B. Holmes, *Synth. Met.* **1993**, *55*, 914

[11] W. Heitz, *Pure. Appl. Chem.*, **1995**, *67*, 1951

[12] M. Suzuki, J. C. Lim, T. Saegusa, *Macromolecules* **1990**, *23*, 1574

[13] S. T. Pasco, P. M. Lahti, F. E. Karasz, *Macromolecules* **1999**, *32*, 6933.

[14] R. F. Heck, *Org. React.* **1982**, *27*, 345

[15] W. Cabri, I. Candiani, *Acc. Chem.* **1995**, *28*, 2-7

[16] J. Tsuji, *Organic Synthesis with Palladium Compounds*, Springer, Berlin, **1980**

[17] W. A. Herrmann, C. Reisinger, K. Oefele, C. Brossmer, M. Beller, H. Fischer, *J. Mol. Catalysis*, **1996**, *108*, 51-56

[18] L. Cassar, *J. Organomet. Chem.*, **1975**, *93*, 253

[19] H. A. Dieck, R. F. Heck, *J. Organomet. Chem.*, **1975**, *93*, 259

[20] K. Sonogashira, Y. Tohda, N. Hagihara, *Tet. Lett.* **1975**, *16*, 4467

[21] C. Weder, M. S. Wrighton, *Macromolecules*, **1996**, *29*, 5157-5165

[22] R. Giesa, J. *Macromol. Sci. Macromol. Chem. Phys.*, **1996**, *4*, 631-670

[23] U. H. F. Bunz, *Chem. Rev.* **2000**, *100*, 1605-1644

[24] T. Vahlenkamp, G. Wegner, *Macromol. Chem. Phys.* **1994**, *195*, 1933

[25] W. Y. Ng, W. Chan, *Adv. Mat.* **1997**, *9*, 716

[26] Z. Bao, Y. Chen, R. Cai, L. Yu, *Macromolecules*, **1993**, *26*, 5281

[27] S. Vanhee, R. Rulkens, U. Lehmann, C. Rosenauer, M. Schulze, W. Köhler, G. Wegner, *Macromolecules*, **1996**, *29*, 5136

[28] M. Rehan, A.D. Schlüter, G. Wegner, *Polymer*, **1989**, *30*, 1060

[29] A. D. Schlüter, G. Wegner, *Acta. Polym.* **1993**, *44*, 59

[30] N. Miyama, T. Yano, A. Suzuki, *Tet. Lett.* **1980**, *21*, 2865

[31] N. Miyama, T. Ishiyama, H. Sasaki, M. Ishikawa, M. Satoh, A. Suzuki, *J. Am. Chem. Soc.* **1989**, *111*, 314

[32] A. Greiner, H. Martelock, A. Noll. N. Siegfried, W. Heitz, *Polymer*, **1991**, *32*, 1857

[33] Z. Bao, R. Cai, L. Yu, *Angew. Chem. Int. Ed. Engl.* **1993**, *32*, 1345-1347

[34] Z. Bao, W. Chan, L. Yu, *Chem. Mater.* **1993**, *5*, 2-3

[35] Z. Bao, W. Chan, L. Yu, *J. Am. Chem. Soc.* **1995**, *117*, 12426-12435

[36] Philip Bentley, PhD Thesis, University of Sheffield, **1999**

[37] H. G. Gilch, W. L. Wheelwright, *J. Polym. Sci.: A-1* **1966**, *4*, 1337

[38] N. N. Barashkov, D. J. Guerrero, H. J. Olivos, J. P. Ferraris, *Synth. Met.* **1995**, *75*, 153

[39] B. R. Hsieh, Y. Yu, E. W. Forsythe, G. M. Schaaf, W. A. Feld, *J. Am. Chem. Soc.* **1998**, *120*, 231

[40] A. J. Heeger, D. Braun, *Chem. Abstr.* **1993**, *118*, 157401j

[41] P. W. M. Bolm, M. J. M. De Jong, J. J. M. Vleggaar, *Appl. Phys. Lett.* **1996**, *68*, 3308-3310

[42] J. Saalbeck, *Ber. Bunsenges. Phys. Chem.* **1996**, *11*, 3174-3187

[43] M. Hirohata, K. Tada, T. Kawai, M. Onoda, K. Yoshino, *Synth. Met.* **1997**, *85*, 1273-1274

Chapter 4: Experimental-Devices

Solid-state solar cells were fabricated using thin films of phenylene-vinylene polymers spun onto the surface of highly dense TiO_2 thin films prepared on ITO substrates. The device fabrication was carried out in a dust free environment to eliminate any contamination. The fabrication procedure of devices consists of four steps as shown in Fig. 4.

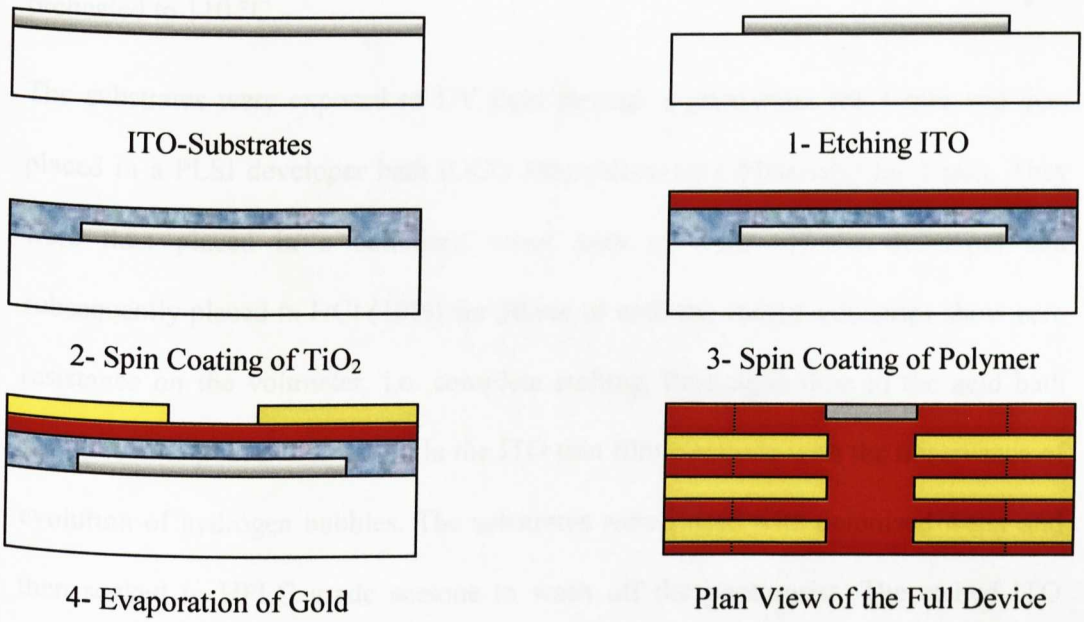

Fig. 4: Schematic diagram of the experimental procedure of the device fabrication

4.1 Device fabrication

4.1.1 Etching of ITO substrates

Indium tin oxide (9 x 9 mm) electrodes on glass substrates (supplied by Balzers) were soaked in a soap solution in an ultrasonic bath for 5 min, rinsed thoroughly with deionised water solution for 5 min and then soaked in boiling HPLC grade isopropyl

alcohol for 1 min. A voltmeter (switched at DC and 2 kΩ) was used to recognise the ITO side from the glass side prior to coating with the photoresist.

Under UV-free yellow neon light, the clean substrates were spin-coated with an RS 690-855 photoresist (RS Component Ltd) at 100 rpm for 1 sec, followed by 3000 rpm for 25 sec. The coated substrates were placed for 1 min on a hot plate that was preheated to 110 °C.

The substrates were exposed to UV light through a photomask for 4 min and then placed in a PLSI developer bath (OCG Microelectronics Materials) for 1 min. They were then placed in a deionised water bath to wash off the developer and subsequently placed in HCl (10%) for 30 sec or until the etched side strips show zero resistance on the voltmeter, i.e. complete etching. Prolonged time in the acid bath would lead to pinhole formation in the ITO thin film electrode with the observance of evolution of hydrogen bubbles. The substrates were rinsed with deionised water and then soaked in HPLC grade acetone to wash off the photoresist. The etched ITO substrates were then cleaned following the same cleaning procedure as explained above prior to the photoresist coating step.

4.1.2 Preparation of titania thin films

The sol-gel process was used to prepare thin films of anatase titania by hydrolysis of titanium tetraisopropoxide, spin coating and a high temperature sintering of the spun film.

$$Ti(O^iPr)_4 + 4H_2O \rightleftharpoons Ti(OH)_4 + 4\ ^iPrOH$$

$$Ti(OH)_4 \rightleftharpoons TiO_2 + 2H_2O$$

4.1.2.1 Spin coating technique

Titanium tetraisopropoxide (Aldrich, 99.99%) was used as the titania precursor. A stable sol was prepared at room temperature by adding titanium tetraisopropoxide [$Ti(O^iPr)_4$] to a stirred mixture of denaturated ethanol (Aldrich, 99.9%) and acetic acid (Aldrich, 99.7%) as the catalyst in the volume ratio of 1:20:0.1, respectively.

In order to produce a stable sol, water should not be added to the reaction mixture and the hydrolysis should proceed through atmospheric water as titanium tetraisopropoxide is very hygroscopic and reacts readily with water, which can lead to the precipitation of a highly condensed powder of TiO_2. Therefore, the humidity level of the clean room was always checked prior to the sol preparation. The sol was prepared in a sealed conical flask to minimise the contact between the reaction mixture and air in order to allow for slow hydrolysis.

The mixture was stirred for 10 min at room temperature until a homogenous colourless stable sol is produced. The etched ITO substrates were coated with the titania sol at 2500 rpm for 40 sec.

The formed gel films were then sintered in a temperature controlled resistance tube furnace under a nitrogen trickle. The temperature was slowly ramped at the rate of 1 °C/min up to 550 °C, held at this temperature for 30 min and then cooled at the rate of

1 °C/min to room temperature. The gel substrates were contained in a silica tube during heat treatment.

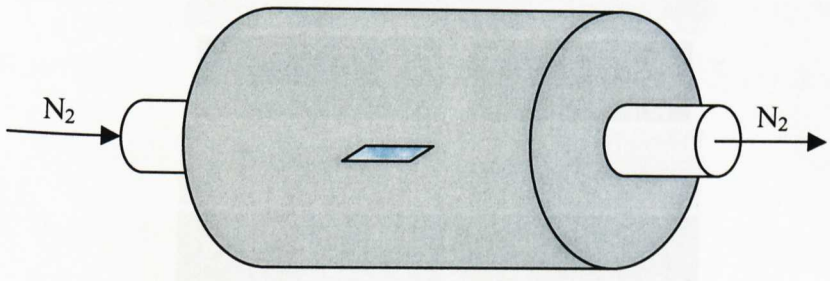

Fig. 4.1.2: Schematic presentation of the tube furnace

The thickness of the sol-gel processed titania films was measured by a Dektak Profilometer. In this measurement, a longitudinal scratch is made in the titania film and the Profilometer needle scans the surface horizontally to measure the height difference across the scratch. For accurate results, several scratches were made in the titania film on both ITO and glass areas of the substrate and the average of these values was recorded. The thickness of the titania films varied with the $Ti(O^iPr)_4$ precursor concentration. Several $Ti(O^iPr)_4$: EtOH volume ratios were employed to produce various thicknesses of titania to study the effect of TiO_2 film thickness on device performance. The results are summarised in Table 4.1.2.

$Ti(O^iPr)_4$: EtOH	Thickness (nm)
1 : 4	120
1 : 6	70
1 : 10	50
1 : 20	40

Table 4.1.2: Showing the effect of precursor concentration on the spin-coated films thickness

4.1.2.2 Dip coating technique

The dip coating technique was carried out by Q. Fan[1] at the University of Sheffield for the preparation of titania thin film. The sol was prepared in a similar fashion as described before using the volume ratio of 1:9:0.1 of the starting material, respectively. The etched ITO substrates were dipped into the TiO_2 sol using NIMA dipping equipment and withdrawn at a speed of 20 mm/min. The dip-coated gel films were dried for about 1 hour under ambient conditions and then sintered in the tube furnace under dynamic air using the same heat treatment as explained before. After sintering, the crystalline structure of TiO_2 films was studied by X-ray diffraction analysis (XRD) and high resolution transmission electron microscope (TEM)[1]. There are three crystalline structures of TiO_2, namely brookite, anatase and rutile. Comparison of the XRD pattern of the sintered TiO_2 film to that of pure anatase TiO_2 showed that anatase TiO_2 structure is dominant. TEM micrographs of TiO_2 films

sintered for half an hour at a fixed temperature of 550 °C without ramping showed the existence of pores in between the crystallites in the form of irregular lines or patterns. In contrast, such patterns are absent from the micrograph produces by sintering with careful temperature ramping to 550 °C. The porosity in TiO_2 films is therefore highly dependent on the sintering process.

It is believed that rapid heating to 550 °C causes fast removal of unwanted solvent and catalyst residues from the material and the resulting TiO_2 is porous. On the other hand, the tightly controlled temperature profile and the slow heat ramp to 550 °C allowed slow removal of the remaining residues from the TiO_2 gel films and as a result of that, the produced TiO_2 films were highly dense.

4.1.3 Spin coating of polymers

MEH-PPV (3 mg) was dissolved in THF (1 ml). The solution was then filtered with a 0.45 μm glass fibre filter prior to spin coating. The spin-coating of the polymer onto the titania substrates was carried out in air for all devices except only for one device, where the titania substrates and the polymer solution were transferred into a nitrogen filled glove-box and the substrates were spin-coated with the polymer solution at 3000 rpm for 40 sec and then 4000 rpm for 10 sec to produce thin films of 80 nm thickness. THF was found to be the best solvent for preparing the polymer solution. Other solvents such as toluene and xylene were also used to dissolve the polymers, however the polymer tends to precipitate out from these solutions on standing.

4.1.4 Evaporation of gold

A gold back contact was applied by Electrical Vapour Deposition technique using Edwards Evaporator (West Technology Systems). Typically 90 nm of gold was applied from gold wire of 1 mm diameter (NetMet, 99.999%). The gold wire (250 mg) was coiled and then placed in a tungsten boat. The substrates were mounted into the metal evaporator facing down and exposed to gold through a deposition mask. Prior to evaporation, high vacuum was applied to the deposition system until the pressure reached (3×10^{-6} Torr). The gold wire was carefully evaporated by slowly increasing the voltage applied to the tungsten boat. An initial buffer layer of 3 nm was slowly deposited at a deposition rate of 0.1 nm/sec. The rate was then raised gradually to reach 1 nm/sec at the end of deposition. Gold was the metal of choice as gold has a high work function of 5.1 eV that matches the HOMO energy level of the polymer to minimise the energy barrier at the polymer/metal interface.

In one of the devices, prior to the deposition of gold, a thin chromium layer (3 nm) was deposited from a chromium rod (NetMet, 99.99%) at a deposition rate of 0.1 nm/sec in order to increase the adhesion properties between MEH-PPV and gold.

4.2 Device illustration

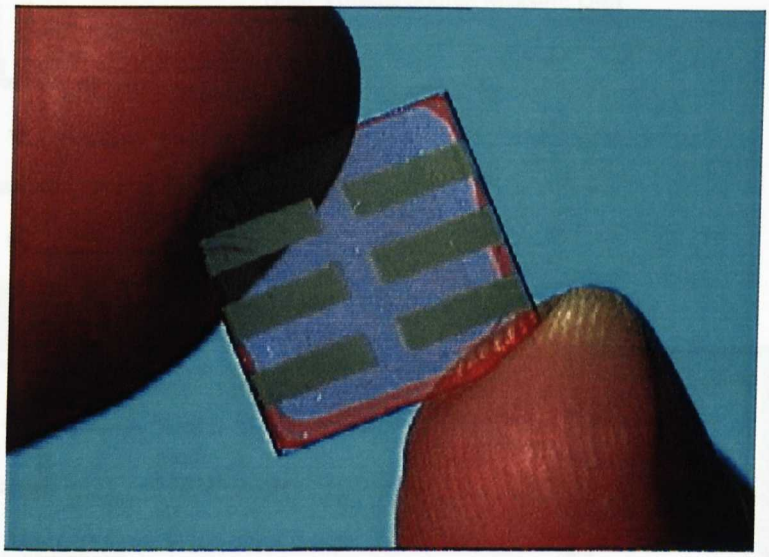

Fig. 4.2: Picture of the fabricated device

4.3 Characterisation of devices

Current-voltage (I-V) characteristics were measured using a Keithley 2400 source unit in vacuum condition and under illumination through the glass side by a xenon light source with an intensity of 0.3 mW/cm^2 for the monochromatic light of 520 nm wavelength and a solar simulator Am1.5 (84 mW/cm^2) as shown in Fig. 4.3. Photocurrent action spectra are taken with the xenon lamp and a monochromator.

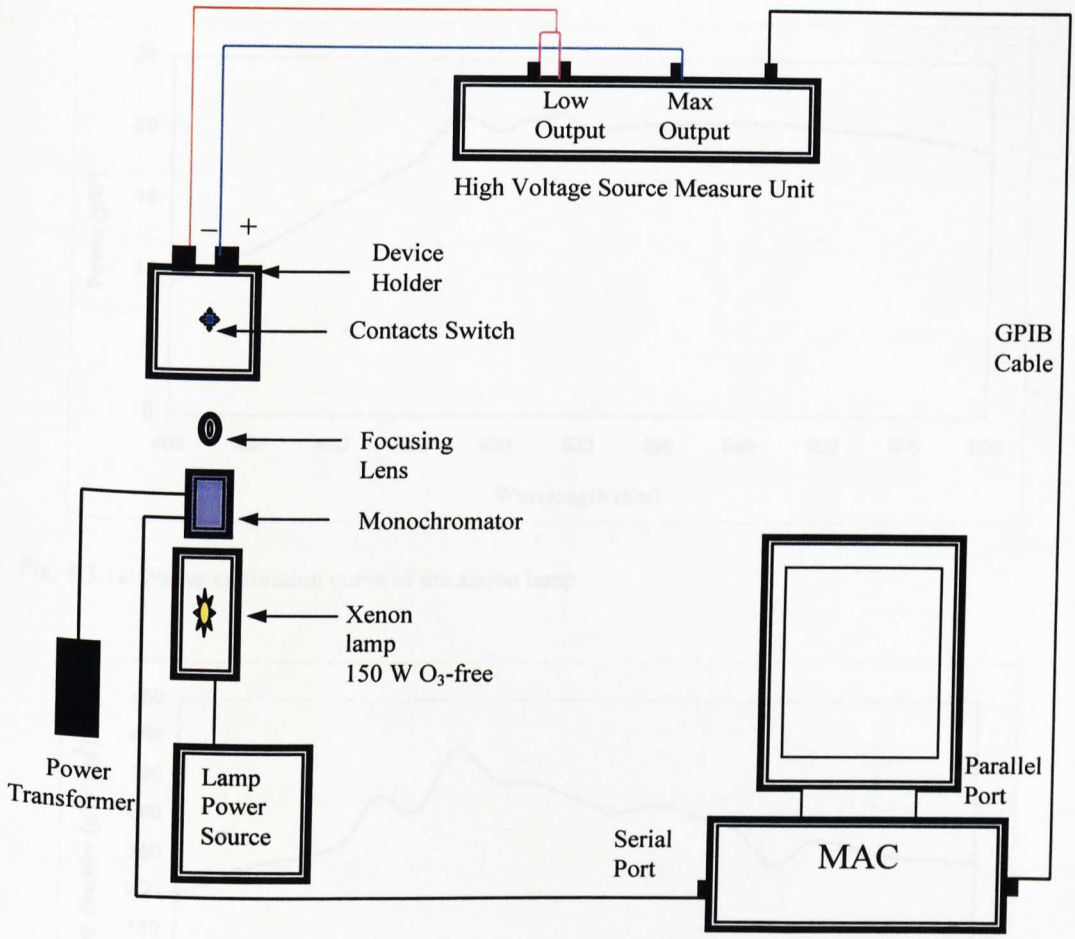

Fig 4.3: Schematic representation of the IV measurement setup

4.3.1 Calibration and measurement

The power of the xenon lamp was calibrated using a power meter within the range between 400 and 600 nm. In Fig. 4.3.1a, the absolute power of the lamp is plotted versus wavelength. The light spot area was also measured for each wavelength for the power density calibration as shown in Fig. 4.3.1b.

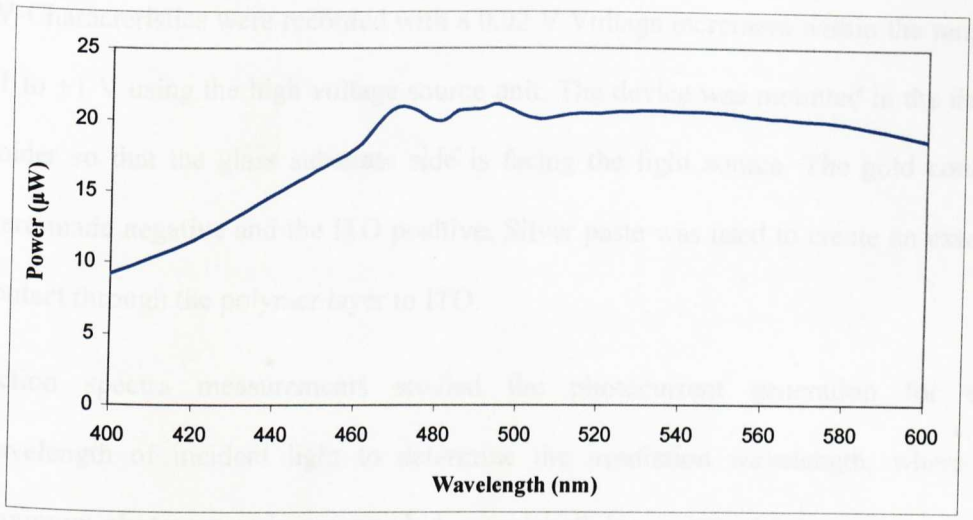

Fig. 4.3.1a: Power calibration curve of the xenon lamp

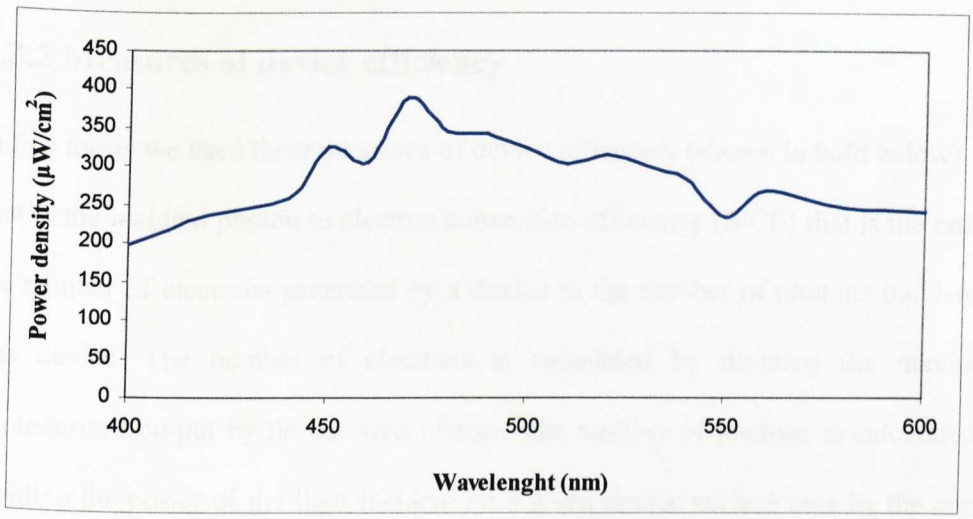

Fig. 4.3.1b: Power density calibration curve of the xenon lamp

The power calibration of the solar simulator was supplied by the manufacture for two distances, 10 and 20 mm, from the sample. The power of the solar simulator is controlled by the slit width of the fibre optic filament.

IV-Characteristics were recorded with a 0.02 V Voltage increment within the range of −1 to +1 V using the high voltage source unit. The device was mounted in the device holder so that the glass substrate side is facing the light source. The gold contacts were made negative and the ITO positive. Silver paste was used to create an external contact through the polymer layer to ITO.

Action spectra measurements studied the photocurrent generation for each wavelength of incident light to determine the irradiation wavelength, where the maximum photocurrent is generated. A wavelength increment of 5 nm was controlled by a monochromator.

4.3.2 Measures of device efficiency

In this thesis we used three measures of device efficiency (shown in bold below). The first is the incident photon to electron conversion efficiency (IPCE) that is the ratio of the number of electrons generated by a device to the number of photons incident on this device. The number of electrons is calculated by dividing the maximum photocurrent output by the electron charge. The number of photons is calculated by dividing the power of the light incident on a given device surface area by the energy of these photons. The photons energy depends on the wavelength of the incident light.

$$\textbf{Incident Photon to Current Efficiency} = \frac{\text{Number of electrons flowing per second}}{\text{Number of incident photons per second}}$$

$$\text{Number of electrons flowing per second} = \frac{\text{Current (Amp)}}{\text{Electron charge (Coulomb)}}$$

$$\text{Number of incident photon per second} = \frac{\text{Power of the light source (Watt)}}{\text{Energy of photons (Joule)}}$$

Power of light source (W) = Source power intensity (W/cm^2) * Device surface area (cm^2)

Energy of a photon of particular wavelength (Joule) = hc/λ

$h = 6.63 \times 10^{-34}$, $C = 3 \times 10^8$(m/s), $e = 1.6 \times 10^{-19}$ (coulomb), Watt = Joule/sec

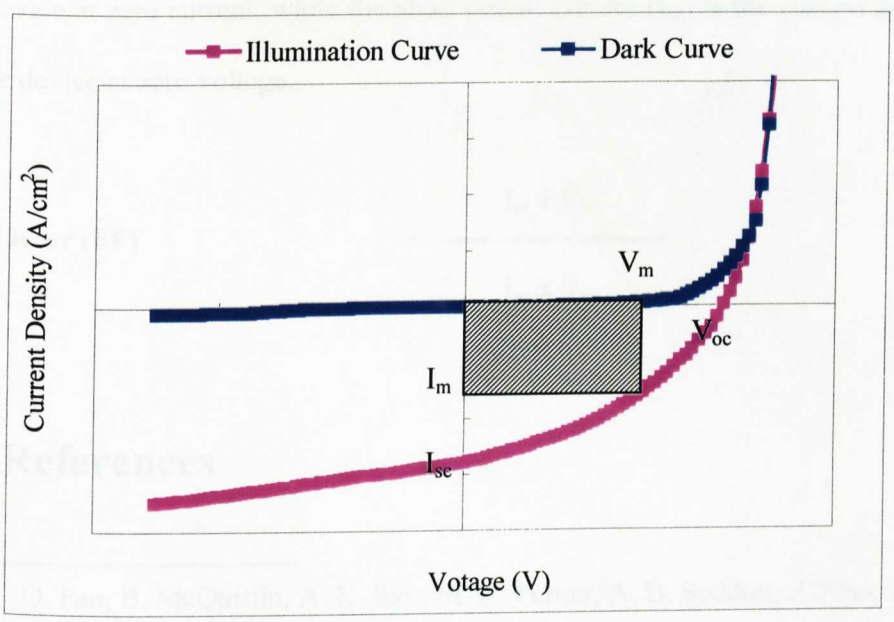

Fig. 4.3.2: An IV-diagram showing the maximum power rectangular area

The second measure is the energy conversion efficiency, which is the ratio of the power output to power input. The power output is the product of the maximum voltage (V_m) and the maximum current (I_m) determined by drawing the maximum power rectangular area under the IV-curve in the 4th quadrant as shown in Fig. 4.3.2. The power input is the incident light power intensity.

$$\textbf{Energy Conversion Efficiency} = \frac{\text{Power Output}}{\text{Power Input}} = \frac{I_m \times V_m}{\text{Power density} \times \text{Area}}$$

The third measure is the fill factor (FF), which is the ratio of the power output to the product of the open circuit voltage (V_{oc}) and the short circuit current (I_{sc}) taken from the illumination curve. The open circuit voltage (V_{oc}) is the voltage recorded across the device at zero current, while the short circuit current (I_{sc}) is the current generated by the device at zero voltage.

$$\textbf{Fill Factor (FF)} = \frac{I_m \times V_m}{I_{sc} \times V_{oc}}$$

4.4 References

[1] Q. Fan, B. McQuillin, A. K. Ray, M. L. Turner, A. B. Seddon, *J. Phys. D: Appl. Phys.* **2000**, *33*, 2683-2686

Chapter 5: Results and Discussion-Devices

5.1 Characterisation of photovoltaic performance

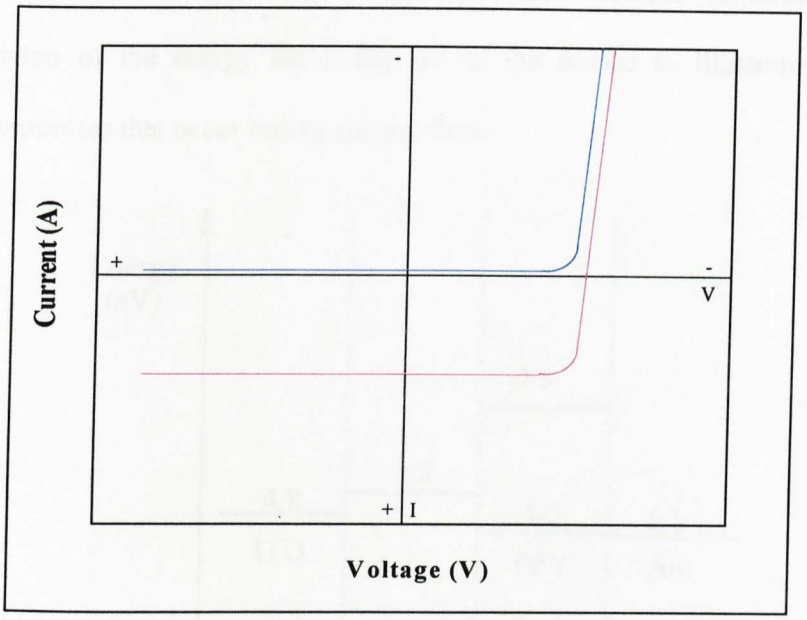

Fig. 5.1 IV-Characteristics of an idealised photovoltaic cell

Fig. 5.1 represents the IV-characteristics of an idealised p-n photovoltaic cell. In the dark (blue curve), there is no current flowing through the cell in forward bias. However, in reverse bias, current flows when the applied voltage overcomes the cell junction potential. Under illumination (red curve), a constant current is generated in forward bias, which is independent on the applied voltage. The reason for the generation of this voltage-independent current under illumination is the generation of excitons upon absorption of light and due to the potential set at the cell interface these excitons dissociate resulting in current generation. The amplitude of this current is dependent on the number of photons of the incident light.

5.2 Energy level study

Discussion of the performance of the fabricated devices requires an initial consideration of the energy band diagram of the device to illustrate the charge transfer processes that occur during current flow.

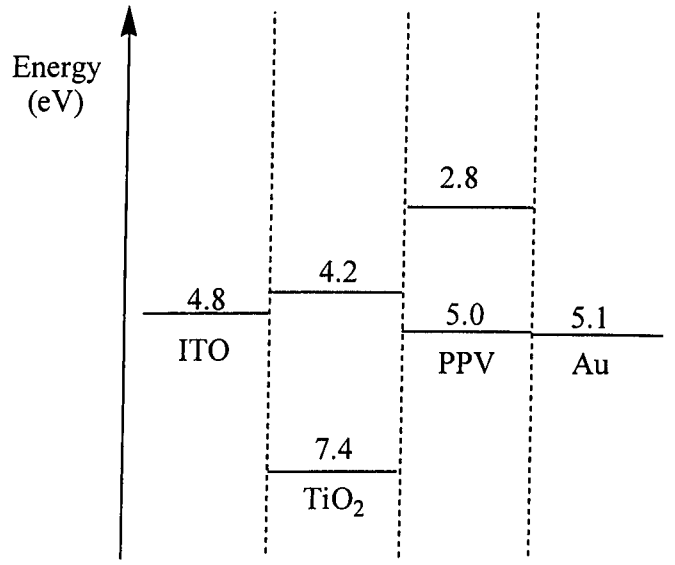

Fig. 5.2a: Energy levels of the proposed device structure in open circuit condition

Fig. 5.2a shows the relative energy levels of our photovoltaic structure[1,2], whereas Fig. 5.2b shows the energy level structure when the device is short-circuited[3]. On the basis of the energy levels of PPV and TiO_2 (Fig. 5.2b), dissociation of excitons at PPV/TiO_2 interface is energetically allowed.

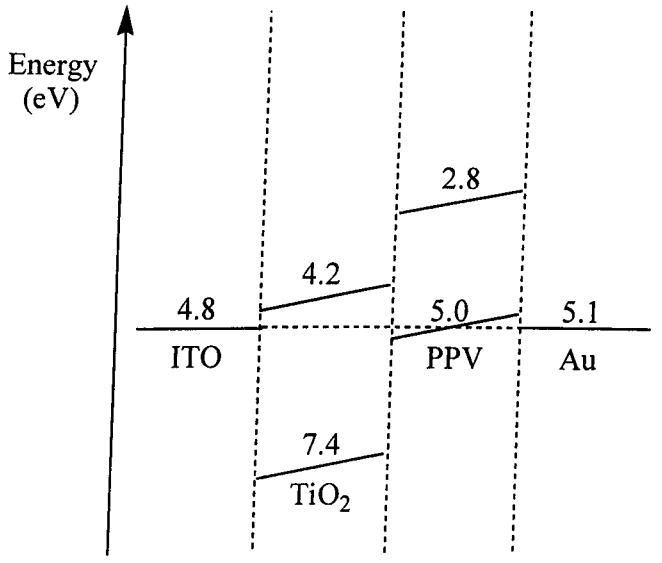

Fig.5.2b: Energy levels of the proposed device structure in short circuit condition

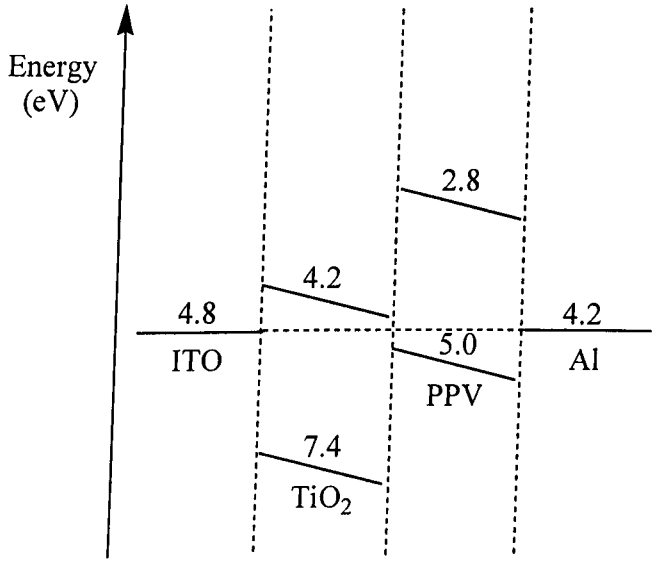

Fig.5.2c: Energy levels of the ITO/TiO_2/PPV/Al device in short circuit condition

Gold was the metal of choice as previous studies at the University of Sheffield carried out by Q. Fan showed that using the device structure of ITO/TiO_2/PPV/Al results in biasing the device in the opposite direction (see Fig. 5.2c) and consequently the

dissociation of excitons at the PPV/TiO_2 interface becomes disfavoured due to the large energy barrier at the interfaces. The work function of gold (5.1 eV) also offers a closer match to the HOMO level of PPV. The current flow of our device structure will be discussed in details in the following section.

Fig. 5.2d shows that the flow of current through the cell in the dark in the forward bias requires hole injection from the gold electrode into the valence band of MEH-PPV, and hole transfer from MEH-PPV to the valence band of TiO_2. The latter process is not allowed, as the energy barrier is too large.

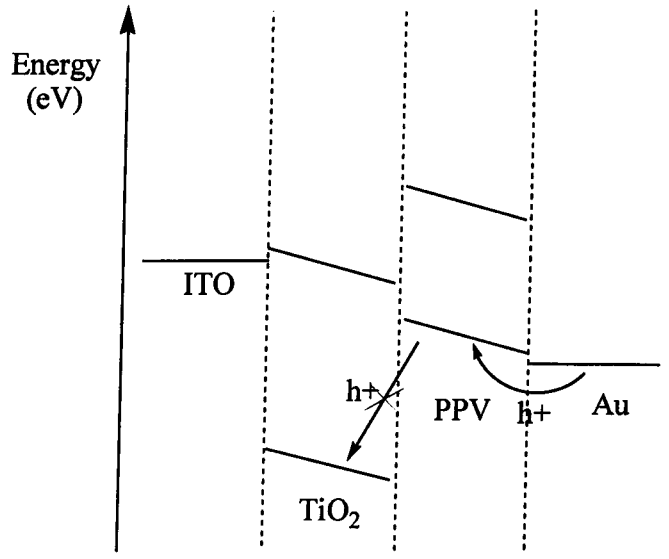

Fig. 5.2d: Energy levels of the proposed device structure in forward bias in the dark

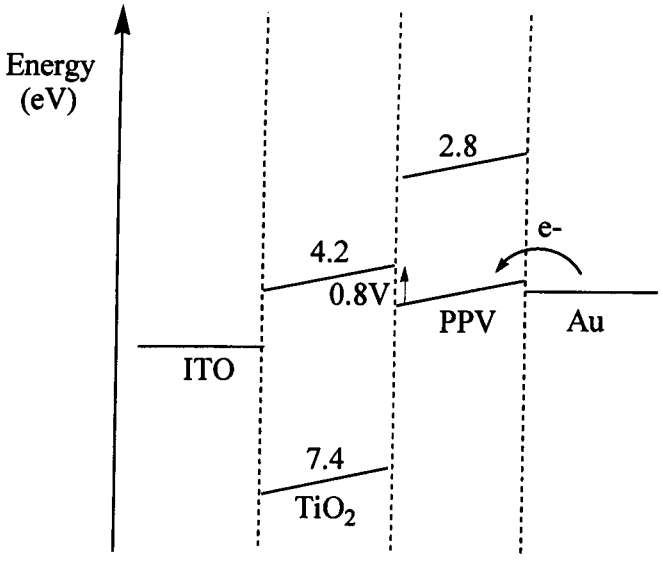

Fig. 5.2e: Energy levels of the proposed device structure in reverse bias in the dark

Under reverse bias (Fig. 5.2e), the flow of current requires electron injection from the gold electrode into the HOMO of MEH-PPV, and an electron transfer to the conduction band of TiO_2. Although the latter process is allowed, there is an energy barrier of ~ 0.8 V that can only be overcome at the open circuit voltage.

Under illumination, absorption of photons by MEH-PPV leads to the generation of excitons that may dissociate at the MEH-PPV/TiO_2 interface. In forward bias, the generated electrons are injected into the gold electrode. At the ITO electrode, electrons are injected into the conduction band of TiO_2. This process is allowed under illumination due to the photoconducting nature of TiO_2 as shown in Fig. 5.2f.

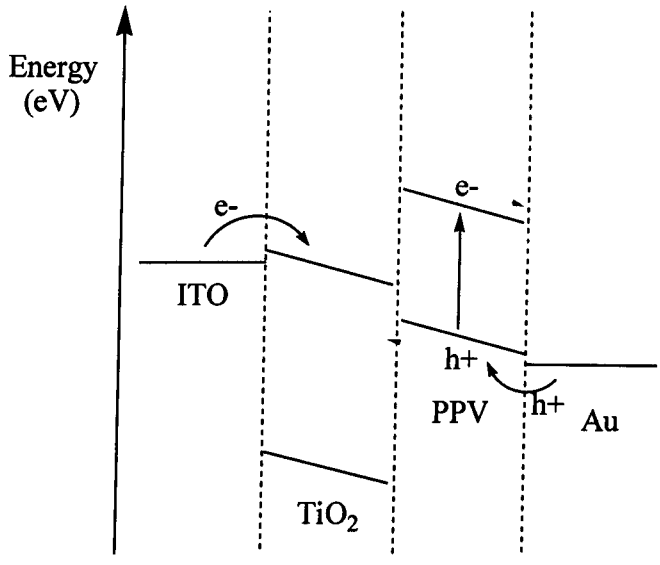

Fig. 5.2f: Energy levels of the proposed device structure in forward bias under illumination

Under reverse bias (Fig. 5.2g), the exciton formation is followed by electron injection into the conduction band of TiO_2 and hole injection into the gold electrode.

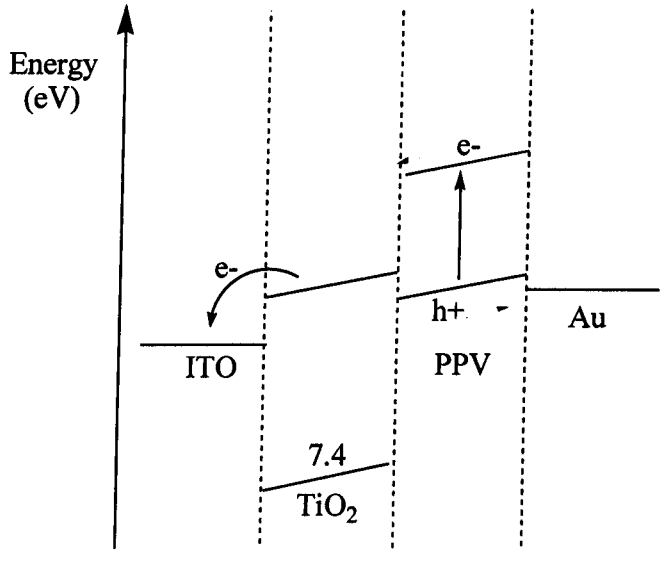

Fig. 5.2g: Energy levels of the proposed device structure in reverse bias under illumination

5.3 Characterisation of devices

5.3.1 ITO/dip-coated TiO_2/PPV12-1/Au

5.3.1.1 IV-Characteristics with monochromatic light (468 nm)

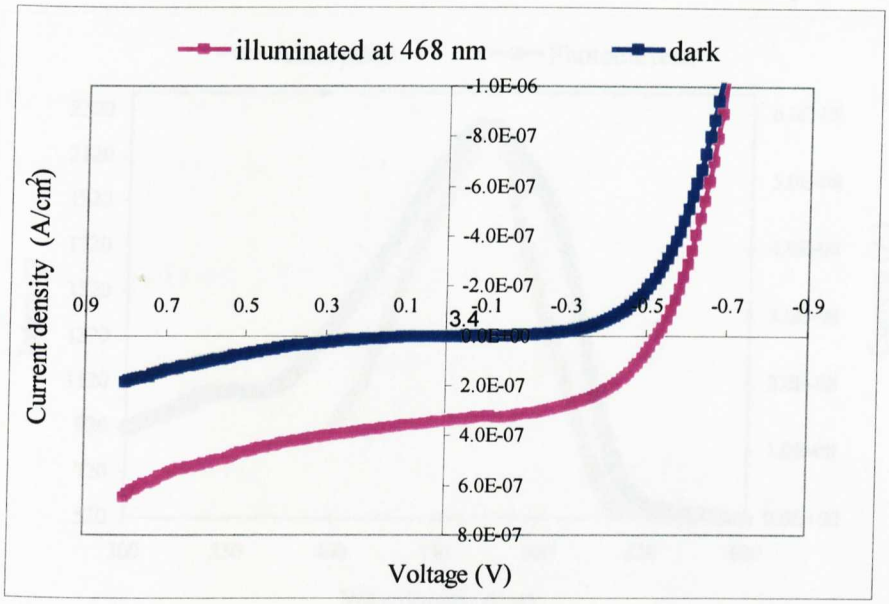

Fig. 5.3.1.1: IV-Characteristics of ITO/dip-coated TiO_2/PPV12-1/Au

This device was fabricated from poly(1,4-phenylenevinylene), PPV12-1, prepared by the Heck reaction that is capable of producing a thin film of even thickness. The greatest film thickness we could achieve with this polymer was 40 nm and this was attributed to the low molecular weight of this polymer. The anatase titania substrate[4] used in this device was prepared by dip-coating technique as explained previously in the Experimental-Devices Chapter. IV-characteristics showed a small leakage current in forward bias (0.18 $\mu A/cm^2$ at 0.8 V), which was presumably due to the presence of charge carriers within the device that lead to current generation[5]. The maximum

obtained photocurrent of this device occurred at a wavelength (468 nm) close to the maximum absorption wavelength of PPV12-1 (470 nm) spun on a glass substrate, i.e. symbatic behaviour is observed for the photosensitiser polymer used, PPV12-1. The device efficiency values are summarised in Table 5.3.1.1.

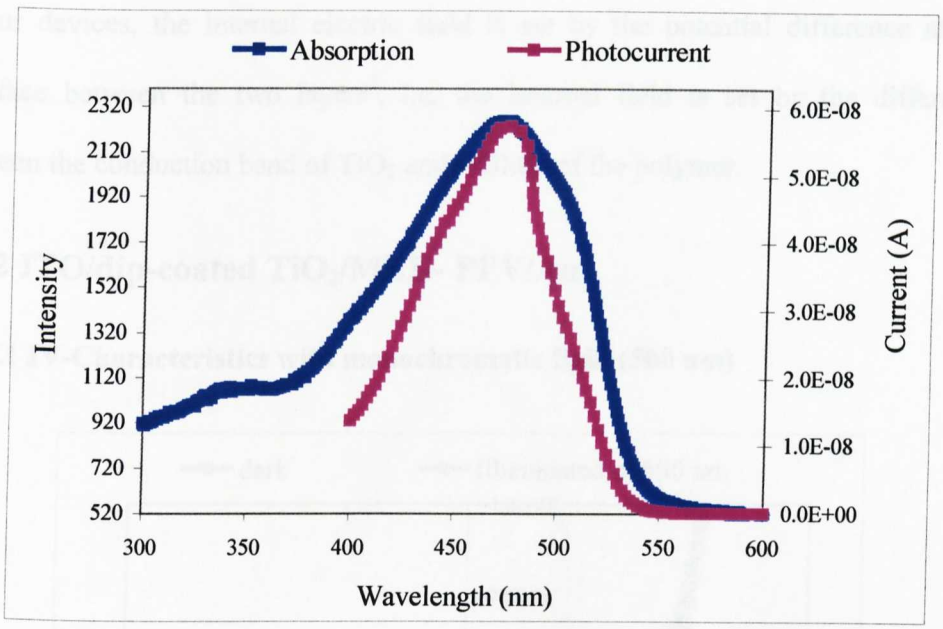

Fig. 5.3.1.2: Absorption and action spectra of PPV12-1 and ITO/dip-coated TiO_2/PPV12-1/Au

Short-circuit current (I_{sc})	1.4 x 10^{-8} A
Open-circuit voltage (V_{oc})	0.52 V
Fill factor	0.5
Incident Photon to Current Efficiency (IPCE)	0.56%
Energy conversion efficiency	0.07%

Table 5.3.1.1: Efficiency values of ITO/dip-coated TiO_2/PPV12-1/Au

In traditional donor-acceptor composite single layer devices, the internal electric field is mainly due to the asymmetry between the electrode work functions[2,3,6]. This cannot account for the observed open circuit voltage (0.52 V), where symmetric contacts, such as gold and ITO with work function of 5.1 ± 0.1 and 4.8 ± 0.2, respectively[1,2,3,5].

In our devices, the internal electric field is set by the potential difference at the interface between the two layers[3], i.e. the internal field is set by the difference between the conduction band of TiO_2 and HOMO of the polymer.

5.3.2 ITO/dip-coated TiO_2/MEH- PPV/Au

5.3.2.1 IV-Characteristics with monochromatic light (500 nm)

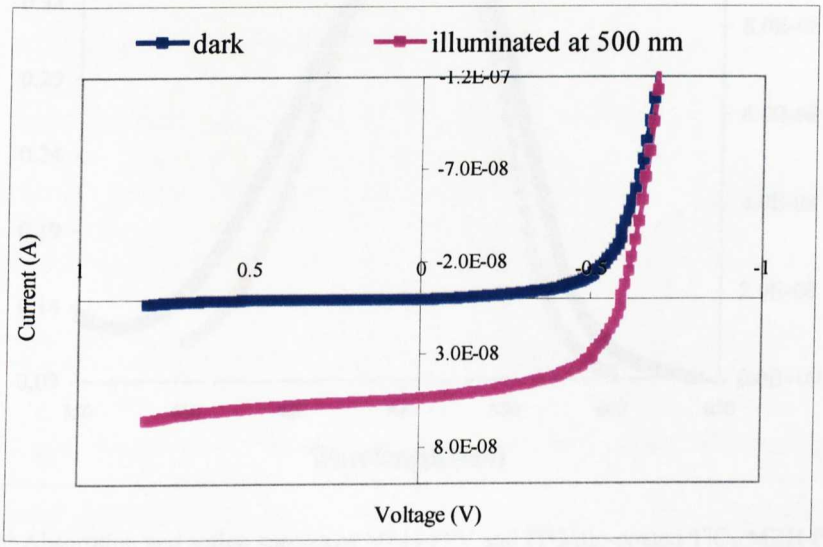

Fig. 5.3.2.1a: IV-Characteristics of ITO/dip-coated TiO_2/MEH-PPV/Au

In these devices, we employed MEH-PPV prepared by the Gilch reaction as the photosensitiser and hole transport layer. Using MEH-PPV much thicker films were

possible and the best devices used a film thickness of 80 nm. The titania films used in these devices were produced by the same technique used for the previous device.

No leakage current was observed in the forward bias i.e. this device shows classic p-n diode rectification behaviour. Fig. 5.3.2.1b shows symbatic behaviour of MEH-PPV between the action and absorption spectra as the maximum photocurrent at 500 nm coincides perfectly with the maximum absorption of the polymer. The device efficiency values are summarised in Table 5.3.2.1.

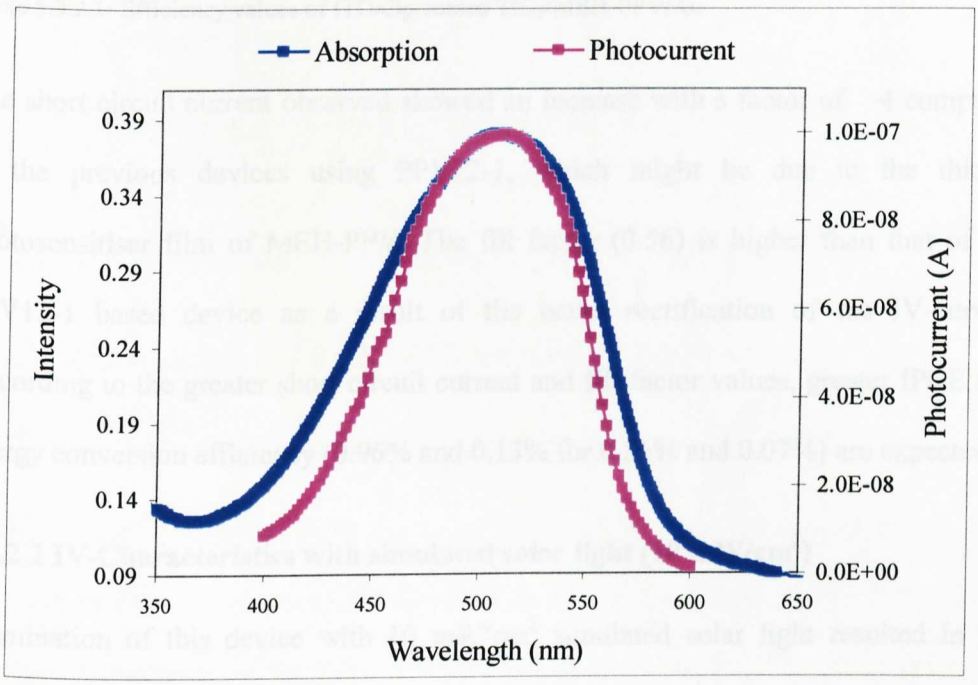

Fig. 5.3.2.1b: Absorption and action spectra of MEH-PPV and ITO/dip-coated TiO_2/MEH-PPV/Au

Short-circuit current (I_{sc})	5.3 x 10^{-8} A
Open-circuit voltage (V_{oc})	0.59 V
Fill factor	0.56
Incident Photon to Current Efficiency (IPCE)	0.97%
Energy conversion efficiency	0.13%

Table 5.3.2.1: Efficiency values of ITO/dip-coated TiO_2/MEH-PPV/Au

The short circuit current observed showed an increase with a factor of 4 compared to the previous devices using PPV12-1, which might be due to the thicker photosensitiser film of MEH-PPV. The fill factor (0.56) is higher than that of the PPV12-1 based device as a result of the better rectification of the IV-curves. According to the greater short circuit current and fill factor values, greater IPCE and energy conversion efficiency (0.96% and 0.13% for 0.56% and 0.07%) are expected.

5.3.2.2 IV-Characteristics with simulated solar light (10 mW/cm^2)

Illumination of this device with 10 mW/cm^2 simulated solar light resulted in the device becoming ohmic with no rectification (Fig. 5.3.2.2). This suggested that the device was short-circuited by illumination with high intensity light. Even though the measurements were performed in high vacuum, it is possible that polymer is photooxidised at the interface with TiO_2, presumably by oxygen trapped at the interface during the spin coating of the polymer that was carried out in air.

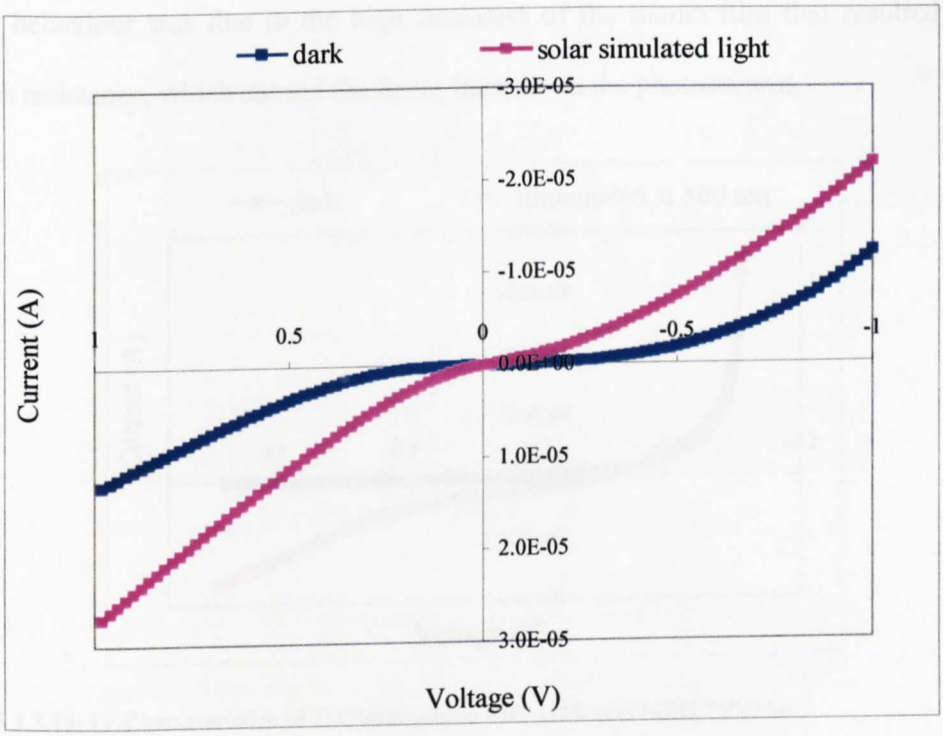

Fig. 5.3.2.2: IV-Characteristics of ITO/dip-coated TiO_2/MEH-PPV/Au

5.3.3 ITO/spin-coated TiO_2 (120 nm)/MEH-PPV/Au

5.3.3.1 IV-Characteristics with monochromatic light

These devices employed TiO_2 substrates prepared by spin-coating technique. The preparation of such titania films was carried out at the Department of Physics as previously explained in the Experimental for Devices Chapter. The thickness of the TiO_2 film used in this device was 120 nm. IV-characteristics showed a perfectly classic diode behaviour in the dark. However, the IV-curve under illumination with monochromatic light at 500 nm was not consistent with that in the dark in forward bias. Under illumination the photocurrent increased linearly with the applied field.

This behaviour was due to the high thickness of the titania film that resulted in a series resistance, which caused the linear increase in the photocurrent.

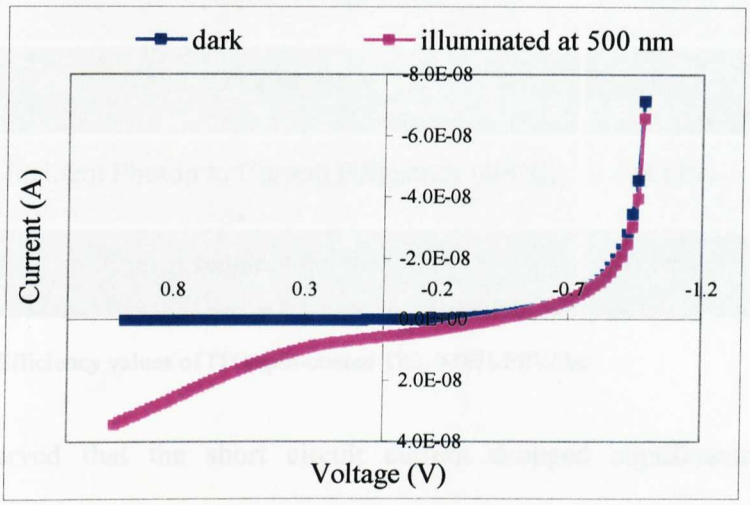

Fig. 5.3.3.1a: IV-Characteristics of ITO/spin-coated TiO_2 (120 nm)/MEH-PPV/Au

Attempts at annealing these devices at 80 °C in vacuum did not result in any increase in the photocurrent gain as shown in Fig. 5.3.3.1b

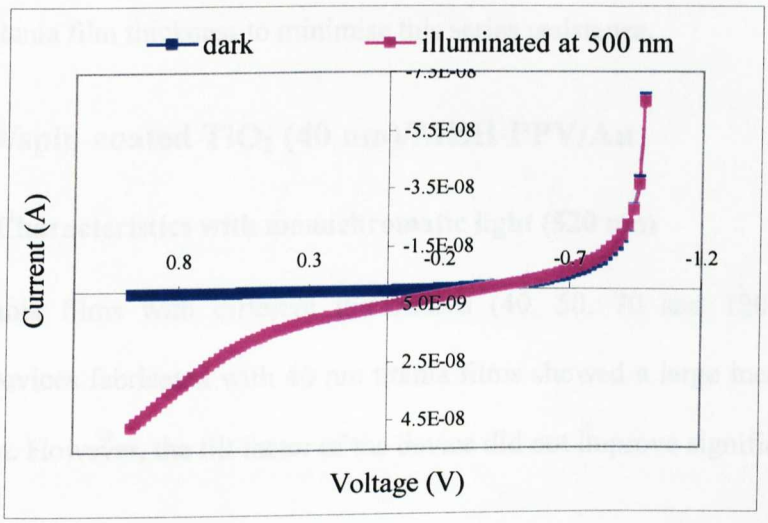

Fig. 5.3.3.1b: IV-Characteristics of ITO/spin-coated TiO_2 (120 nm)/MEH-PPV/Au (annealed)

Short-circuit current (I_{sc})	5.8 x 10^{-9} A
Open-circuit voltage (V_{oc})	0.42 V
Fill factor	0.31
Incident Photon to Current Efficiency (IPCE)	0.11%
Energy conversion efficiency	0.006%

Table 5.3.3.1: Efficiency values of ITO/spin-coated TiO_2/MEH-PPV/Au

It was observed that the short circuit current dropped significantly from the previously fabricated device fabricated with dip-coated titania film, from 5.3x10^{-8} A to 5.8x10^{-9} A.

At this stage, it was thought that the decrease in the photocurrent in these devices is due to the high series resistance of the titania film and therefore it was decided to lower the titania film thickness to minimise this series resistance.

5.3.4 ITO/spin-coated TiO_2 (40 nm)/MEH-PPV/Au

5.3.4.1 IV-Characteristics with monochromatic light (520 nm)

Several titania films with different thicknesses (40, 50, 70 and 120 nm) were prepared. Devices fabricated with 40 nm titania films showed a large increase in the photocurrent. However, the fill factor of the device did not improve significantly.

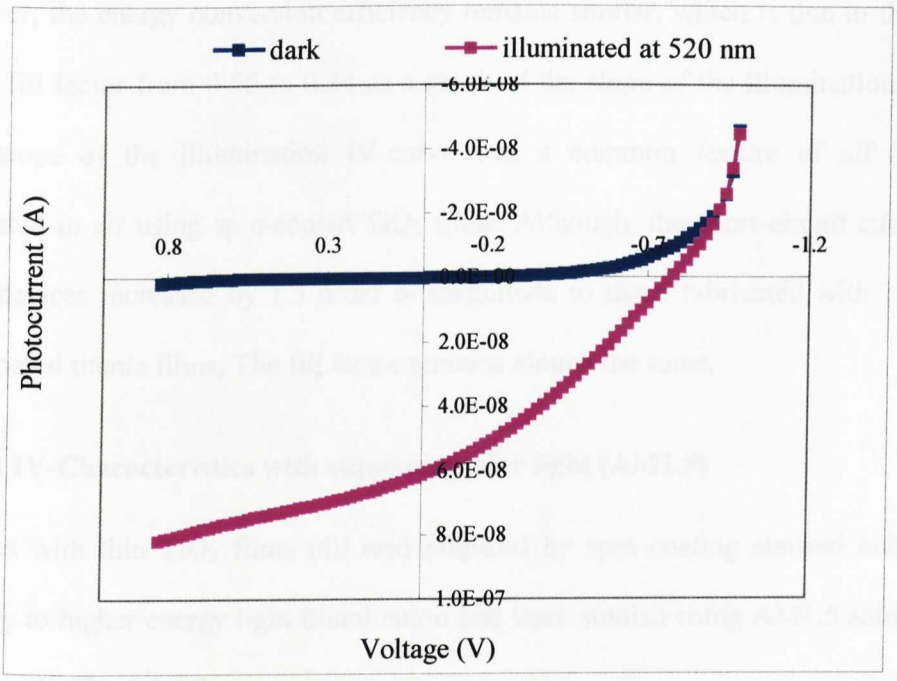

Fig. 5.3.4.1: IV-Characteristics of ITO/spin-coated TiO_2 (40 nm)/MEH-PPV/Au

Short-circuit current (I_{sc})	6.14 x 10^{-8} A
Open-circuit voltage (V_{oc})	0.76 V
Fill factor	0.34
Incident Photon to Current Efficiency (IPCE)	1.6%
Energy conversion efficiency	0.15%

Table 5.3.4.1: Efficiency values for ITO/spin-coated TiO_2 (40 nm)/MEH-PPV/Au

As shown in Table 5.3.4.1, the photon to electron conversion efficiency increases remarkably from the previous device fabricated with 50 nm dip-coated TiO_2 film,

however, the energy conversion efficiency remains similar, which is due to the drop in the fill factor from 0.56 to 0.34 as a result of the slope of the illumination curve. This slope of the illumination IV-curve was a common feature of all devices fabricated in air using spin-coated TiO_2 films. Although, the short-circuit current in these devices increased by 1.5 order of magnitude to those fabricated with 120 nm spin-coated titania films, The fill factor remains almost the same.

5.3.4.2 IV-Characteristics with simulated solar light (AM1.5)

Devices with thin TiO_2 films (40 nm) prepared by spin coating showed enhanced stability to higher energy light illumination and were studied using AM1.5 solar light as shown in Fig. 5.3.4.2.

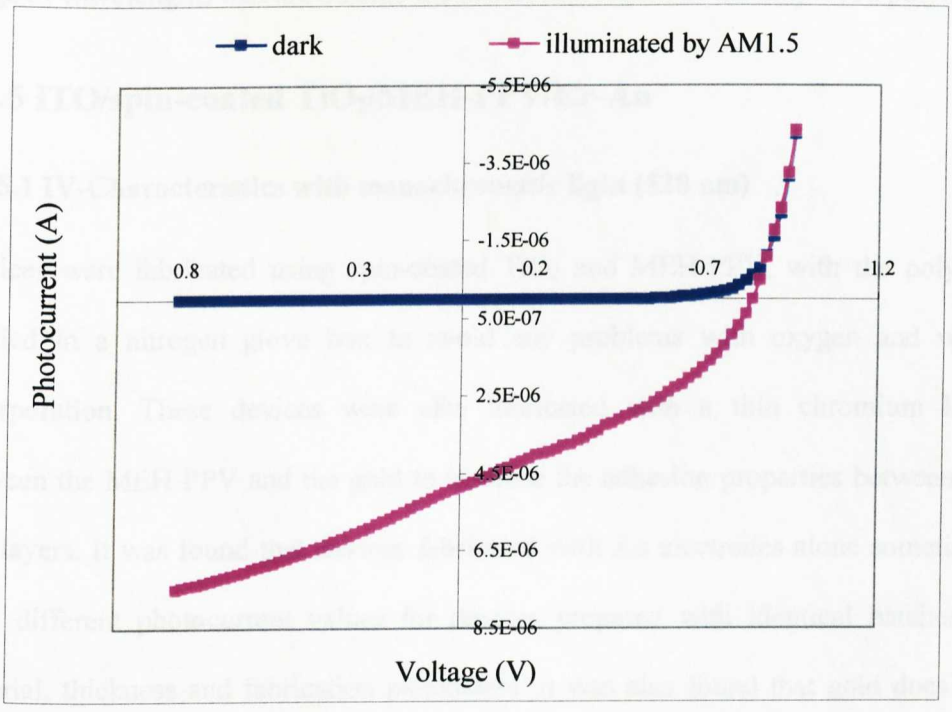

Fig. 5.3.4.2: IV-Characteristics of ITO/spin-coated TiO_2 (40 nm)/MEH-PPV/Au

Short-circuit current (I_{sc})	4.8 x 10^{-6} A
Open-circuit voltage (V_{oc})	0.82 V
Fill factor	0. 38
Incident Photon to Current Efficiency (IPCE)	0.8%
Energy conversion efficiency	0.11%

Table 5.3.4.2: Efficiency values for ITO/spin-coated TiO_2/MEH-PPV/Au for solar light AM1.5 study

The IPCE under AM1.5 illumination was 0.8%, which is lower than that obtained for monochromatic irradiation at 500 nm as the solar simulated light consists of a wide range of wavelengths that are outside the absorption region of the employed polymer.

5.3.5 ITO/spin-coated TiO_2/MEH-PPV/Cr-Au

5.3.5.1 IV-Characteristics with monochromatic light (520 nm)

Devices were fabricated using spin-coated TiO_2 and MEH-PPV, with the polymer applied in a nitrogen glove box to avoid any problems with oxygen and water incorporation. These devices were also fabricated with a thin chromium layer between the MEH-PPV and the gold to increase the adhesion properties between the two layers. It was found that devices fabricated with Au electrodes alone sometimes gave different photocurrent values for devices prepared with identical batches of material, thickness and fabrication parameters. It was also found that gold does not

adhere well to the conjugated polymers and this may result in a non-ohmic contact between gold and MEH-PPV.

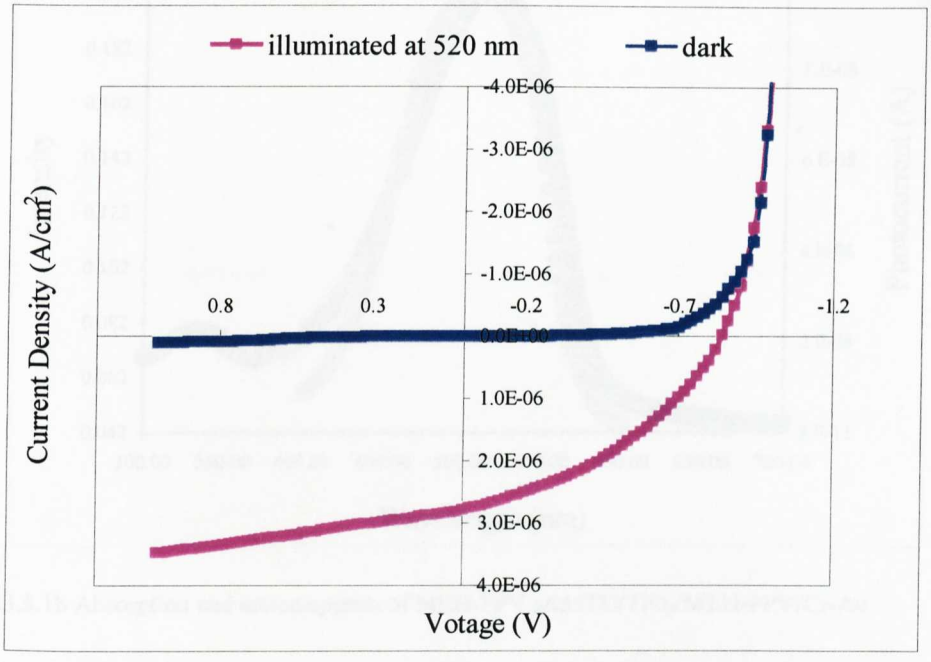

Fig. 5.3.5.1a: IV-Characteristics of ITO/spin-coated TiO_2/MEH-PPV/Cr-Au illuminated by 520 nm

The action spectrum of the device accurately resembles the absorption spectrum of the polymer film spun on glass as shown in Fig. 5.3.5.1b. The device efficiency values are summarised in Table 5.3.5.1.

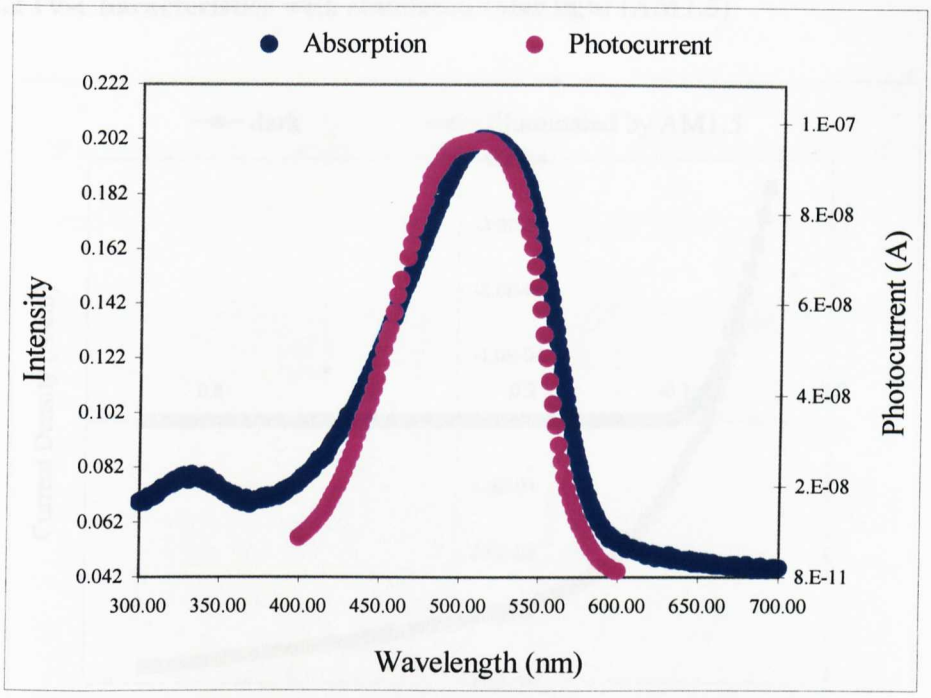

Fig. 5.3.5.1b Absorption and action spectra of MEH-PPV and ITO/TiO_2/MEH-PPV/Cr-Au

Short-circuit current (I_{sc})	2.78 x 10^{-6} A/cm^2
Open-circuit voltage (V_{oc})	0.8 V
Fill factor	0. 46
Incident Photon to Current Efficiency (IPCE)	2.3%
Energy conversion efficiency	0.38%

Table 5.3.5.1: Efficiency values for ITO/spin-coated TiO_2/MEH-PPV/Au for monochromatic light

5.3.5.2 IV-Characteristics with simulated solar light (AM1.5)

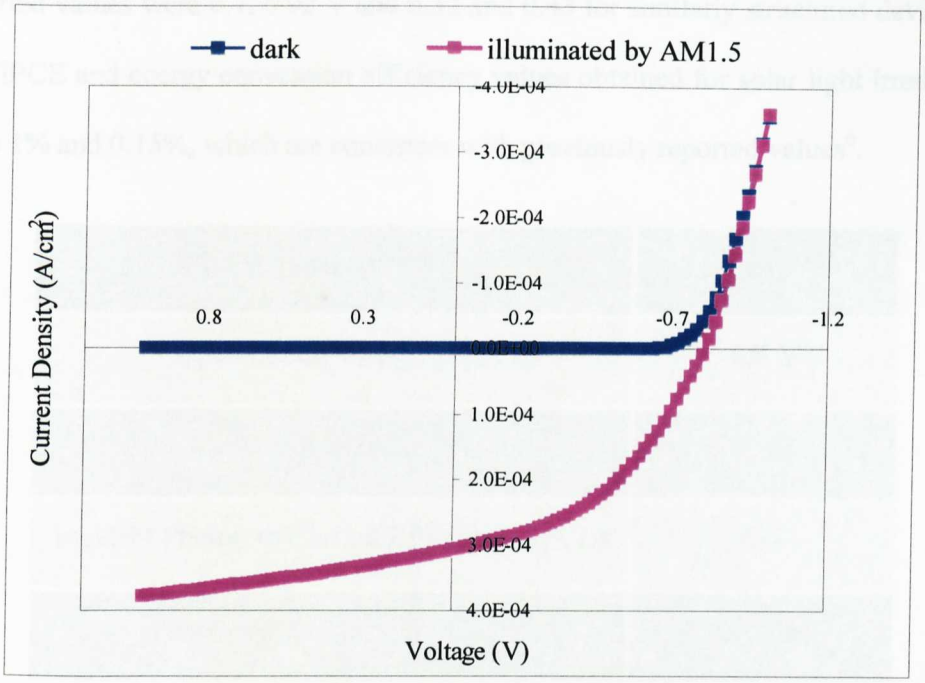

Fig. 5.3.5.2a: IV-Characteristics of ITO/spin-coated TiO_2 (40 nm)/MEH-PPV/Cr-Au illuminated by AM1.5

It is quite clear, that preparation of the devices under an oxygen and moisture free environment had a profound effect on the performance. The photocurrent was increased, as was the incident photon to electron conversion efficiency to 2.3%, compared to 1.6% for an exactly similar device prepared in air. The conversion efficiency also increased from 0.15% to 0.38%. In addition, the slope of the illumination curve was much reduced, i.e. a lower series resistance was achieved.

The device prepared in nitrogen showed a greater stability to illumination with solar light and intensities up to AM1 could be employed as shown in Fig. 5.3.5.2a. The device efficiency values are summarised in Table 5.3.5.2.

The observed open circuit voltage and the fill factor were 0.8 V and 0.43. Previously reported values were 0.7, 0.92 V and 0.52 and 0.43 for similarly structured devices[3,7]. The IPCE and energy conversion efficiency values obtained for solar light irradiation were 1% and 0.15%, which are consistent with previously reported values[6].

Short-circuit current (I_{sc})	0.31 x 10^{-3} A/cm^2
Open-circuit voltage (V_{oc})	0.8 V
Fill factor	0. 43
Incident Photon to Current Efficiency (IPCE)	1%
Energy conversion efficiency	0.15%

Table 5.3.5.2: Efficiency values for ITO/spin-coated TiO_2/MEH-PPV/Au for solar light study

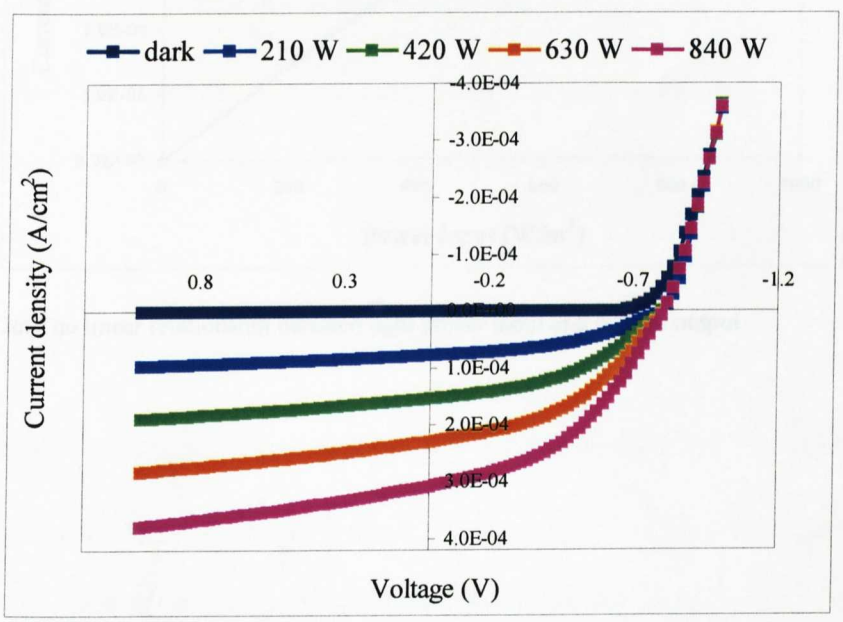

Fig. 5.3.5.2b: IV-Characteristics of ITO/ TiO_2/MEH-PPV/Cr-Au illuminated by various power input

The response of the device to different light power input values was studied and the IV-characteristics are shown in Fig. 5.3.5.2b. The relationship between the light power input and the current output was also studied and this was found to be linear as expected (see Fig. 5.3.5.2c).

The linear power input to current output relationship and the consistent illumination curve shape curve at different light power input demonstrates that the power conversion efficiency of these devices is independent of the input power.

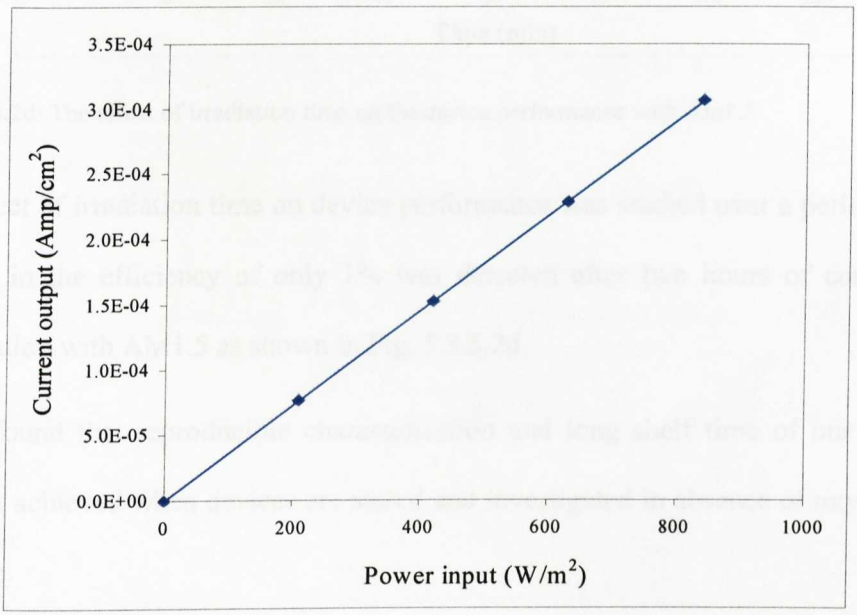

Fig. 5.3.5.2c: The linear relationship between light power input and current output

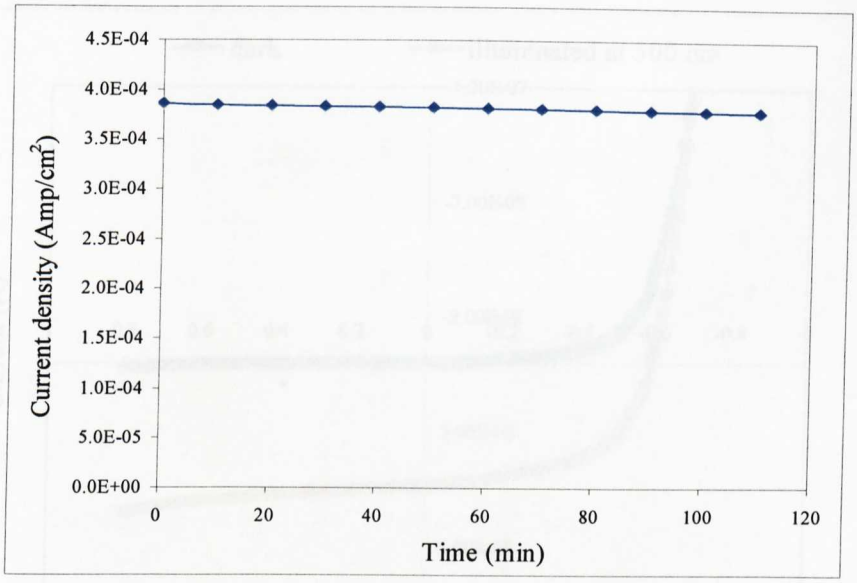

Fig. 5.3.5.2d: The effect of irradiation time on the device performance with Am1.5

The effect of irradiation time on device performance was studied over a period of 2h. A drop in the efficiency of only 1% was detected after two hours of continuous illumination with AM1.5 as shown in Fig. 5.3.5.2d.

It was found that reproducible characterisation and long shelf time of our devices could be achieved when devices are stored and investigated in absence of oxygen and moisture.

5.4 Discussion of devices results

5.4.1 Comparison between dip-coated and spin-coated titania films

Characterisation of devices fabricated with dip-coated titania films showed that only few of the six contacts produced IV-curves of classic photovoltaic diodes.

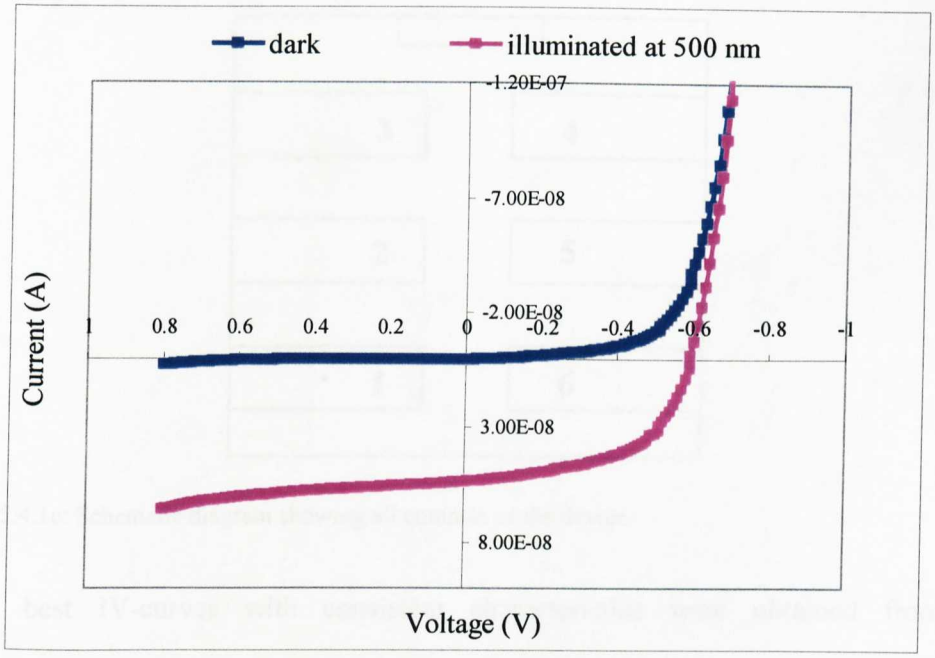

Fig. 5.4.1a: IV-Characteristics of contact 2 of ITO/dip-coated TiO_2/MEH-PPV/Au device

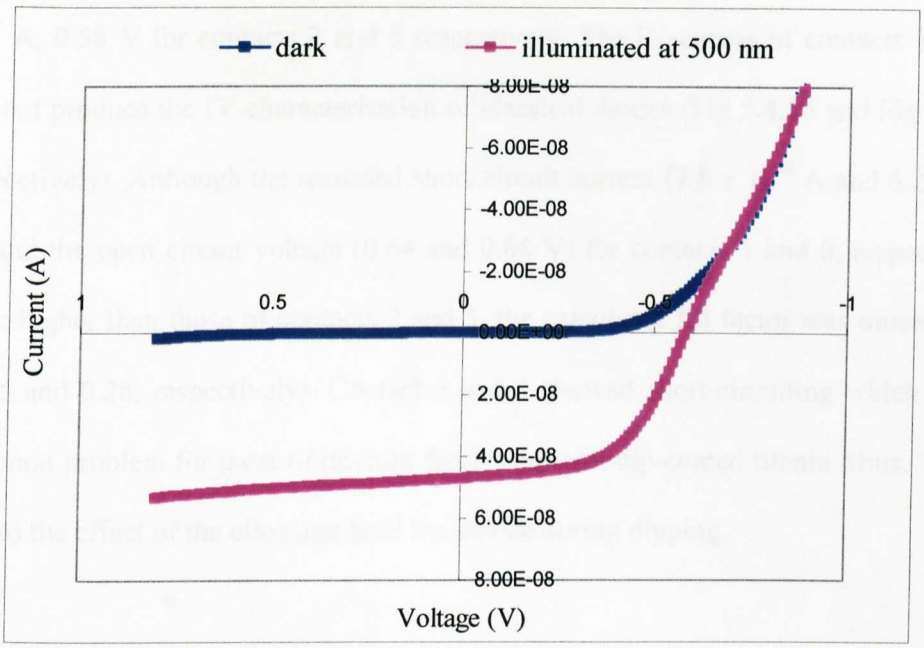

Fig. 5.4.1b: IV-Characteristics of contact 5 of ITO/dip-coated TiO_2/MEH-PPV/Au device

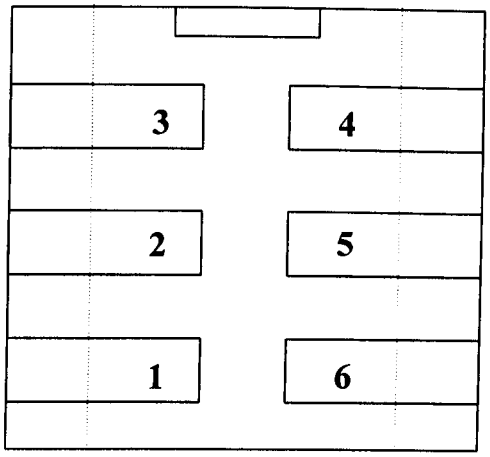

Fig. 5.4.1c: Schematic diagram showing all contacts of the device

The best IV-curves with consistent characteristics were obtained from the characterisation of contacts 2 and 5 (Fig. 5.4.1a and Fig. 5.4.1b, respectively). The short circuit current and the open circuit voltage were 5.3 x 10^{-8} A, 0.59 V and 4.7 x 10^{-8} A, 0.58 V for contacts 2 and 5 respectively. The IV-curves of contacts 1 and 6 did not produce the IV-characterisation of classical diodes (Fig 5.4.1d and Fig 5.4.1e, respectively). Although the recorded short circuit current (7.8 x 10^{-8} A and 6.2 x 10^{-8} A) and the open circuit voltage (0.64 and 0.66 V) for contacts 1 and 6, respectively, were higher than those of contacts 2 and 5, the calculated fill factor was much lower (0.35 and 0.28, respectively). Contact 3 and 4 showed short-circuiting which was a common problem for most of devices fabricated with dip-coated titania films. This is due to the effect of the clips that hold the device during dipping.

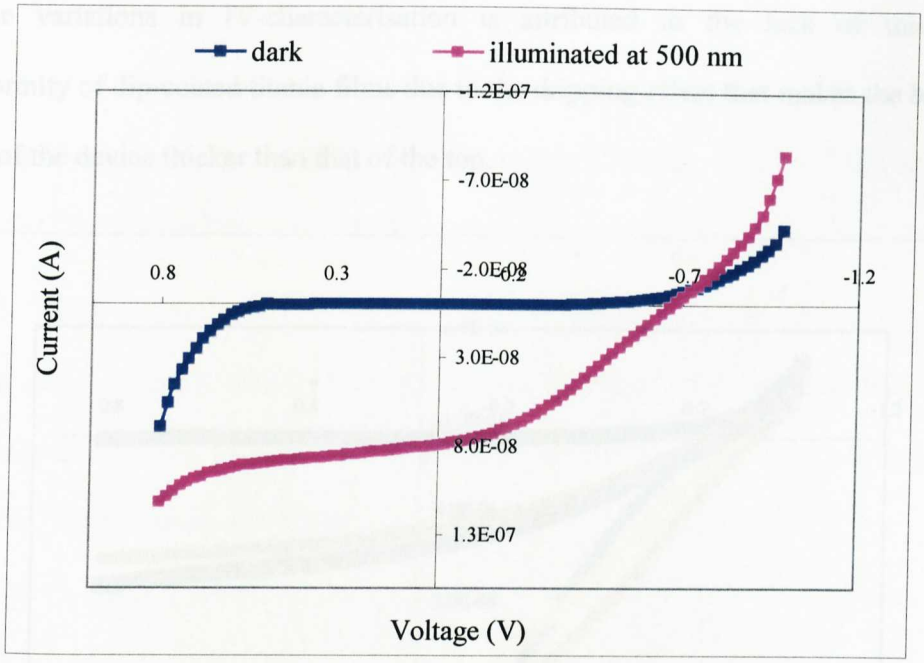

Fig. 5.4.1d: IV-Characteristics of contact 1 of ITO/dip-coated TiO_2/MEH-PPV/Au device

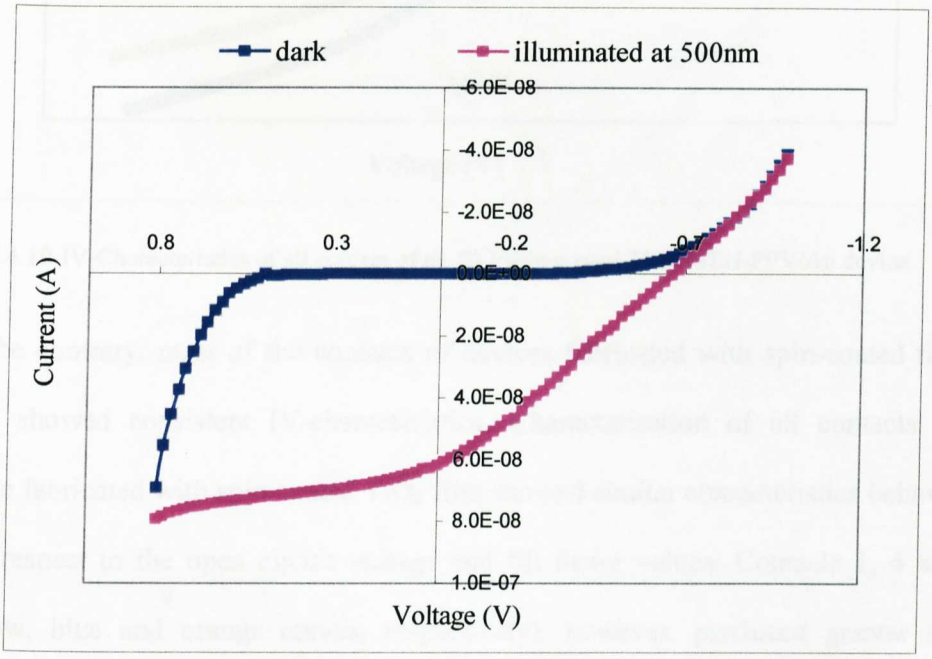

Fig. 5.4.1e: IV-Characteristics of contact 6 of ITO/dip-coated TiO_2/MEH-PPV/Au device

These variations in IV-characterisation is attributed to the lack of thickness uniformity of dip-coated titania films due to the dripping effect that makes the bottom area of the device thicker than that of the top.

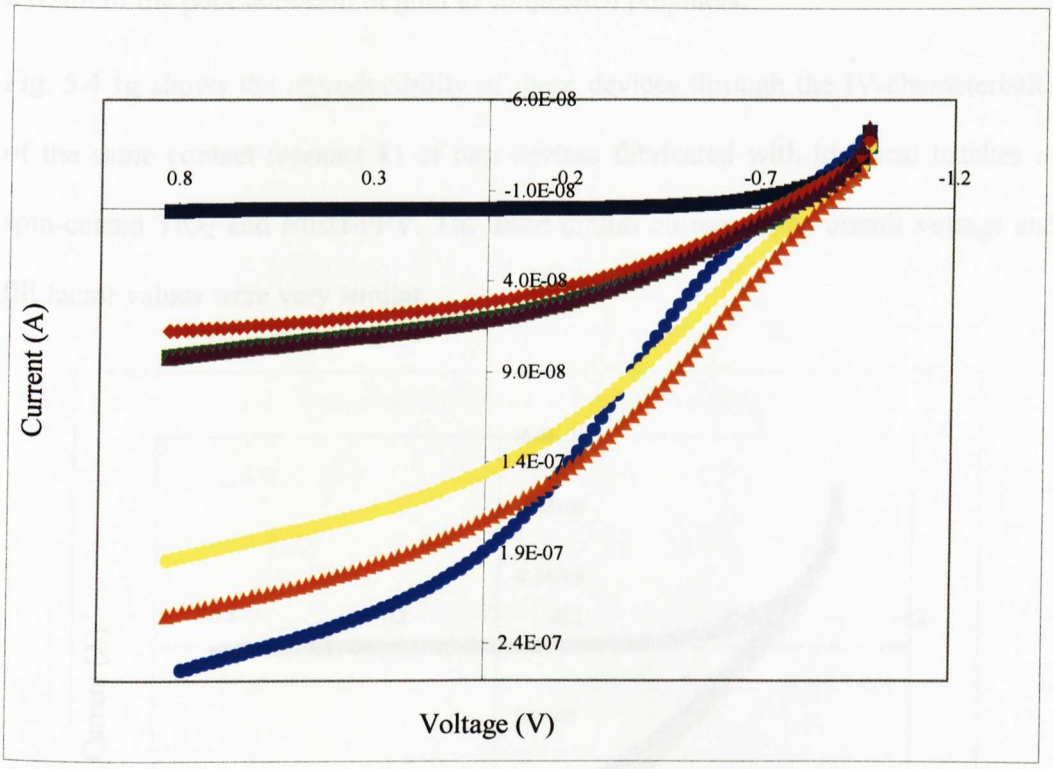

Fig. 5.4.1f: IV-Characteristics of all contact of an ITO/spin-coated TiO_2/MEH-PPV/Au device

On the contrary, most of the contacts of devices fabricated with spin-coated titania films showed consistent IV-characteristics. Characterisation of all contacts of a device fabricated with spin-coated TiO_2 film showed similar characteristics behaviour with respect to the open circuit voltage and fill factor values. Contacts 1, 4 and 6 (yellow, blue and orange curves, respectively), however, produced greater short circuit current as shown in Fig. 5.4.1f whereas the open circuit voltage and the fill

factor remain similar to contacts, 2, 3 and 5 (violet, green and red curves respectively). This discrepancy in short circuit current values of different contacts is presumably related to the possible non-ohmic contact between gold and MEH-PPV as a result of the poor adhesion of gold to conjugated polymers.

Fig. 5.4.1g shows the reproducibility of these devices through the IV-characteristics of the same contact (contact 2) of two devices fabricated with identical batches of spin-coated TiO_2 and MEH-PPV. The short circuit current, open circuit voltage and fill factor values were very similar.

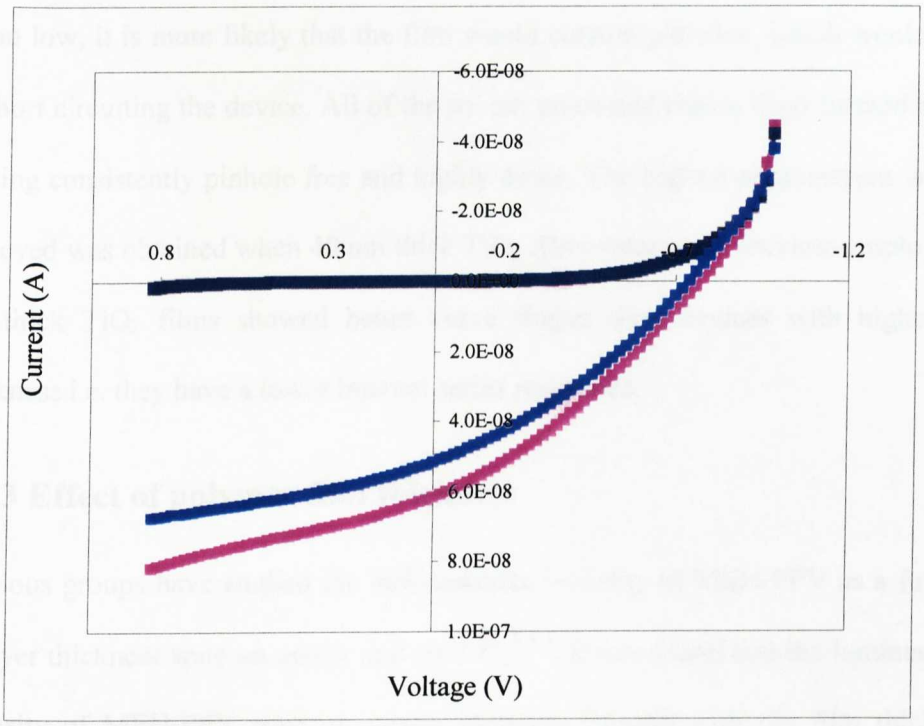

Fig. 5.4.1g: IV-Characteristics of contact 2 of two ITO/spin-coated TiO_2/MEH-PPV/Au devices

The second major difference, we observed, is that all devices fabricated with dip-coated titania films were short-circuited when illuminated with solar simulated light,

even when low light intensity solar simulated light of 10 mW/cm^2 was applied. On the contrary, spin-coated titania based devices showed great stability to simulated solar light with intensities up to AM1 with reproducible IV-characteristics.

5.4.2 Effect of TiO_2 film thickness

Several titania thin films of different thicknesses have been employed in the photovoltaic device structure of ITO/TiO_2/MEH-PPV/Au to optimise the performance of the device i.e. to achieve high photocurrent. The thicker the TiO_2 film, the higher the series resistance and hence the lower the photocurrent. If the titania film thickness is too low, it is more likely that the film would contain pinholes, which would result in short circuiting the device. All of the sol gel processed titania films formed by spin coating consistently pinhole free and highly dense. The highest photocurrent we have achieved was obtained when 40 nm thick TiO_2 films were used. Devices employed 40 nm thick TiO_2 films showed better curve shapes than devices with higher film thickness i.e. they have a lower internal series resistance.

5.4.3 Effect of polymer film thickness

Previous groups have studied the luminescence intensity of MEH-PPV as a function of layer thickness spun on quartz and on TiO_2[7,8,9]. It was found that the luminescence intensity of MEH-PPV spun on quartz increases linearly with the film thickness. However, luminescence intensity of MEH-PPV spun on TiO_2 showed two regimes. At thicknesses below 20 nm the luminescence is almost completely quenched, but above this threshold the luminescence increases linearly with the same slope as on

quartz suggesting that the exciton diffusion length in of MEH-PPV spun films is ~ 20 nm, i.e. excitons generated in the bulk of the polymer layer (within a distance greater than 20 nm away from the MEH-PPV/TiO_2 interface) would not contribute to the photocurrent. Our results showed that devices that employed polymer films with thicknesses below 40 nm were short-circuited. This could be attributed to two reasons; the first is due to the surface roughness of the ITO substrates and the second is owing to the gold diffusion on evaporation. It was found that film thickness of 80 nm of the polymer is an ideal compromise between a thin film thickness and short-circuit free devices.

5.4.4 Comparison of devices efficiency with previously reported devices

5.4.4.1 Monochromatic light efficiencies

Dip-coated titania based devices sensitised by PPV12-1 under illumination with 468 nm monochromatic light of 0.1 mW/cm^2 intensity revealed IPCE efficiency of 0.56%, power conversion efficiency of 0.07% and a fill factor of 0.5. The higher molecular weight MEH-PPV/dip-coated titania based device revealed better efficiencies, where the IPCE was 0.97% and the power conversion efficiency was 0.13% with a fill factor of 0.56 under illumination of 500 nm monochromatic light with similar light intensity. The best results were obtained from devices fabricated in nitrogen with spin-coated titania sensitised by MEH-PPV. The IPCE and the power conversion

efficiency under illumination with 520 nm monochromatic light were 2.3% and 0.38%, respectively. The fill factor was 0.46.

The photovoltaic properties of single layer PPV sandwiched between ITO and Al electrodes showed a power conversion efficiency of approximately 0.1% and a low fill factor of 0.22 under monochromatic light intensities of 1 mW/cm^2. The relationship between the optical absorption of PPV alone and the spectrally resolved photocurrent of these devices were found to be antibatic[10,11]. In these devices the potential difference between the electrodes should be high enough to overcome the coulomb attraction barrier of the photogenerated excitons so that efficient charge generation takes place. Typical quantum yields of 20% could be achieved at –10 V bias[12]. Without the high reverse voltages the absorbed photons will mainly create excitons that decay (either radiatively with photoluminescence or non-radiatively). To overcome this limitation of photoinduced charge carrier generation, a donor-acceptor approach using a composite thin film of conjugated polymer/fullerene mixture was successfully introduced[13]. Heeger *et al*[14] reported 0.04% power conversion efficiency for the first bilayer ITO/MEH-PPV/fullerene/Au device, with 100 nm film thickness for both layers, under illumination with 514.5 nm monochromatic light of 1 mW/cm^2 intensity. The open circuit voltage and the fill factor were 0.44 V and 0.48 respectively. This type of devices also suffered from antibatic behaviour. The reported values were close to those obtained from the characterisation of our first device fabricated with PPV12-1. However, the power conversion efficiency in our device is slightly higher. The low power conversion efficiency in these devices was

attributed to the limited carrier collection efficiency of separated charges at the interface and the recombination of the photoexcitons that are created far from the donor-acceptor junction. Consequently, interpenetrating phase-separated MEH-PPV/fullerene based devices were fabricated to overcome charge carriers recombination in the polymer layer. The IPCE efficiency and power conversion efficiency under monochromatic light for a composite thin film with 80 wt.% of a soluble fullerene derivative were 29% and 2.9%, respectively[15]. Although these devices show much higher efficiencies compared to our best devices characterisation, they are operated at a bias of –2 V. The 0.72 V open circuit voltage reported was independent of the work function difference between the electrodes and was set by the difference between the LUMO of fullerene (4.1 eV) and the HOMO of MEH-PPV (5 eV). This is in agreement with our interpretation to the values of the observed open circuit voltage in our devices. Devices based on thin film composites of PPV and electron acceptor nanocrystals such as CdSe[16] and TiO_2[2] showed IPCE efficiency of 12% for a MEH-PPV/CdSe composite based device with 90 wt % of CdSe and 1% for PPV/TiO_2 composite based device with 25 wt % of TiO_2 under illumination of monochromatic light of 514 and 495 nm, respectively. These devices were not able to produce IV-curves of classic p-n diodes.

The use of polymers as both donor and acceptor was introduced by the Cavendish Laboratory in Cambridge[17]. The two layers are blends of donor and acceptor conjugated polymers, POPT and CN-MEH-PPV, respectively. This device produced 29% IPCE efficiency and 4.8% power conversion efficiency under illumination of 480 nm

monochromatic light. Despite the higher efficiency obtained in this device, the IV-curve did not follow the classic diode behaviour and the device was operated at –2 V bias.

5.4.5 Solar light efficiencies

The best results were obtained from devices fabricated in nitrogen with spin-coated titania sensitised by MEH-PPV. The IPCE and the power conversion efficiency were 1% and 0.15%, respectively with a fill factor of 0.43 under illumination with simulated solar light AM1.5. These values were consistent with previously reported device of similar structure[6]. The laminated POPT/CN-MEH-PPV based device[17] showed an overall power conversion efficiency of 1.9% under AM1.5 simulated solar light illumination.

5.5 Strategies to increase devices efficiency

5.5.2 Inclusion of a porous layer of titania

The inclusion of a porous layer of titania on the top of the dense layer should increase the titania surface area and allow for an improved contact with the polymer molecules. This should result in an improved charge dissociation and higher device efficiency.

Our initial attempts at inclusion of a second porous layer of TiO_2 used a fast heat ramp profile to sinter the second layer. This layer was heat treated with heat ramp of 10 °C/min in order to produce a porous thin film of TiO_2. Devices fabricated with this layer resulted in a high series resistance and low photocurrent as shown in Fig. 5.5.2.

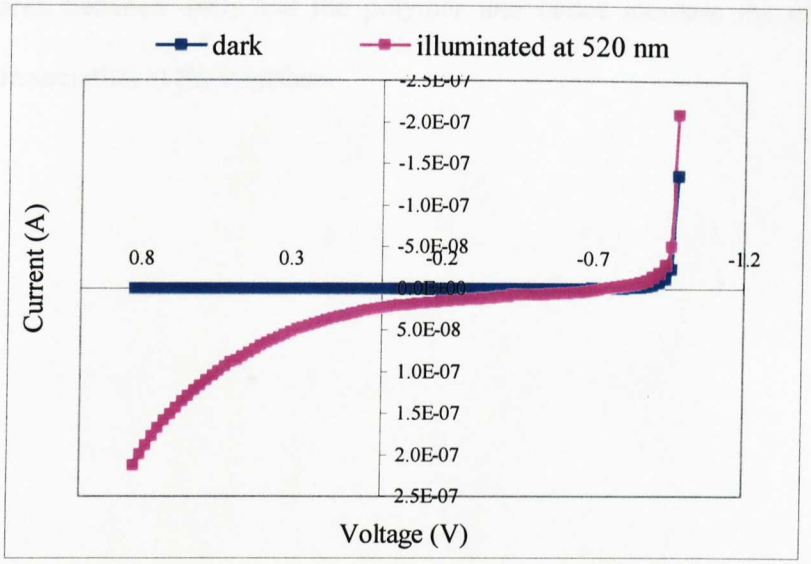

Fig. 5.5.2: IV-Characteristics of ITO/2 layers of spin-coated TiO_2/MEH-PPV/Au device

The shape of the IV-curves of these devices was similar to those of devices fabricated with thicker titania substrate (120 nm thickness). However, the photocurrent obtained was greater by a factor of two.

The high series resistance and low photocurrent in these devices is attributed to the thick titania films. This suggests that the second layer was rather dense and not as porous as we expected. This means that the heat ramp of 10 °C/min is not fast enough to create porous titania film. A faster heat ramp was not possible as the maximum heating capacity of the furnace used in sintering titania films is 10 °C/min.

5.5.1 Annealing of the polymer layer

Annealing of the polymer layer at the glass transition temperature allows the polymer molecules to fill in the pores of TiO_2, which will result in maximising the interfacial

contact area between TiO_2 and the polymer and hence increase the efficiency of exciton dissociation at the interface.

5.6 References

[1] J. Holzl and F. K. Schelte, *Springer Tracts in Modern Physics, Springer*, Berlin, **1979**, *85*

[2] J. S. Salafsky, *Physical review B*, **1999**, *39*, 10885-10894

[3] A. C. Arango, S. A. Carter, J. C. Scott, P. J. Brock, *Appl. Phys. Lett.* **1999**, *74*, 1698

[4] Q. Fan, B. McQuillin, A. K. Ray, M. L. Turner, A. B. Seddon, *J. Phys. D: Appl. Phys.* **2000**, *33*, 2683-2686

[5] R. N. Marks, J. J. M. Halls, D. D. C. Bradley, R. H. friend, A. B. Holmes, *J. Phys.: Condens. Matter*, **1994**, *6*, 1379-1394

[6] G. Yu, A. J. Heeger, *J. Appl. Phys.* **1995**, *78*, 4510

[7] T. J. Savenjie, J. M. Warman, A. Goossens, *Chem. Phys. Lett.* **1998**, *287*, 148-153.

[8] N. C. Greenham, X. Peng, A. P. Alivisatos, *Phys. Rev. B*, **1996**, *54*, 17628

[9] M. G. Harrison, J. Gruner, G. C. W. Spencer, *Phys. Rev. B*, **1997**, *55*, 7831

[10] H. Antoniadis, B. R. Hsieh, M. A. Abkowitz, S. A. Jenkhe, M. Stolka, *Synth. Met.* **1994**, *62*, 265

[11] W. Riess, S. Krag, V. Dyakonov, M. Meier, M. Schwoerer, *J. of Luminescence*, **1994**, *906*, 60

[12] G. Yu, C. Zhang, A. J. Heeger, *Appl. Phys. Lett.* **1994**, *64*, 1540

---

[13] J. J. M. Halls, K. Pichler, R. H. Friend, S. C. Moratti, A. B. Holmes, *Appl. Phys. Lett.* **1996**, *68*, 3120

[14] N. S. Sariciftci, D. Braun, C. Zhang, V. I. Srdanov, A. J. Heeger, G. Stucky, F. Wudl, *Appl. Phys. Lett.* **1993**, *62*, 585

[15] N. S. Sariciftci, A. J. Heeger, *Handbook of Organic Conductive Molecules and Polymers*, **1997**, *1*, H. S. Nalwa (Ed.), John Wiley & Sons, New York

[16] N. C. Greenham, X. Peng, A. P. Alivisatos, *Phys. Rev. B*, **1996**, *54*, 17628

[17] M. Granstroem, K. Petritsch, A. C. Arias, A. Lux, M. R. Andersson, R. H. Friend, *Nature*, **1998**, *395*, 257

Chapter 6: Conclusions and Future Work

6.1 Synthesis

The aim of this thesis was to synthesise conjugated polymers that are highly photoabsorbing in the visible region of the spectrum and are capable of charge donation when set in intimate contact with an electron acceptor semiconductor for the fabrication of conjugated polymer based solid-state photovoltaics.

Two different classes of conjugated polymers were synthesised, poly(1,4-phenylene-ethynylene) and poly(1,4-phenylene-vinylene) polymers, via various synthetic routes, such as Heck, Stille and Gilch reactions. The Gilch reaction yielded higher molecular weight polymers than the palladium catalysed polymerisation reactions.

Further synthetic work should focus on the incorporation of push-pull system via the attachment of electron-drawing and electron-donating groups as substituents such as nitro and amino groups to the main chain to enhance the conjugation and hence further red shift the photoabsorption of the polymers. An interesting polymeric structure would be poly(1,4-phenylene-vinylene-thienylene) as the incorporation of thiophene into poly(1,4-phenylene-vinylene) polymers should red-shift the absorption of these polymers.

The choice of the solubilising side chain groups should focus on the branched alkoxy chains as MEH-PPV showed the best solubility among all synthesised polymers. Long alkoxy chains should not be symmetrically attached to the monomeric aryl rings as synthesised polymers with symmetrically substituted long alkoxy chains showed poor solubility in THF, toluene, xylene and chloroform.

6.2 Devices

Thin films of controlled thickness of the synthesised polymers were produced by spin coating technique for use as the light harvesting hole transport layer. The maximum absorption of these polymers in the solid state lies between 450 to 500 nm.

We have produced thin films of controlled thickness of TiO_2 by the sol gel process for use as the electron acceptor layer.

It was found that the film thickness of these materials has a profound effect on the device performance. It was found that the thinner the TiO_2 film, the less the series resistance of the film and hence the greater the generated photocurrent. The thinnest pinhole free titania film prepared had a thickness of 40 nm.

Ideally, the polymer film thickness would be ca 20 nm to match the maximum exciton diffusion length within the polymer film. However such low thickness was found to be too thin to produce short circuit free devices and transmits too much of the incident light. It was found that a film thickness of 80 nm of the polymer is an ideal compromise.

We have demonstrated that devices fabricated using these polymers convert 2.3% of incident photons into electrons and 0.38% of incident light into electrical power when monochromatic light is the source of light, whereas 1% and 0.15% respectively are achieved with solar simulator AM1.5 light source.

Characterisation of these devices revealed a linear relationship between the light power input and the generated photocurrent. In addition, the power conversion efficiency was found to be independent of the input power.

Further enhancement of device efficiency can be achieved by the enhancement of the interface structure. This could be achieved by the inclusion of a porous TiO_2 layer. The inclusion of a high surface area porous layer of titania on the top of the dense layer will maximise the area of contact between TiO_2 and the polymer and consequently improve the exciton dissociation at the interface and the device efficiency. The porous TiO_2 layer should be prepared by direct firing of the TiO_2 gel film at high temperatures (500–550 °C) and not by slow temperature programming.

Annealing of the polymer layer at the glass transition temperature should allow the polymer molecules to fill in the pores of TiO_2, which will also help to maximise the interfacial contact area and hence increase the efficiency of exciton dissociation at the interface.

In order to achieve consistent device characterisation, the fabrication of the devices should always be carried out in a clean room environment with moisture and temperature control. In addition, the spin coating of the polymer layer on the titania layer should be done in a glove box to avoid trapping oxygen at the interface as this has a tremendous effect on the device performance and stability.

Encapsulation of these devices will allow them to be operated and stored in absence of oxygen and moisture. This should maintain their efficiency and increase their operational and storage life time.